Function within Disorder: HSPB1 and HSPB5 Modulate Tau Aggregation

Mia Cervantes

A dissertation
submitted in partial fulfillment of the
requirements for the degree of

Doctor of Philosophy

University of Washington
2026

Reading Committee:
Rachel Klevit, Chair
Abhinav Nath
Claudia Vasquez

Program Authorized to Offer Degree:
Biochemistry

University of Washington

Abstract

Function within Disorder: HSPB1 and HSPB5 Modulate Tau Aggregation

Mia Cervantes

Chairs of Supervisory Committee:
Rachel Klevit
Department of Biochemistry

In numerous neurogenerative diseases, microtubule-associated protein tau forms fibrillar aggregates that are hallmarks of disease pathology. Small heat shock proteins (sHSPs) are ATP-independent molecular chaperones that play a critical role in maintaining protein homeostasis. Two sHSPs, HSPB1 (Hsp27) and HSPB5 (aB-crystallin), are constitutively expressed in the brain and neurons. Here, we show that HSPB1 and HSPB5 delay tau aggregation *in vitro* through distinct mechanisms determined by their disordered N-terminal regions (NTRs). HSPB1 inhibits tau aggregation under non-stress conditions, whereas HSPB5 requires activation by pH acidosis. Using chimeric constructs in which small NTR subregions are swapped, we identify different functional regions within the NTRs that modulate chaperone function for tau. The regions identified contain known sites of phosphorylation, suggesting that they are also functional control points that respond to cellular stress conditions. To further define how NTR sequence features encode function, NTR-ACD interaction network is perturbed through domain swaps, mutation, and hetero-oligomerization. Our findings support a model in which specific functional

motifs within disordered NTRs of sHSPs govern activity and client preference in response to cellular stress. Finally, this thesis presents a systematic framework for organizing sHSP NTRs into five distinct Function Regions (FR-A through FR-E) across ten human sHSPs. This work also establishes experimental tools for understanding sHSP oligomerization and function.

TABLE OF CONTENTS

LIST OF FIGURES

ACKNOWLEDGMENTS

I am incredibly grateful to have crossed paths with so many remarkable people during my PhD at the University of Washington. First and foremost, I would like to sincerely thank my co-advisors, Dr. Rachel Klevit and Dr. Abhinav Nath. I am deeply appreciative of their constant support, encouragement and thoughtful discussion about both my research and career development. From them, I have learned so much about what it means to do "good science"; to think critically, ask careful questions, and pursue answers with rigor and curiosity. I am also thankful for the unique opportunities they supported, including attending academic conferences where I was able to explore new places and connect with peers in the scientific community. Coming into University of Washington, I was eager to study the intricacies of intrinsically disordered proteins and understand how protein aggregation can lead to human disease. My thesis project, exploring interactions between small heat shock protein and tau, encompassed both of these curiosities, and while challenging, I thoroughly enjoyed peeling back the many layers of complexity within these systems. I am also grateful for my committee members, Matt Bush, Claudia Vasquez, and Mike Guttman for sharing their expertise and for the many insightful discussions over the years. I would like to thank all current and past members of the Klevit and Nath labs for their helpful discussion, collaboration, support and for making each day in the lab so much fun. I am especially thankful to Maria Janowska, Ellie James, Lisa Tuttle, and Peter Brzovic for their constant support, mentorship and for sharing their expertise over the years. I am also thankful for the two undergraduate students I had the privilege to mentor, Logan Davis and Anya Higashionna, for being able to share excitement for our research projects together.

During graduate school, I have been a part of wonderful scientific communities, including the Biological Physics Structure and Design program, Pharmacological Sciences

Training Program, and departments of Biochemistry and Medicinal Chemistry. I have benefited greatly from the collaborative and supportive environments that these communities fostered and learned a lot from members of these communities. I want to especially thank Erin Krischner, the BPSD program coordinator and my BPSD/Biochemistry cohorts for their support over the years.

Finally, I would like to thank my support system: my incredible friends, family, and animals, all of whom have been the backbone of this journey through their unconditional love and support. I am endlessly grateful to my parents who always encouraged and supported me to forge my own paths; my sisters for always making my day brighter; and my animals Luka, Lenny, and Miriel for their companionship. I have loved our daily morning walks with Luka to start the day, and my cats Lenny and Miriel for the purrs. Lastly, I want to thank my fiancé KJ for his love and support over the years. Moving to a new state and starting a new chapter is scary, but taking that step together had made everything so much easier. I am incredibly lucky to have these people in my life and will forever cherish my time at the University of Washington.

1. Introduction

1.1 Small heat shock protein function and organization

Small heat shock protein function

Cells rely on an interconnected network of molecular chaperones to maintain protein homeostasis and prevent irreversible aggregation (1-2). Small heat shock proteins (sHSPs) are a first line of defense in maintaining a healthy cellular condition by stabilizing misfolding proteins in an ATP-independent manner. The misfolded protein, or "client", is stabilized by an sHSP until it can subsequently refold spontaneously or through the action of ATP-dependent chaperones like Hsp70 (3). Expressed throughout human tissues (4), sHSPs are sensitive to cellular stress signals, including oxidation, post-translational modifications, acidosis, and heat shock. In response to stress signals, sHSPs undergo structural rearrangements to take on more active states where chaperone activity is enhanced (5-7).

The natural propensity of sHSPs to delay protein aggregation makes them attractive therapeutic targets for protein aggregation diseases including tauopathies. Indeed, efforts have been made to design small molecules or peptides that bind to sHSPs in the hope of controllably activating their chaperone effect (8-9). However, such approaches are limited by an incomplete understanding of how sHSPs are structurally organized, how they transition between inactive and active states, and how they recognize client proteins. This lack of understanding stems from properties of sHSPs that make them not amenable to traditional biochemical/biophysical techniques: they are largely (>50%) disordered and form large, polydisperse ensembles of oligomers ranging from dimers to 40-mers.

Small heat shock protein architecture

sHSPs are composed of three domains: a disordered N-terminal region (NTR), a conserved and folded α-crystallin domain (ACD), and a disordered C-terminal region (CTR) (Figure 1.1). Since the NTR and CTR that flank the ACD are highly disordered and flexible, isolated ACDs remain the only structurally characterized component of sHSPs. Despite the gap in structural understanding of the whole protein, several key interactions have been identified that may contribute to sHSP oligomerization and activity. Dimerization of ACDs is a foundational process in the assembly of higher-order oligomers. Structural studies revealed that the ACD dimer bears three defined grooves: one dimer groove at the interface between two ACD protomers, and two hydrophobic edge grooves formed by β4-β8 strands of each ACD protomer (10). Both central and edge grooves are thought to act as a binding template for potential binding partners, including but not limited to clients, co-chaperones, and other sHSP protomers (11). In basal (non-stressed) conditions, the NTRs of sHSPs have been described to be sequestered within oligomers through interactions with the ACD grooves (14). Despite having only three (1 central groove, 2 edge grooves) binding pockets, each ACD dimer unit has been shown to have multiple binding partners (clients, co-chaperones, inter-/intra-molecular interactions with other sHSP, etc.). The presence of more binding sequences than binding sites is thought to be a major contributor to the heterogeneity of sHSP oligomers. These interactions are relatively long-lived and not random; in some cases, they are also orientation-specific. The term "**quasi-ordered**" is used to describe this ensemble of heterogeneous yet specific interactions facilitated by the NTRs (11). This structural plasticity and dynamics, governed by networks of inter- and intra-interactions, make sHSP a challenging system to study.

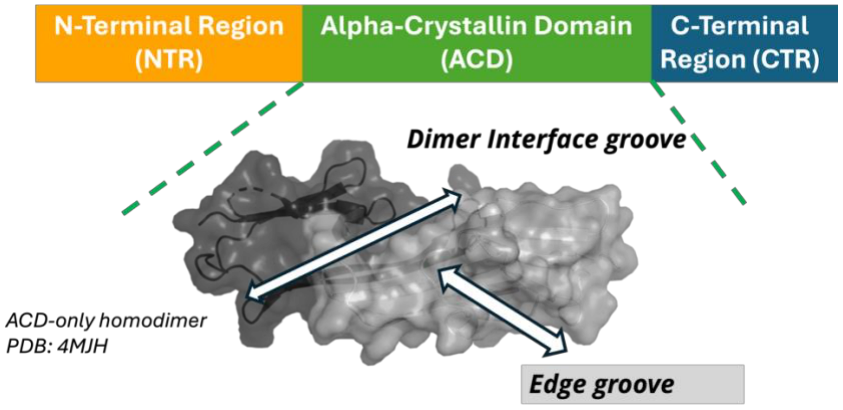

Figure 1.1 Architecture of small heat shock protein. Each sHSP is comprised of three domains: the disordered NTR (orange), structured ACD (green), and short disordered CTR (blue). ACD is the only structured domain of the protein that forms IgG-like beta-sheet sandwich. Edge groove and Dimer interface groove are indicated in arrows.

1.2 Functional sub-regions in human small heat shock protein NTRs

Small heat shock proteins are notoriously difficult to study, truly a monster of a biochemical beast! One major challenge in the sHSP field is the high level of complexity in sHSP organization and the lack of a systematic framework for examining and identifying patterns that underlie specific functions or interactions. One of the most important functions of sHSPs is to intervene in protein aggregation. However, protein aggregation itself is an inherently heterogeneous process and is difficult to reproduce consistently. Small variations in buffer composition, temperature, or agitation, can alter aggregation kinetics, making comparisons across studies difficult. Adding to this complexity, sHSPs themselves are also sensitive to experimental conditions, as mentioned above. As a result, systematic comparisons are rarely performed for sHSPs, limiting the ability to understand general features of sHSP biology.

As highlighted in the previous section, we have a relatively strong understanding of the structured ACD, including the specific grooves involved in oligomerization and client binding. However, an increasing number of studies point to the intrinsically disordered N-terminal region (NTR) to be essential for nearly every aspect of sHSP behavior, from oligomer plasticity to specific client chaperone activity. Despite this, no unifying or systematic organizational framework exists for the NTRs across the 10 human sHSPs. Evidence presented in this thesis, along with many other studies (11-14), indicates that short NTR segments carry distinct functional roles and likely encode client-specific interaction modes.

Identifying and systematically organizing these NTR-subregions would help reveal common sequence patterns, shared biophysical properties, and interactive or regulatory sites within sHSPs. Building a framework for systematic organization would be invaluable for understanding the diverse functions of the NTR, uncovering common regulatory mechanisms, and explaining how these proteins achieve specificity despite their dynamic and disordered nature. To address this gap, this chapter proposes an organization for the NTRs of the 10 human sHSP into subregions defined by short sequence elements with specific or unique motifs and biophysical characteristics. Organization of NTR sub-regions in HSPB1 has been previously described (11), but the selection of sub-regions was guided by peptides used for NMR studies. The sub-region definition used in Chapter 2 of my thesis is also based on the Clouser 2019 framework (Figure 1.2). However, sub-regions selection was only specific to HSPB1 features, so we sought to develop an organization scheme applicable to all 10 human sHSPs. Some human sHSPs have almost no information available regarding their structure or functions. Here, selection of NTR sub-regions was determined based on similar sequence, function, or binding. The NTRs share a high proline content distributed throughout the sequence, thus each sub-region

(with some exceptions) commonly ends with a proline residue. The newly proposed subregions are termed Functional Regions A-E (Table 1), to imply that each sub-region is associated with a specific function, binding, sequence features, and empirical observations (including HDX-MS for proteins with available data). Defining the NTR sub-regions as functional regions enables a more systematic and idiosyncratic approach for identifying shared roles, motifs, and biophysical features. With the exception of HSPB1 and HSPB3, all human sHSPs contain 5 recognizable sub-regions (Functional Regions A-E). HSPB1 contains an extra Insertion region and HSPB3 lacks FR-B. The hydrophobicity of each sub-region is also examined using the Hopp-Woods scale to better characterize shared intrinsic properties within their NTRs.

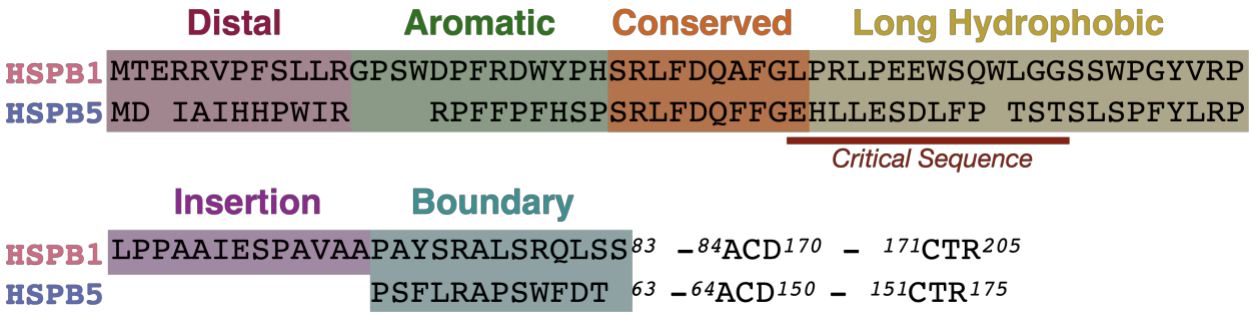

Figure 1.2: Sequence alignment of HSPB1 and HSPB5 NTR residues used in Chapter 2 thesis. The NTRs of HSPB1 and HSPB5 are divided into 5-6 short subregions, following Clouser et al. nomenclature for HSPB1.

	FR-A	FR-B	FR-C	FR-D	Insertion	FR-E	Tissue localization
HSPB1	1-14	15-25	26-34	35-57	58-71	72-94	ubiquitous
HSPB2	1-9	10-21	22-30	31-51	-	52-61	skeletal muscle and heart
HSPB3	1-14		14-22	23-45	-	46-58	skeletal muscle and heart
HSPB4	1-11	12-19	20-28	29-50	-	51-59	eye lens
HSPB5	1-13	14-20	21-29	30-51	-	52-74	ubiquitous
HSPB6	1-15	16-25	26-34	35-58	-	59-73	ubiquitous
HSPB7	1-12	13-24	25-33	34-58	-	59-70	skeletal muscle and heart
HSPB8	1-17	18-27	28-36	37-66	-	67-79	ubiquitous
HSPB9	1-7	7-11	12-20	21-37	-	38-44	testis
HSPB10	1-12	13-24	25-33	34-83	-	84-96	testis

Table 1.1: NTR organized in functional regions A-E (FR). NTR residues are organized in 5 different functional regions (FR) for all 10 human sHSPs. Tissue localization for each sHSP is also shown in the last row. HSPB1 and HSPB5, the two small heat shock proteins that are discussed in this thesis is highlighted in pink (HSPB1) and blue (HSPB5).

Functional Region A (FR-A)

Functional Region A (FR-A) has been referred to as the "Distal" region in prior work (11-14). FR-A comprises the most N-terminal portion of the sHSP and in several sHSPs (HSPB1,HSPB3 HSPB5, HSPB6), FR-A has an "IxI" motif that has been implicated in binding the ACD edge groove (11). The presence of an IxI motif in FR-A is not universal across all human sHSPs and several proteins contain more than one IxI motif (Table 1.2). The motifs also differ among sHSPs: for example, FR-A of HSPB1 (^{6}VPFLS) is not strictly an "IxI" but rather has alternating hydrophobic residues that could bind in a manner similar to the alternating Ile in IxI. A canonical IxI exists in HSPB3 (^{4}IIL), HSPB4 (^{3}VTI), and HSPB5 (^{3}IAI). In addition, HSPB3 and HSPB6 exhibit "double IxI" features in their FR-A (^{10}IEIPV in HSPB3 and ^{3}IPVPV in HSPB6) while

50% of the human sHSPs (HSPB2, HSPB7, HSPB8, HSPB9, HSPB10) lack an obvious IxI motif altogether. This variability suggests that while edge groove engagement is a broadly conserved feature of FR-A in 50% of human sHSPs, the specific sequence requirements to achieve this interaction are flexible. Further, IxI-mediated binding to the edge groove in some sHSPs might be weaker than in others due to differences in IxI sequence and affinity and/or differences in the properties of the ACD groove. Previous HDX-MS supports this interpretation, as FR-A exists in variable sequestration patterns across proteins or conditions (Chapter 2-3). In the case of HSPB1 and HSPB5 oligomers, FR-A peptides exhibit bimodal exchange behavior, suggesting existence of two major conformations: one in which FR-A is more protected, presumably because it is bound to the ACD edge groove and a second population in which FR-A is solvent exposed and dynamic (11,14,15).

Sequence information	Start residue	Sequence	End residue	Theoretical pI
HSPB1	1	MTERR**VPFSL**L RGP	14	11.70
HSPB2	1	MSGRSVP HAHP	11	9.54
HSPB3	1	MAK**IIL**R HL**IEIPV**	14	8.52
HSPB4	1	MD **VTI**Q HPWFKRT	13	8.52
HSPB5	1	MD **IAI** HHPWIRRP	13	9.39
HSPB6	1	ME**IPVPV**QPSWLRRA	15	9.35
HSPB7	1	MSHRTSST FRAERS	14	11.70
HSPB8	1	MADGQMPFSCHYPSRLR	17	8.0
HSPB9	1	MQRVGNTFSNE	11	5.75
HSPB10	1	MAALSCLLDSVR	12	5.59

Table 1.2: Sequence information for the FR-A regions, including residue numbers, amino acid sequence, and theoretical isoelectric point (pI). Sequence features are color coded within each FR-A sequence: positively charged residues (blue), negatively charged residues (red), proline

residues (purple), and aromatic residues (orange). The "IxI" sequence motif, which binds to the ACD edge groove, is shown in bold.

Analysis of FR-A hydrophobicity using the Hopp & Woods scale (Uniprot.org/ProtScale) reveals an overall pattern in which a hydrophobic segment spanning approximately residues 4-10 is sandwiched between stretches of polar residues (Figure 1.3). The IxI motif often falls within this hydrophobic patch. This sequence organization may be a strategy used by IDRs where polar residues preserve disorder and solubility, while the hydrophobic patch holds motifs that serve as important interaction modules.

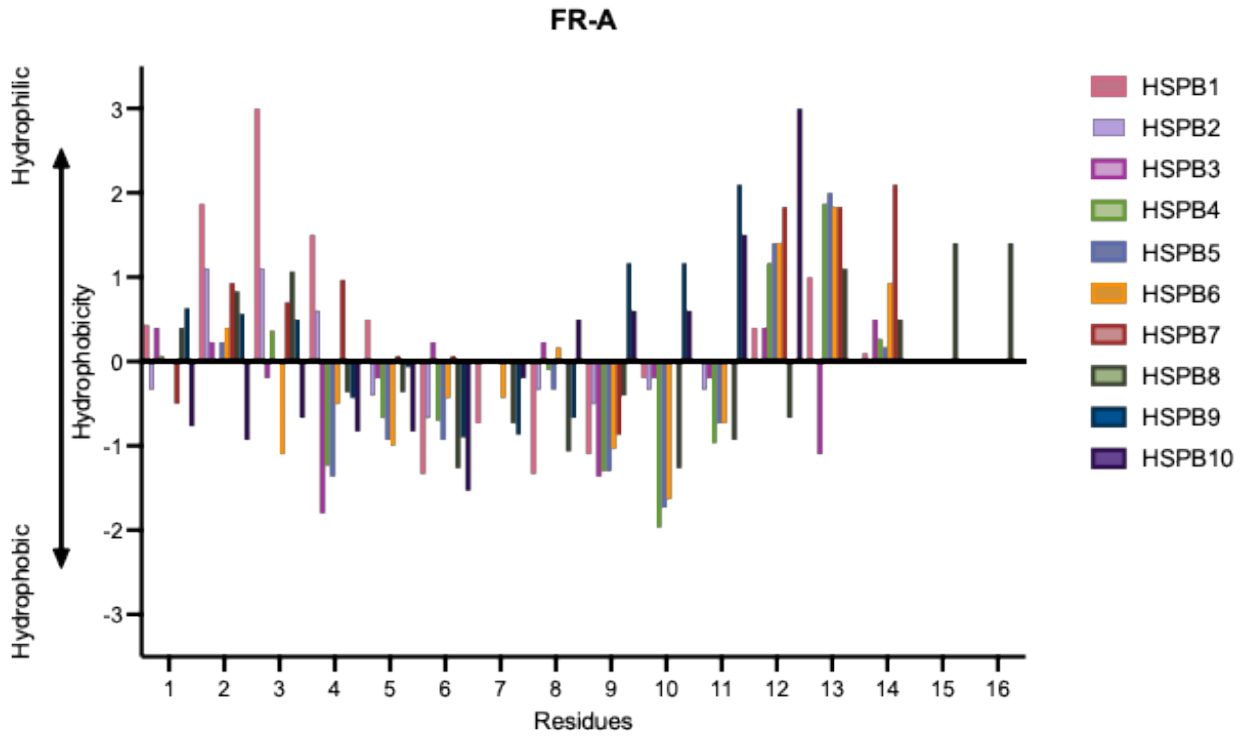

Figure 1.3: Hydrophobicity plot of the FR-A region calculated using the Hopp & Woods scale using with the ProtScale function on UniPro.org. Positive values indicate hydrophilicity and negative values indicate hydrophobicity, as shown by the arrow on the left side of the figure.

Hydrophobicity value for each residue was calculated using a three residue sliding window, with individual amino acid values based on Hopp & Wood hydrophobicity scale (see Appendix Figure 1). Residue numbers correspond to HSPB1, with residues from other sHSP aligned accordingly. Each sHSP is annotated in different colors as shown in the side legend.

FR-A is enriched in sequence features commonly associated with IDRs, including a high content of proline, polar, and charged residues (Table 1.3). Protein folding is discouraged in IDRs partly because their sequence composition is depleted in hydrophobic amino acids that can engage in intramolecular interactions (16). Enrichment of proline residues is also characteristic of IDRs. Proline has unique chemistry due to its cyclic side chain yet its effects on IDR ensembles remain highly debated. Prolines are generally considered disorder-promoting, due in part to steric effects that make chain dimensions more *expanded* and suppress transient helicity and beta-strand formation (17). Proline has also been shown to form polyproline II (PPII) structure, a helical secondary structural element with three residues per turn, that yields a locally expanded conformation (18-21). Conversely, recent work suggests that proline can have a dual role in IDR structure by not only promoting disorder but also compaction. Isolated prolines can promote local turns and increase intramolecular contacts, resulting in more *compact* ensembles (22-23). Thus, proline residues can influence disordered ensembles toward expansion or compaction depending on sequence and environmental context. In most FR-A sequences, prolines are relatively evenly distributed rather than clustered, with HSPB6 being the exception due to the high proline content within its IxI motif. Evenly spaced prolines may help to maintain FR-A in a disordered and soluble state by preventing secondary structure formation. Alternatively, these prolines may facilitate conformational switching by cis/trans isomerization,

allowing the region to sample bound and unbound conformations efficiently. While it is difficult to assign a single role to FR-A prolines without additional experiments, the conserved content of prolines across FR-A sequences highlights their importance in the dynamics and conformational plasticity of FR-A mediated interactions.

sHSP	- (E,D)	+ (R,K)	Net charge	P-site	Histidine	Proline	Aromatic (W,F,Y)
HSPB1	1	3	+2	-	0	P7,P14	1
HSPB2	0	1	+1	-	2	P7, P11	0
HSPB3	1	2	+1	-	1	P13	0
HSPB4	1	2	+1	-	1	P8	2
HSPB5	1	2	+1	-	2	P8, P13	1
HSPB6	1	2	+1	-	0	P4, P6, P9	1
HSPB7	1	3	+2	S7,S14	1		1
HSPB8	1	2	+1	-	1	P7, P13	1
HSPB9	1	1	0	-	0		1
HSPB10	1	1	0	-	0		0

Table 1.3: Sequence feature information for the FR-A regions, including numbers of charged residues, net charge, phosphorylation site (P-site), histidine, proline, and aromatic residues

Another notable feature of FR-A in several sHSPs is the presence of an aromatic residue (W or F) followed by 1-2 basic residues near the C-terminal end of the sub-region, three residues after the IxI-motif. Examples include HSPB4 (^{9}WFKR), HSPB5 (^{9}WIRR), and HSPB6 (^{11}WLRR). Variants of this motif can be described generally as (ΦxRR, ΦxKK, ΦxRK (Φ = F, Y, or W)). Such motifs could strengthen intramolecular docking interactions for the bound FR-A population. Aromatic residues can stabilize binding through hydrophobic packing, π- π interactions, and cation- π (24-27), while adjacent basic residues (R/K) can bind with negatively

charged patches on the ACD surface. Together, these interactions could reinforce ACD binding in addition to the IxI binding with the ACD edge groove, thereby increasing the stability of the bound state. Further mapping of the ACD electrostatic landscape around the edge groove in which FR-A binds would be valuable for determining whether these residues contribute to differences in NTR sequestration between sHSPs.

Functional Region B (FR-B)

Functional region B (FR-B) had been described previously as the "Aromatic" region in HSPB1, as it contains an unusually high density of aromatic residues (11). FR-B is characterized by a distinctive grammar of aromatic residues interspersed among prolines (Table 1.4). This motif-like sequence is observed across several sHSPs, suggesting that FR-B may hold functional roles or interactions. The proline spacing in FR-B likely contributes to maintaining disorder, while aromatic residues could engage in numbers of interactions as stated in FR-A section. Aromatic residues in IDRs are frequently associated with transient intramolecular stabilization and, in some contexts, client binding (28). Based on the study presented in Chapter 2 of this thesis, FR-B is hypothesized to contribute directly to chaperone activity *in vitro* (14). FR-B is also a hotspot for regulatory elements, including phosphorylation sites and histidine in several sHSPs (Table 1.5). PTMs and pH-sensitive Histidine residues within IDRs have been proposed to edit the "grammar" of IDR ensembles by changing their sequence chemistry, hence modulating the conformation in a reversible and controllable way (29). In sHSPs, phosphorylation and histidine could represent mechanisms by which FR-B tunes the balance between NTR sequestration and exposure. Consistent with this model, in HSPB1, NMR experiments using a peptide corresponding to FR-B show chemical shift perturbations in the

ACD upon peptide addition, and these perturbations are weakened when the analogous peptide is phosphorylated at S15 (11). In other words, FR-B appears to participate in NTR-ACD interactions and PTMs can regulate the equilibrium between bound and unbound NTR states.

While there are some shared features in this region, the FR-B sequences are variable across the human sHSP. Some proteins, such as HSPB7, contain serine-repeats, while others like HSPB4 and HSPB5 are short and hydrophobic, and HSPB1 exhibits alternating hydrophobic/polar patterns (Figure 1.4). HSPB8 and HSPB10 are also different in this region, showing more charged residues and fewer hydrophobic/aromatic residues. FR-B is also absent in HSPB3 and HSPB9, suggesting that this region is not universally required and may instead provide protein-specific regulatory or functional roles.

Sequence information	Start residue	Sequence	End residue	Theoretical pI
HSPB1	15	SWDPFRDWYPH	25	5.19
HSPB2	12	AT AEYEFANP	21	3.80
HSPB3	-	–	-	-
HSPB4	14	LG P FY P	19	5.52
HSPB5	14	FF P FHSP	20	6.74
HSPB6	16	SA PLPGLSAP	25	5.24
HSPB7	15	FHSSSSSSS	24	6.74
HSPB8	18	RDPFRDSPLS	27	5.96
HSPB9	-	–	-	-
HSPB10	13	RDIKKVDRELRQ	24	9.98

Table 1.4: Sequence information for the FR-B regions, including residue numbers, amino acid sequence, and theoretical isoelectric point (pI). Sequence features are color coded within each

FR-B sequence: positively charged residues (blue), negatively charged residues (red), proline residues (purple), and aromatic residues (orange).

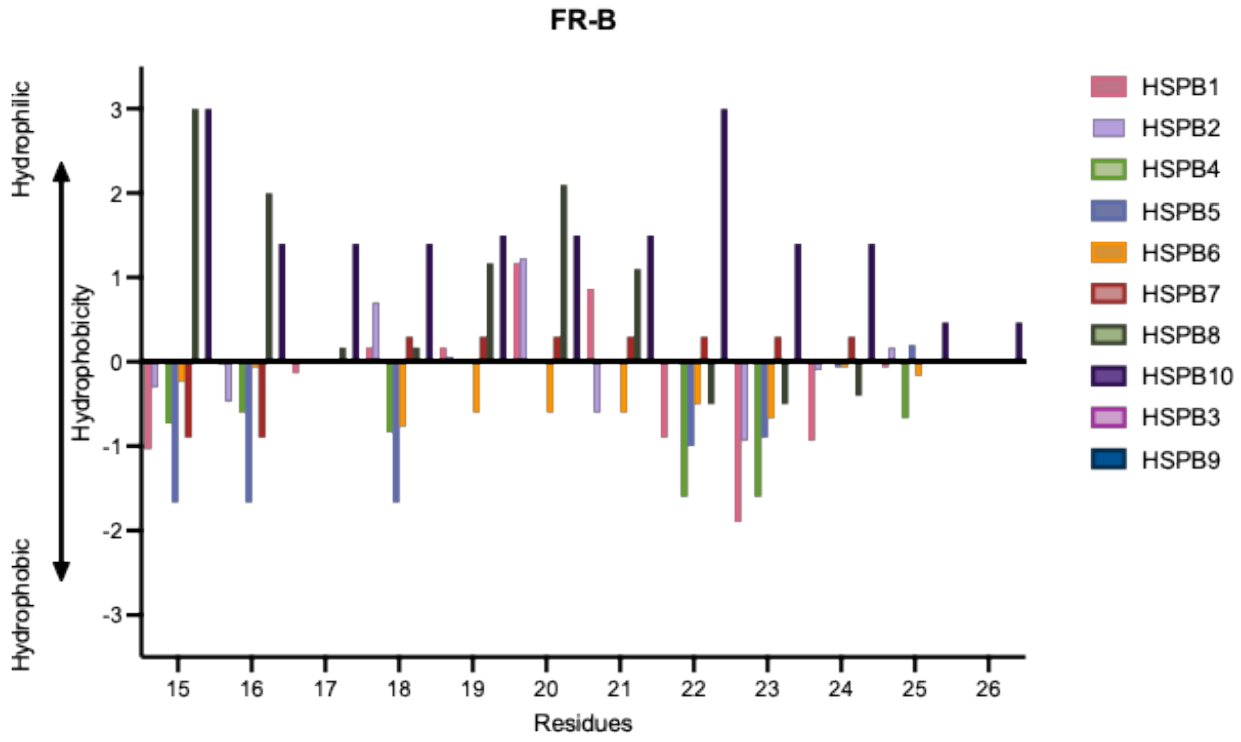

Figure 1.4: Hydrophobicity plot of the FR-B region calculated using the Hopp & Woods scale using with the ProtScale function on UniPro.org. Positive values indicate hydrophilicity and negative values indicate hydrophobicity, as shown by the arrow on the left side of the figure. Hydrophobicity value for each residue was calculated using a three residue sliding window, with individual amino acid values based on Hopp & Wood hydrophobicity scale (see Appendix Figure 1). Residue numbers correspond to HSPB1, with residues from other sHSP aligned accordingly. Each sHSP is annotated in different colors as shown in the side legend.

sHSP	- (E,D)	+ (R,K)	Net charge	Phos-site	Histidine	Proline	Aromatic (W,F,Y)
HSPB1	2	1	-1	S15	1	P18,P24	4
HSPB2	2	0	-2	-	0	P21	2
HSPB3	-	-	-	-	-	-	-
HSPB4	0	0	0	-	1	P16,P19	2
HSPB5	0	0	0	S19	1	P16, P20	3
HSPB6	0	0	0	S16	0	P18, P20, P25	0
HSPB7	0	0	0	-	1	-	1
HSPB8	2	2	0	S24	0	P20, P25	1
HSPB9	-	-	-	-	-	-	-
HSPB10	3	5	+2	-	0	-	0

Table 1.5: Sequence feature information for the FR-B regions, including numbers of charged residues, net charge, phosphorylation site (P-site), histidine, proline, and aromatic residues.

Functional Region C (FR-C)

Functional Region C (FR-C) is the most conserved region within the NTR across the sHSP family. This conservation suggests strong evolutionary pressure to preserve its role in sHSP architecture. FR-C commonly begins with serine, followed by a conserved arrangement of charged and hydrophobic residues, then often includes one or more phenylalanine and a small residue like glycine near the C-terminal end (Table 1.6, Figure 1.5). Unlike other functional NTR regions, FR-C contains no known phosphorylation sites and no histidines (Table 1.7). FR-Cs have been observed to bind to central grooves in several sHSPs (11,13). This suggests that FR-C is a key structural or functional element that is not itself regulated through pH or phosphorylation, but instead through binding to the ACD dimer interface. HSPB7 has the most divergent FR-C sequence in human sHSPs, suggesting either altered organization or reduced

reliance on this conserved interaction. More broadly, the high conservation of FR-C highlights this region as a core element of the quasi-order network shared across the sHSP family. Future experiments testing whether FR-C is exchangeable between sHSPs would provide insights into which protein-specific interactions govern sHSP structure and function.

Sequence information	Start residue	Sequence	End residue	Theoretical pI
HSPB1	26	SRLFDQAFG	34	5.55
HSPB2	22	SRLGEQRFG	30	9.31
HSPB3	14	VRYQEEFEA	22	4.25
HSPB4	20	SRLFDQFFG	28	5.55
HSPB5	21	SRLFDQFFG	29	5.55
HSPB6	26	GRLFDQRFG	34	9.60
HSPB7	25	STSSSASRA	33	9.47
HSPB8	28	SRLLDDGFG	36	4.21
HSPB9	12	SRVASRCPS	20	10.35
HSPB10	25	LRCIDEFST	33	4.37

Table 1.6: Sequence information for the FR-C regions, including residue numbers, amino acid sequence, and theoretical isoelectric point (pI). Sequence features are color coded within each FR-C sequence: positively charged residues (blue), negatively charged residues (red), proline residues (purple), and aromatic residues (orange).

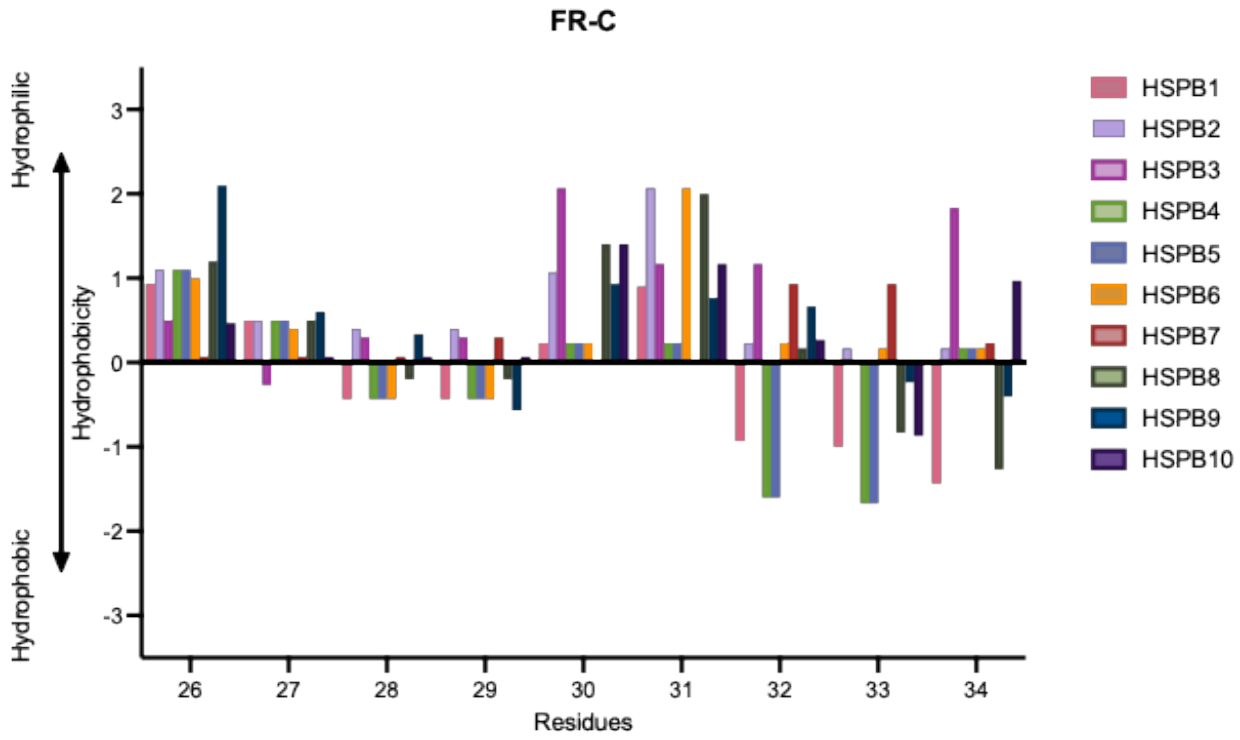

Figure 1.5: Hydrophobicity plot of the FR-C region calculated using the Hopp & Woods scale using with the ProtScale function on UniPro.org. Positive values indicate hydrophilicity and negative values indicate hydrophobicity, as shown by the arrow on the left side of the figure. Hydrophobicity value for each residue was calculated using a three residue sliding window, with individual amino acid values based on Hopp & Wood hydrophobicity scale (see Appendix Figure 1). Residue numbers correspond to HSPB1, with residues from other sHSP aligned accordingly. Each sHSP is annotated in different colors as shown in the side legend.

sHSP	- (E,D)	+ (R,K)	Net charge	P-site	Histidine	Proline	Aromatic (W,F,Y)
HSPB1	1	1	0	-	0	-	2
HSPB2	1	2	+1	-	0	-	1
HSPB3	3	1	-2	-	0	-	2
HSPB4	1	1	0	-	0	-	3
HSPB5	1	1	0	-	0	-	3
HSPB6	1	2	+1	-	0	-	2
HSPB7	0	1	+1	-	0	-	0
HSPB8	2	1	-1	-	0	-	1
HSPB9	0	2	+2	-	0	P19	0
HSPB10	2	1	-1	-	0	-	1

Table 1.7: Sequence feature information for the FR-C regions, including numbers of charged residues, net charge, phosphorylation site (P-site), histidine, proline, and aromatic residues.

Functional Region D (FR-D)

Functional Region (FR-D) corresponds to a region previously described in HSPB5 as a Long Hydrophobic and in HSPB1 as a "Trp-rich" region (11). FR-D contains multiple prolines, aromatic, and aliphatic residues, producing a strongly hydrophobic character relative to other NTR regions (Table 1.8). Hydrophobicity is broadly conserved across the sHSP, especially after the first ~7 residues of FR-D. The net charge of FR-D is slightly negative in most sHSPs, with HSPB1 having a neutral net charge and HSPB9 having a positive net charge. Although hydrophobic residues dominate, FR-D also contains charged residues that tend to cluster, particularly at the N-terminal end of the sequence. Notably, like FR-A, FR-D displays an alternating pattern of polar and hydrophobic residue patches, beginning with a short polar segment followed by an extended hydrophobic stretch (Figure 1.6). In most sHSPs, this

hydrophobic stretch contains multiple aromatic residues interspersed with prolines, similar to the pattern observed in FR-B. The sequence composition here may be supporting transient intra-inter-molecular interaction and/or client engagement. Indeed, FR-D of HSPB5 contains residues ("Critical region") implicated in chaperone function and activation (12). The presence of hydrophobic elements in other sHSPs raises the possibility that FR-D provides a conserved client-binding surface or other functionally relevant interactions. At the same time, sequence differences within FR-D could give rise to divergent functions or client specificity in this region. FR-D also harbors phosphorylation sites in multiple sHSPs (HSPB4, HSPB5, HSPB7, and HSPB8) as well as histidines in some proteins, suggesting that this region may also be regulated by cellular conditions (Table 1.9).

Sequence information	Start residue	Sequence	End residue	Theoretical pI
HSPB1	35	LPRLPEEWSQWLGGSSWPGYV RP	57	6.14
HSPB2	31	EGLLPEEIL TPTLYHGYYV RP	51	4.75
HSPB3	23	RGLEDCRLDHALYALPGPTIV DL	45	4.66
HSPB4	29	EGLFEYDLLPFLSSTISPYY RQ	50	4.14
HSPB5	30	EHLLESDLFP TSTSLSPFYLRP	51	4.65
HSPB6	35	EGLLEAELAALCP TTLAPYYLRAP	58	4.25
HSPB7	34	LPAQDPPMEKALSMFSDDFGS FMRP	58	4.23
HSPB8	37	MDPFPDDLTASWPDWALPRLS SAWPGTLRS	66	4.14
HSPB9	21	VGLAERNRVATMPVRLL	37	11.70
HSPB10	34	RCLCDLYMHPYCCCDLHPYPY CLCYSKRSRSCGLCDLYPCCL CDYKLYCL	83	7.57

Table 1.8: Sequence information for the FR-D regions, including residue numbers, amino acid sequence, and theoretical isoelectric point (pI). Sequence features are color coded within each FR-D sequence: positively charged residues (blue), negatively charged residues (red), proline residues (purple), and aromatic residues (orange).

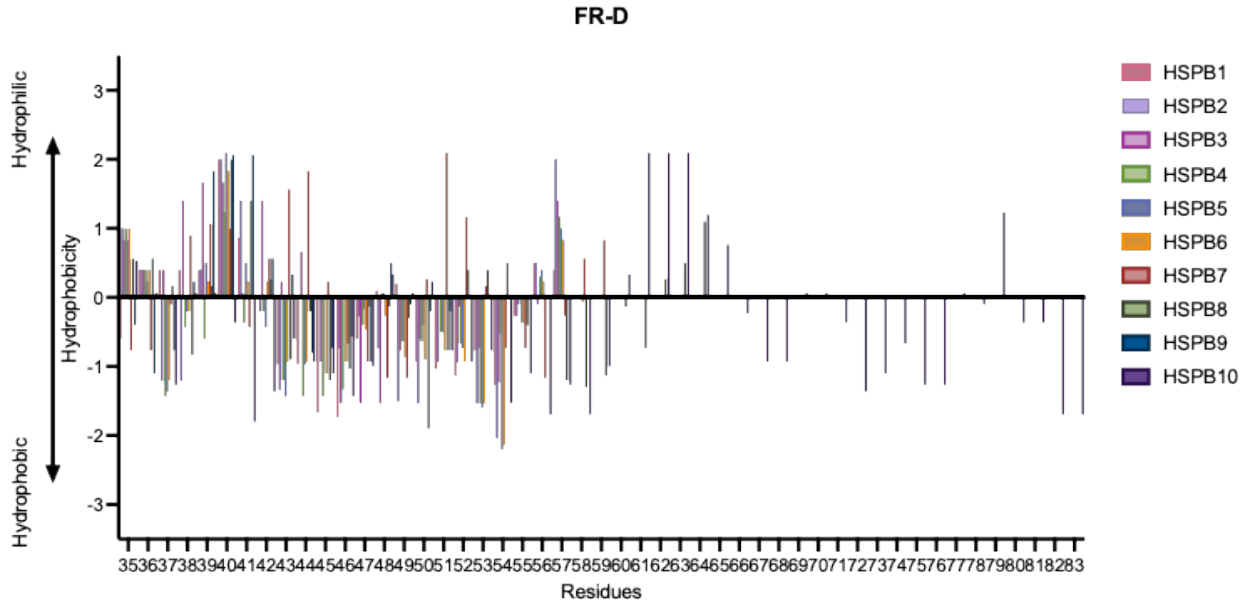

Figure 1.6: Hydrophobicity plot of the FR-D region calculated using the Hopp & Woods scale using with the ProtScale function on UniPro.org. Positive values indicate hydrophilicity and negative values indicate hydrophobicity, as shown by the arrow on the left side of the figure. Hydrophobicity value for each residue was calculated using a three residue sliding window, with individual amino acid values based on Hopp & Wood hydrophobicity scale (see Appendix Figure 1). Residue numbers correspond to HSPB1, with residues from other sHSP aligned accordingly. Each sHSP is annotated in different colors as shown in the side legend.

sHSP	- (E,D)	+ (R,K)	Net charge	P-site	Histidine	Proline	Aromatic (W,F,Y)
HSPB1	2	2	0	-	0	P36,P39,P52,P57	2
HSPB2	3	1	-2	-	1	P35,P41,P51	3
HSPB3	4	2	-2	-	1	P38,P40	1
HSPB4	3	1	-2	S45	0	P38,P46	5
HSPB5	3	1	-2	S45	1	P39,P46,P51	3
HSPB6	3	1	-2	-	0	P47,P52,P58	2
HSPB7	4	2	-2	S46,S49	0	P35,P39,P40,P58	3
HSPB8	4	2	-2	S57,S63	0	P39,P41,P49,P54,P61	4
HSPB9	1	3	+2	-	0	P33	0
HSPB10	4	5	+1	-	2	P43,P51,P53,P72	8

Table 1.9: Sequence feature information for the FR-D regions, including numbers of charged residues, net charge, phosphorylation site (P-site), histidine, proline, and aromatic residues.

Functional Region E (FR-E)

Functional Region (FR-E) lies at the boundary between the NTR and the ACD. This region represents one of the more interactive and heterogeneous regions of the sHSP sequence (Table 1.10). FR-E is enriched in phosphorylation sites and in some sHSPs, histidines (Table 1.11). Partial structural information for FR-E has been captured in prior studies, because short NTR extensions are often included in "ACD-only" constructs used for crystallography or NMR (30-33). These structures indicate that FR-E can adopt multiple conformational states, and in some contexts, can form beta-strand interactions that integrate into the ACD core while in others it remains disordered and untethered. FR-E sequences often contain a mixture of charged residues and small, flexible residues such as glycine and alanine, producing a polar region with conformational plasticity (Figure 1.7). Several sequence features may support this flexibility: 1)

abundant glycine could lower steric constraints within FR-E, accommodating either bound or unbound populations; and 2) in several sHSPs, FR-E holds clustered proline/aromatic sequences similar to those observed in FR-B and FR-D. HSPB1 differs substantially in this region, potentially due to the presence of unique insertion sequence preceding FR-E (discussed below). HSPB9 and HSPB10 are also unusual, with HSPB10 being positively charged across much of FR-E and HSPB9 having a net negative charge.

Sequence information	Start residue	Sequence	End residue	Theoretical pI
HSPB1	72	AYSRALSRQLSSGVSEIRHTADR	94	10.67
HSPB2	52	RAAPAGEGSRAGASELRLSEGK	73	8.74
HSPB3	46	RKTRAAQSPPVDSAAETPPREGK	68	9.98
HSPB4	51	SLFR TVLDSGISEVRSDRDK	70	5.89
HSPB5	52	PSFLRAPSWF DTGLSEMRLEKDR	74	6.64
HSPB6	59	SVALPVAQVPTDPGH	73	5.06
HSPB7	59	HSEPLAFPARPGGAGNIKTLGDA	81	6.75
HSPB8	67	GMVPRGPTATARFGVPAEGRT PPPFPGEP	95	9.51
HSPB9	38	RDSPAAQEDNDHARDG	53	4.35
HSPB10	84	RPSLRSLERKAIRIRAIEDEK RELAKLRRTTNRILASSCCSS NILGS	128	10.78

Table 1.10: Sequence information for the FR-E regions, including residue numbers, amino acid sequence, and theoretical isoelectric point (pI). Sequence features are color coded within each FR-E sequence: positively charged residues (blue), negatively charged residues (red), proline residues (purple), and aromatic residues (orange).

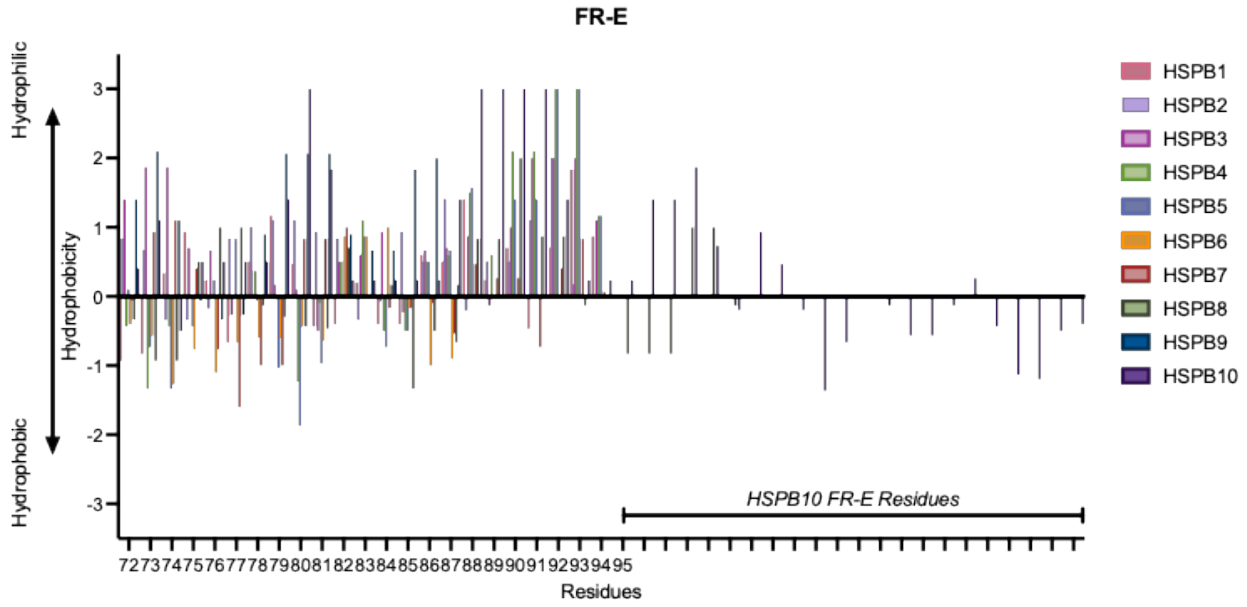

Figure 1.7: Hydrophobicity plot of the FR-E region calculated using the Hopp & Woods scale using with the ProtScale function on UniPro.org. Positive values indicate hydrophilicity and negative values indicate hydrophobicity, as shown by the arrow on the left side of the figure. Hydrophobicity value for each residue was calculated using a three residue sliding window, with individual amino acid values based on Hopp & Wood hydrophobicity scale (see Appendix Figure 1). Residue numbers correspond to HSPB1, with residues from other sHSP aligned accordingly. Each sHSP is annotated in different colors as shown in the side legend.

sHSP	- (E,D)	+ (R,K)	Net charge	Phos-site	Histidine	Proline	Aromatic (W,F,Y)
HSPB1	2	4	+2	S78,S82	1	-	1
HSPB2	3	4	+1	-	0	P55	0
HSPB3	3	5	-2	S53	0	P54,P55,P63,P64	0
HSPB4	4	4	0	-	0	-	1
HSPB5	4	4	0	S59	0	P52,P58	3
HSPB6	1	0	1	-	1	P58,P63,P70	0
HSPB7	2	2	0	S60	1	P62,P66,P69	1
HSPB8	2	3	+1	-	0	8 total Prolines	2
HSPB9	5	2	-3	-	1	P41	0
HSPB10	5	11	+6	-	0	P85	0

Table 1.11: Sequence feature information for the FR-E regions, including numbers of charged residues, net charge, phosphorylation site (P-site), histidine, proline, and aromatic residues.

HSPB1 Insertion Region

A major distinguishing feature of HSPB1 is the presence of an additional short segment within the NTR, referred to as the Insertion region (Table 1.12). This region is highly solvent exposed in HSPB1 as evidenced by HDX-MS (14). The HSPB1 Insertion region has been shown to modulate oligomeric assembly (34) and to increase heterogeneity and polydispersity of HSPB1 (12). This segment is proline rich and aliphatic, and may introduce additional disorder or steric effects (Figure 1.8, Table 1.13). The sequence also appears to be highly soluble, consistent with the high exposure observed by HDX-MS. This property may explain the higher overall exposure of the HSPB1 NTR relative to HSPB5 (See Thesis Chapter 2). It is also noteworthy that the Insertion region is conserved across HSPB1 homologs, suggesting that it provides an evolutionarily conserved function specific to HSPB1. Although there do not appear to be any

other human sHSPs that contain an insertion region, further sequence analysis into whether if there are any similar sequences or "insertion" in other non-human sHSPs could be useful to better define the role of this peptide.

Sequence information	Start residue	Sequence	End residue	Theoretical pI
HSPB1	58	LPPAAIESPAVAAP	71	4.0

Table 1.12: Sequence information for the HSPB1 insertion region, including residue numbers, amino acid sequence, and theoretical isoelectric point (pI). Sequence features are color coded: positively charged residues (blue), negatively charged residues (red), proline residues (purple), and aromatic residues (orange).

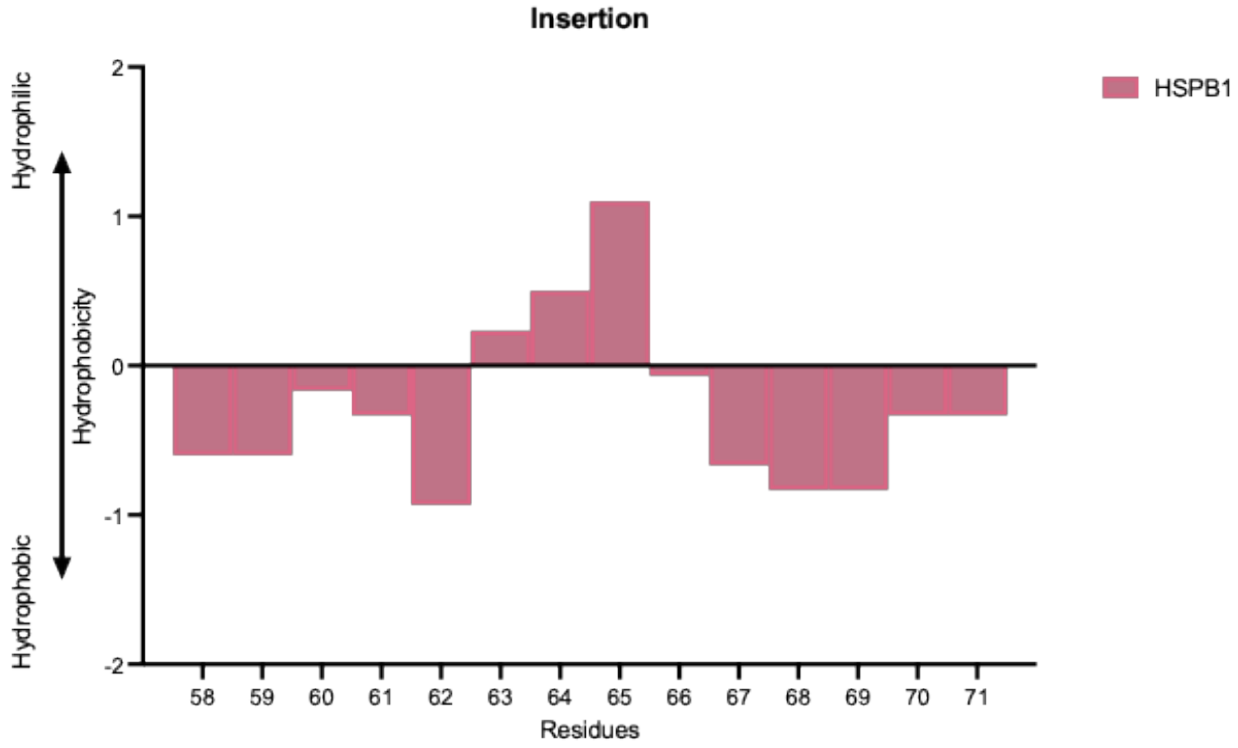

Figure 1.8: Hydrophobicity plot of the HSPB1 Insertion region calculated using the Hopp & Woods scale using with the ProtScale function on UniPro.org. Positive values indicate

hydrophilicity and negative values indicate hydrophobicity, as shown by the arrow on the left side of the figure. Hydrophobicity value for each residue was calculated using a three residue sliding window, with individual amino acid values based on Hopp & Wood hydrophobicity scale (see Appendix Figure 1)

sHSP	- (E,D)	+ (R,K)	Net charge	Phos-site	Histidine	Proline	Aromatic (W,F,Y)
HSPB1	1	0	-1	-	0	P59,P60,P66,P71	0

Table 1.13: Sequence feature information for HSPB1 Insertion region, including numbers of charged residues, net charge, phosphorylation site (P-site), histidine, proline, and aromatic residues.

1.3 Amyloidogenic protein tau as a client for HSPB1 and HSPB5

To function properly, organisms have evolved mechanisms to manage misfolded proteins and aggregates. In healthy cells, these protective systems, including chaperones and clearance pathways, operate efficiently, maintaining cellular equilibrium. However, in aging or diseased organisms, these mechanisms begin to falter, allowing age-related pathologies to emerge. Among the most debilitating conditions affecting older populations are neurodegenerative diseases, such as Alzheimer's disease. Alzheimer's disease is marked by a progressive failure of proteostasis, where toxic species accumulate and cellular defense systems are unable to manage the burden. The molecular mechanisms underlying disease initiation and progression, as well as the cellular defenses against these toxic species, remain incompletely understood.

Although the full molecular basis of Alzheimer's disease is not yet understood, decades of work highlight two defining neuropathological features: the formation of extracellular amyloid plaques composed of amyloid-beta (A-beta) peptide and neurofibrillary tangles composed of hyperphosphorylated tau protein (35-39). Both molecules accumulate in the brains of patients with neurodegenerative disease, but it remains debated whether these events are causative, and how they mechanistically contribute to brain degeneration (40-41). A-beta is a peptide generated from amyloid precursor protein (APP), a transmembrane protein that is cleaved by α- or β-secretases, a process thought to play roles in neuronal development and growth (42). Tau, a microtubule associated protein, is essential for maintaining neuronal microtubule stability and dynamics (43). In a set of neurogenerative diseases, tau becomes hyperphosphorylated and dissociates from microtubules to form amyloid fibrils that are hallmarks of disease pathology. These diseases are termed "tauopathies" and include Alzheimer's disease and frontotemporal dementia (44). Due to the intrinsically disordered nature of tau that defies traditional structural biology tools and drug development pipeline, progress toward therapeutics that directly engage tau has been extremely challenging (45).

Of 10 sHSP expressed in humans, HSPB1 (B1/Hsp27) and HSPB5 (B5/αB-crystallin) are two of the most abundant, and are both constitutively expressed in the brain and neurons (15-16). Not only are levels of HSPB1 and HSPB5 upregulated in Alzheimer's disease, but these two proteins also colocalize with tau fibrils in tauopathy brains and have been shown to play protective roles against tauopathies (17-19). Despite these observations, the molecular mechanisms by which these sHSP recognize and chaperone tau remain poorly defined. Further understanding of how HSPB1 and HSPB5 play protective roles against tauopathies could help better understand the proteostasis system in disease and provide new avenues for therapeutics.

1.4 Scope of Thesis

In this thesis, I compare HSPB1 and HSPB5 in their sequence features, structural organization, oligomeric assembly, and chaperone activity. By applying a shared set of experimental approaches across both proteins, I aim to build a mechanistic framework for how sHSPs encode client specificity and stress responsiveness within their quasi-ordered network. In Chapter 2, I examine the role of NTR-ACD interactions by disrupting these contacts via domain and targeted NTR sub-region swaps between HSPB1 and HSPB5. This strategy enabled the identification of NTR regions that contribute to oligomer assembly and chaperone function for tau aggregation. In Chapter 3, I perturb the quasi-ordered network using disease-associated mutations, blocking ACD edge groove (Bump mutation), and hetero-oligomerization between HSPB1 and HSPB5. These perturbations are used to test how disrupting specific interaction hubs alter sHSP architecture and how reorganization these interactions influence chaperone function. In these chapters, I characterize chaperone activity using *in vitro* tau aggregation assays to connect functional outcomes to structural changes. Structural changes are captured by Hydrogen-deuterium exchange mass spectrometry (HDX-MS) to map changes in protection and accessibility across each domain. Mass photometry is used to quantify changes in oligomer size distributions in response to perturbations in NTR-ACD interactions. Together, these approaches allow for the relationship between structure and function to be examined in a sHSP system that is otherwise resistant to traditional high-resolution structural methods. Chapter 4 describes optimization and method development for the experimental techniques that were essential for uncovering multiple layers of sHSP structure and behavior.

Overall, the findings presented here challenge the notion that sHSPs operate through a single conserved mechanism. Instead, they support a modular model in which specific NTR

subregions confer client specificity and stress responsiveness, while the ACD provides a scaffold that regulates NTR exposure. The ACD may also directly contribute to client engagement (Chapter 4). In sum, the results presented here support a model in which sHSP chaperone activity is governed by regulated NTR exposure, shaped by sequence-encoded stress sensors and oligomeric scaffolding. This framework provides rationale for how sHSPs achieve client specificity, respond to environmental cues, and adapt to proteotoxic stress. It also opens new avenues for therapeutic intervention by targeting NTR–ACD interactions, modulating phosphorylation states, or designing molecules that mimic stress-induced conformational shifts. Understanding these mechanisms is essential not only for decoding sHSP biology, but also for harnessing their protective potential in neurodegenerative disease.

References

1. Haslbeck, M., Franzmann, T., Weinfurtner, D. et al. Some like it hot: the structure and function of small heat-shock proteins. Nat Struct Mol Biol 12, 842–846 (2005).
2. Hartl, F. Ulrich, Andreas Bracher, and Manajit Hayer-Hartl. "Molecular chaperones in protein folding and proteostasis." Nature 475.7356 (2011): 324-332.
3. Gonçalves, Conrado C., et al. "The chaperone HSPB1 prepares protein aggregates for resolubilization by HSP70." Scientific reports 11.1 (2021): 17139.
4. Mymrikov, Evgeny V., et al. "The chaperone activity and substrate spectrum of human small heat shock proteins." Journal of Biological Chemistry 292.2 (2017): 672-684.
5. Banzet, Nathalie, et al. "Accumulation of small heat shock proteins, including mitochondrial HSP22, induced by oxidative stress and adaptive response in tomato cells." The Plant Journal 13.4 (1998): 519-527.

6. Hayes, David, et al. "Phosphorylation dependence of hsp27 multimeric size and molecular chaperone function." Journal of Biological Chemistry 284.28 (2009): 18801-18807.
7. Acidosis: Rajagopal, Ponni, et al. "A conserved histidine modulates HSPB5 structure to trigger chaperone activity in response to stress-related acidosis." elife 4 (2015): e07304.
8. Makley LN, Johnson OT, Ghanakota P, et al. Chemical validation of a druggable site on Hsp27/HSPB1 using in silico solvent mapping and biophysical methods. Bioorg Med Chem. 2021;34:115990.
9. Freilich, Rebecca et al. “Competing protein-protein interactions regulate binding of Hsp27 to its client protein tau.” Nature communications vol. 9,1 4563.
10. Klevit, Rachel E. "Peeking from behind the veil of enigma: Emerging insights on small heat shock protein structure and function." Cell Stress and Chaperones 25.4 (2020): 573-580.
11. Clouser, Amanda F., et al. "Interplay of disordered and ordered regions of a human small heat shock protein yields an ensemble of ‘quasi-ordered’states." Elife 8 (2019): e50259.
12. Woods CN, Ulmer LD, Guttman M, Bush MF, Klevit RE. Disordered region encodes α-crystallin chaperone activity toward lens client γD-crystallin. Proceedings of the National Academy of Sciences. 2023 Feb7;120(6):e2213765120.
13. Woods CN, Janowska MK, Ulmer LD, Kaur Sidhu J, Stone NL, James EI, Guttman M, Bush MF, Klevit RE. Activation mechanism of Small Heat Shock Protein HSPB5 revealed by disease-associated mutants. Proceedings of the National Academy of Sciences. 2025 May 20;122(20):e2425061122.

14. Cervantes M, Janowska MK, Tuttle LM, Nath A, Klevit RE. Function within Disorder: Small heat shock proteins use different functional regions to chaperone tau aggregation. bioRxiv. 2026:2026-01.
15. Stone NL, Janowska MK, Narisawa L, Tuttle LM, Ulmer LD, Guttman M, Bush MF, Klevit RE. Disorder with consequence: Phosphorylation sites in HSPB5 yield distinct structural outcomes. bioRxiv. 2025 Oct 28:2025-10.
16. Ruff KM, King MR, Ying AW, Liu V, Pant A, Lieberman WE, Shinn MK, Su X, Kadoch C, Pappu RV. Molecular grammars of predicted intrinsically disordered regions that span the human proteome. Cell. 2026 Jan 8;189(1):323-42.
17. Sebák F, Szolomájer J, Papp N, Tóth G, Bodor A. Proline cis/trans isomerization in intrinsically disordered proteins and peptides. Frontiers in Bioscience-Landmark. 2023;28(6).
18. Reiersen H, Rees AR. The hunchback and its neighbours: proline as an environmental modulator. Trends in biochemical sciences. 2001 Nov 1;26(11):679-84.
19. Perez RB, Tischer A, Auton M, Whitten ST. Alanine and proline content modulate global sensitivity to discrete perturbations in disordered proteins. Proteins: Structure, Function, and Bioinformatics. 2014 Dec;82(12):3373-84.
20. Stapley BJ, Creamer TP. A survey of left-handed polyproline II helices. Protein Science. 1999 Mar;8(3):587-95.
21. Cubellis MV, Caillez F, Blundell TL, Lovell SC. Properties of polyproline II, a secondary structure element implicated in protein–protein interactions. Proteins: Structure, Function, and Bioinformatics. 2005 Mar 1;58(4):880-92.

22. Hazra MK, Gilron Y, Levy Y. Not only expansion: Proline content and density also induce disordered protein conformation compaction. Journal of Molecular Biology. 2023 Sep 1;435(17):168196.
23. Mateos B, Conrad-Billroth C, Schiavina M, Beier A, Kontaxis G, Konrat R, Felli IC, Pierattelli R. The ambivalent role of proline residues in an intrinsically disordered protein: from disorder promoters to compaction facilitators. Journal of molecular biology. 2020 Apr 17;432(9):3093-111.
24. Martin EW et al. Valence and patterning of aromatic residues determine the phase behavior of prion-like domains. Science 367, 694–699 (2020). [PubMed: 32029630]
25. Portz B. et al. Structural heterogeneity in the intrinsically disordered RNA polymerase II Cterminal domain. Nat. Commun 8, 15231 (2017). [PubMed: 28497792]
26. Bremer A. et al. Deciphering how naturally occurring sequence features impact the phase behaviours of disordered prion-like domains. Nat. Chem 14, 196–207 (2022). [PubMed: 34931046]
27. Plevin MJ, Bryce DL & Boisbouvier J Direct detection of CH/pi interactions in proteins. Nat. Chem 2, 466–471 (2010). [PubMed: 20489715]
28. Espinoza-Fonseca LM. Aromatic residues link binding and function of intrinsically disordered proteins. Molecular BioSystems. 2012;8(1):237-46.
29. Holehouse AS, Kragelund BB. The molecular basis for cellular function of intrinsically disordered protein regions. Nature Reviews Molecular Cell Biology. 2024 Mar;25(3):187-211.

30. Rajagopal P, Liu Y, Shi L, Clouser AF, Klevit RE. Structure of the α-crystallin domain from the redox-sensitive chaperone, HSPB1. Journal of biomolecular NMR. 2015 Oct;63(2):223-8.
31. Clark AR, Egberts WV, Kondrat FD, Hilton GR, Ray NJ, Cole AR, Carver JA, Benesch JL, Keep NH, Boelens WC, Slingsby C. Terminal regions confer plasticity to the tetrameric assembly of human HspB2 and HspB3. Journal of molecular biology. 2018 Sep 14;430(18):3297-310.
32. Laganowsky A, Benesch JL, Landau M, Ding L, Sawaya MR, Cascio D, Huang Q, Robinson CV, Horwitz J, Eisenberg D. Crystal structures of truncated alphaA and alphaB crystallins reveal structural mechanisms of polydispersity important for eye lens function. Protein science. 2010 May;19(5):1031-43.
33. Weeks SD, Baranova EV, Heirbaut M, Beelen S, Shkumatov AV, Gusev NB, Strelkov SV. Molecular structure and dynamics of the dimeric human small heat shock protein HSPB6. Journal of structural biology. 2014 Mar 1;185(3):342-54.
34. Mchaourab HS, Lin YL, Spiller BW. Crystal structure of an activated variant of small heat shock protein Hsp16. 5. Biochemistry. 2012 Jun 26;51(25):5105-12.
35. Alzheimer A. Über eigenartige Krankheitsfälle des späteren Alters. Zeitschrift für die gesamte Neurologie und Psychiatrie. 1911 Dec 1;4(1):356-85.
36. Crimins JL, Pooler A, Polydoro M, Luebke JI, Spires-Jones TL. The intersection of amyloid beta and tau in glutamatergic synaptic dysfunction and collapse in Alzheimer's disease. Ageing research reviews. 2013 Jun 1;12(3):757-63.
37. Spires-Jones TL, Hyman BT. The intersection of amyloid beta and tau at synapses in Alzheimer’s disease. Neuron. 2014 May 21;82(4):756-71.

38. Glenner GG, Wong CW. Alzheimer's disease: initial report of the purification and characterization of a novel cerebrovascular amyloid protein. Biochemical and biophysical research communications. 1984 May 16;120(3):885-90.

39. Lu JX, Qiang W, Yau WM, Schwieters CD, Meredith SC, Tycko R. Molecular structure of β-amyloid fibrils in Alzheimer's disease brain tissue. Cell. 2013 Sep 12;154(6):1257-68.

40. Mirbaha H, Chen D, Mullapudi V, Terpack SJ, White CL, Joachimiak LA, Diamond MI. Seed-competent tau monomer initiates pathology in a tauopathy mouse model. Journal of Biological Chemistry. 2022 Aug 1;298(8).

41. Tanzi RE. The genetics of Alzheimer disease. Cold Spring Harbor perspectives in medicine. 2012 Oct 1;2(10):a006296.

42. Morley JE, Farr SA. The role of amyloid-beta in the regulation of memory. Biochemical pharmacology. 2014 Apr 15;88(4):479-85.

43. Drubin, David G., and Marc W. Kirschner. "Tau protein function in living cells." The Journal of cell biology 103.6 (1986): 2739-2746.

44. Goedert, M. G. S. M., et al. "Multiple isoforms of human microtubule-associated protein tau: sequences and localization in neurofibrillary tangles of Alzheimer's disease." Neuron 3.4 (1989): 519-526.

45. Jeganathan, Sadasivam, et al. "The natively unfolded character of tau and its aggregation to Alzheimer-like paired helical filaments." Biochemistry 47.40 (2008): 10526-10539.

2. HSPB1 and HSPB5 Use Distinct Functional Regions to Chaperone Tau

Parts of this chapter are adapted from a manuscript under review at Protein Science – [Mia Cervantes, Maria K. Janowska, Lisa M. Tuttle, Abhinav Nath, Rachel E. Klevit], [Function within Disorder: Small heat shock proteins use different functional regions to chaperone tau aggregation.]; Tau aggregation assays by MC, HDX-MS experiments performed by MC and MKJ, HDX-MS Bimodal analysis by LMT.

2.1: Introduction

Cells maintain proteostasis through coordinated systems that recognize, stabilize, and clear misfolded or aggregation-prone proteins. Failure in these systems contributes to age-related pathologies, most notably neurodegenerative diseases such as Alzheimer's disease (AD). AD is the most prevalent of a class of neurodegenerative diseases known collectively as tauopathies in which toxic species of the microtubule-associated protein tau accumulate in brain and neurons (1). Tau is essential for neuronal microtubule stability and dynamics (2). In tauopathies including AD and fronto-temporal dementia, tau becomes hyperphosphorylated, dissociates from microtubules, and can assemble into amyloid fibrils that are hallmarks of disease pathology (3-7). Due to its intrinsic disorder, tau defies traditional structural biology tools and drug development pipelines, making progress towards therapeutics that productively engage tau challenging. As a result, the molecular mechanisms underlying tau toxicity, and the cellular defenses that counter it, remain incompletely understood.

Protein homeostasis is safeguarded by a network of molecular chaperones that suppress irreversible aggregation (8-9). Small heat shock proteins (sHSPs) are a first line of defense in maintaining a healthy proteome by stabilizing partly unfolded or misfolding proteins ("clients") without ATP hydrolysis (10-11). Clients stabilized by sHSPs may refold spontaneously or may be

transferred to ATP-dependent chaperones like Hsp70 (12-13). sHSPs are constitutively expressed in many human tissues (14) and are sensitive to cellular stress signals, such as oxidation, post-translational modifications, and acidosis. These cues trigger structural rearrangements that enhance chaperone activity (15-17), positioning sHSPs to function under both normal and stress conditions.

sHSPs' ability to delay protein aggregation without requiring ATP hydrolysis makes them attractive therapeutic targets for protein aggregation diseases. Indeed, efforts have been made to design small molecules or peptides that can bind to sHSPs to controllably activate their chaperone effect (18). However, progress has been limited by an incomplete understanding of both the structure and mechanisms of how sHSPs interact with clients and of the activation mechanisms. This gap stems from properties of sHSPs that make them challenging to traditional biochemical/biophysical techniques: they are >50% disordered and form ensembles of large polydisperse oligomers ranging from dimers to ~40-mers (19).

All sHSPs share a tripartite architecture comprising a disordered N-terminal region (NTR), a folded α-crystallin domain (ACD), and a disordered C-terminal region (CTR). ACDs form dimers that serve as building blocks for higher order oligomers via inter-subunit interactions with NTRs and CTRs (20-21). Each ACD dimer presents three conserved surface grooves: a "Central" groove at the interface between two ACDs and two "Edge" grooves at opposing ends of a dimer. These grooves accommodate potential binding partners, including but not limited to short stretches of the NTRs and CTRs of other subunits within an oligomer (21-24). Because multiple binding sequences can bind to each groove, oligomers contain more binding partners than binding sites, giving rise to heterogeneity in sHSP oligomers. This "**quasi-**

ordered" organization sequesters disordered regions within oligomers and creates structural and dynamic plasticity that is thought to govern sHSP function (25).

Of the ten human sHSPs, HSPB1 (Hsp27) and HSPB5 (αB-crystallin) are particularly abundant in brain and neurons (14, 26). Both are upregulated in AD, colocalize with tau fibrils in tauopathy brains, and exert protective roles against tau-mediated toxicity (27-32). Despite these shared properties, mechanisms by which HSPB1 and HSPB5 engage tau, and whether they do so through shared or different strategies remain unresolved.

Here, we compare chaperone activities of HSPB1 and HSPB5 toward tau aggregation and define features that give rise to that activity. We aimed to disentangle two features of sHSP oligomers that together govern chaperone function: 1) the **local structural organization** that encodes for discrete chaperone-active regions and 2) the **oligomerization of sHSPs** that mediates the accessibility of specific regions. We find that HSPB1 suppresses tau aggregation under both normal and stress conditions and that HSPB5 requires stress-induced activation, for example, by pH to become effective. To identify the source of this difference, we focused on the NTRs, which are essential for tau chaperoning activity in HSPB1 (33). Using chimeric proteins, we show that scaffolding of intrinsically disordered regions within oligomers dictates chaperone potency. Finer-scaled chimeras in which short subregions of the NTRs were swapped between the two sHSPs identified specific regions that mediate activity. Integrating aggregation assays, NTR accessibility by Hydrogen-Deuterium Exchange (HDX-MS), and oligomeric size distributions by mass photometry (MP), we demonstrate that specific NTR subregions encode client-specific chaperone function. Together, the results provide a mechanistic framework for how sHSP oligomers tune their responses to aggregation-prone clients such as tau.

2.2: Results.

2.2.1: HSPB1 and HSPB5 delay in vitro aggregation of tau using their disordered N-terminal domains.

HSPB1 can inhibit tau aggregation in a range of *in vitro* contexts (Freilich 2018; 33). HSPB5 is also constitutively present in neurons and most other cells (34), so we tested whether it can chaperone tau. To assess the chaperone activity of HSPB1 and HSPB5 towards tau aggregation, we performed in vitro assays in which fibrils are detected by Thioflavin T fluorescence. Spontaneous aggregation of tau is slow and requires an inducer to start aggregation. A sulfated polysaccharide, heparin, has traditionally been used to trigger aggregation of tau (35-37). However, while heparin is produced in mast cells and basophils, it is not in neurons (38-39). We used polyphosphate, a polyanionic chain of phosphate groups, to induce tau aggregation. Polyphosphate is present in neuronal cytoplasm and its levels increase with stress (40-41), thus providing a more realistic context for our *in vitro* studies. Under our assay conditions, polyphosphate induces tau aggregation faster than previously optimized conditions using heparin as the inducer (SI Figure 2). Both HSPB1 and HSPB5 delay tau aggregation, whether induced by heparin or polyphosphate. HSPB1 is more effective than HSPB5 under non-stress ("basal") conditions (pH 7.5, 37C^{o}; Figure 2.1 left).

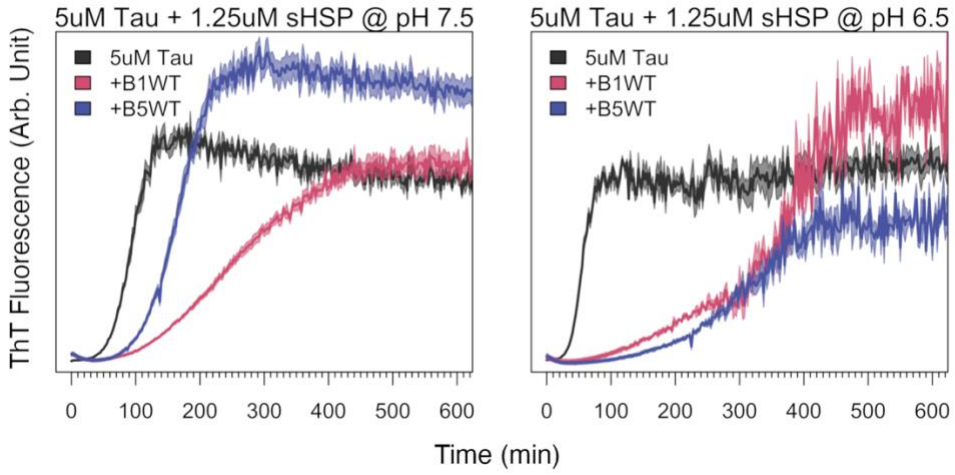

Figure 2.1 - in vitro tau aggregation in the absence and presence of HSPB1 and HSPB5. Changes in Thioflavin T (ThT) dye fluorescence is monitored over the time-course of tau aggregation in presence and absence of sub-stoichiometric concentrations of HSPB1 or HSPB5. HSPB1 and HSPB5 chaperone polyphosphate-induced aggregation of tau at pH 7.5 (Left); HSPB5 becomes activated at pH 6.5 (Right). Both reactions are induced by 1 mg/mL polyphosphate using 5 μM Tau in presence and absence of 1.25 μM sHSP at 37 °C with agitation of the plate prior to each measurement. ThT fluorescence was recorded using excitation at 440 nm and 485 nm emission (arbitrary units). Solid lines represent the average ThT fluorescence, with lighter shaded regions indicating the SEM from 4-6 replicates per condition.

HSPB1 and HSPB5 are sensitive to environmental conditions. Among these, pH-dependent activation is the best characterized and is associated with various stress conditions including those in aging neurons (42). As shown in Figure 2.1A (right panel), both HSPB1 and HSPB5 effectively delay tau aggregation at pH 6.5, despite more rapid aggregation of tau alone

under these conditions. Thus, HSPB1 and HSPB5 have similar chaperoning capacity towards tau, but HSPB5 activity is lower under basal conditions.

The disordered NTR is required for HSPB1's chaperone activity towards tau (33). When tau fibril formation was assessed in the presence of constructs lacking the NTR, "ACD-only" constructs of HSPB1 and HSPB5 both showed only modest chaperone activity at very high concentrations. At equivalent concentrations to full-length counterparts, the activities were negligible (SI Figure 2B-C). Thus, both HSPB1 and HSPB5 require their NTRs to effectively chaperone tau.

2.2.2: Interplay of ordered ACD and disordered NTR modulates HSPB1 and HSPB5 activity.

Interactions between ACDs and NTRs within sHSP oligomers are thought to play a role in their mechanism of action. Surface grooves on ACD dimers scaffold multiple discrete regions within NTRs (21) through inter- and intra-molecular interactions that sequester certain regions and affect activity. Certain HSPB5 NTR regions are more exposed at pH 6.5 than at pH 7.5 (43). Based on the differential tau activity observed between HSPB1 and HSPB5 at pH 7.5, we hypothesized that HSPB5-ACD is more effective at sequestering its chaperone-active regions than HSPB1 under this condition, thereby limiting its chaperone activity.

ACD swapping affects chaperone activity. To test this hypothesis, we created two chimeric proteins in which the ACDs were swapped: B151 (HSPB1 containing HSPB5-ACD) and B515 (HSPB5 containing HSPB1-ACD). Strikingly, ACD swapping has opposite effects on tau chaperone activity. B151 is a better chaperone at pH 7.5 than WT-HSPB1 and B515 is a less effective chaperone than WT-HSPB5 (Figure 2.2A). Quantitatively, the time required to reach 50% of the ThT signal at saturation (T_{50}) increased by three hours for B151 compared to HSPB1,

while B515 reached T_{50} 45 minutes earlier than HSPB5 (SI Figure 2D). These results suggest that the HSPB1 NTR is less effectively sequestered by the HSPB5 ACD and the HSPB5 NTR is likely better sequestered by the HSPB1 ACD of HSPB1.

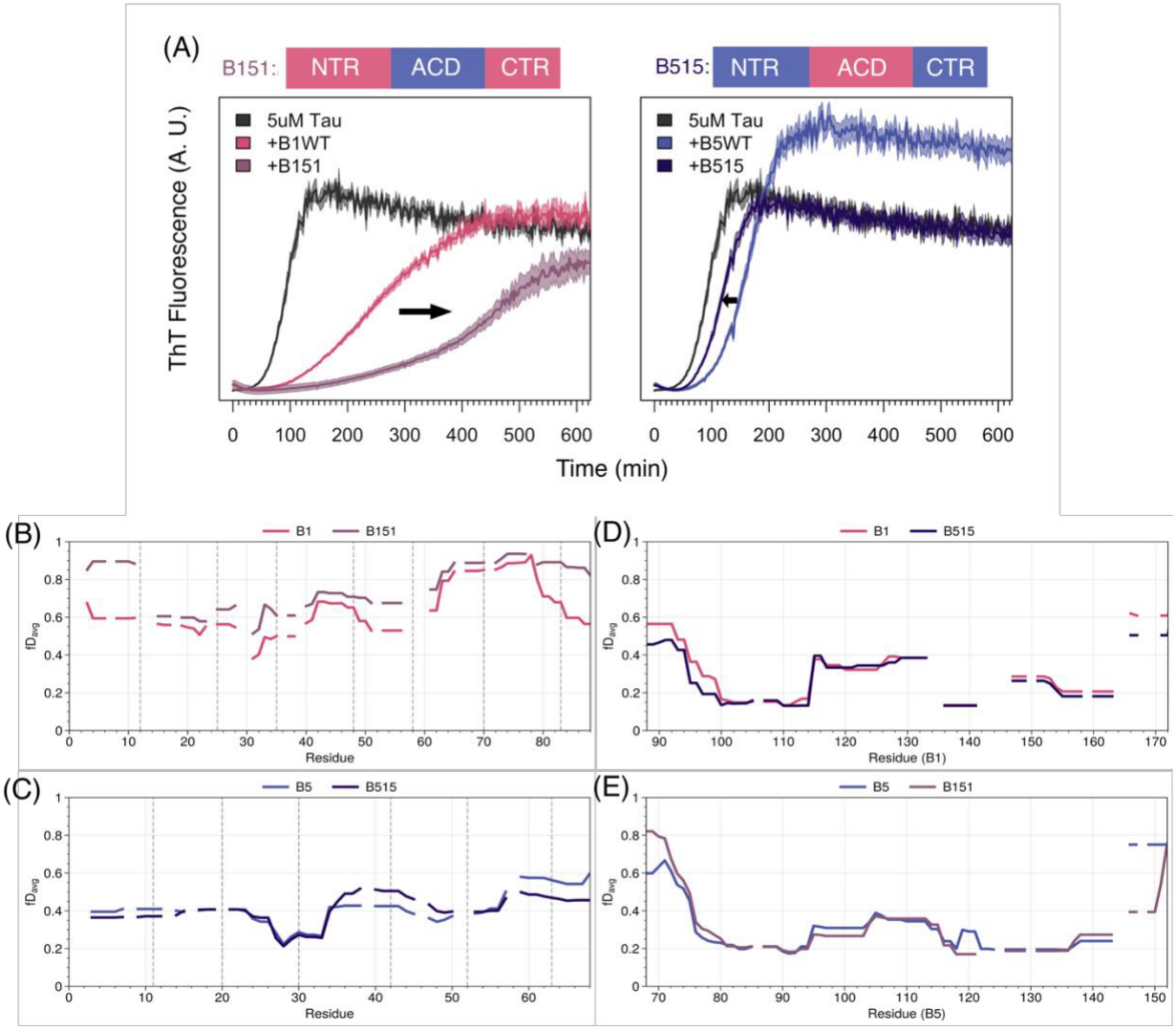

Figure 2.2. Exchanging the ACDs has opposite effects on HSPB1 and HSPB5 chaperone activities. (A) In vitro tau aggregation assay using ThT comparing WT activities of HSPB1 (Left) and HSPB5 to their ACD-swapped constructs (Right). Aggregation reactions are performed at pH 7.5, 37 °C using 5 μM Tau and 0.25 molar equivalent of small heat shock protein. Both

fibrilization reactions are induced with 1 mg/mL polyphosphate. Black arrows show direction of changes in activities going from WT to ACD-swapped construct. (B-C): Comparison of average deuteration uptake for the NTRs of HSPB1 and B151 (B) and HSPB5 and B515 (C). Average deuteration level calculated based on unimodal analysis is shown for corresponding residues. Figure 2.2B shows HSPB1-WT (pink) compared to B151 (purple) after 4 seconds incubation in deuterated buffer. Figure 2.2C shows equivalent for HSPB5-WT (blue) and B515 (dark blue). (D-E):ACD-matched HDX-MS comparison of HSPB1 and HSPB5 WT vs ACD-swapped constructs. Figure 2.2D shows HSPB1-WT ACD (pink) compared to B515 ACD (dark blue). Figure 2.2E shows equivalent for HSPB5-WT (blue) and B151 ACD (purple).

HDX-MS reveals altered NTR scaffolding in chimeras. To directly assess how ACDs identity influences NTR sequestration, we compared WT and chimeric constructs by single time point hydrogen-deuterium exchange mass spectrometry (HDX-MS). HDX-MS uniquely enables near-residue-level interrogation of quasi-ordered polydisperse oligomers of sHSPs in their native state. Because NTR sequestration is most evident at very short exchange times, we performed analysis following a 4-second incubation in D_2O-based buffer.

Peptide-level data were aggregated to obtain near-residue-level fractional D-uptake values, using the approach described in (44), shown in Figure 2.2. To ensure comparison between identical sequences, data are plotted by region: NTR comparisons include WT-HSPB1 versus B151 and WT-HSPB5 versus B515 (Figure 2.2B); ACD comparisons include WT-HSPB1 versus B515 and WT-HSPB5 versus B151 (Figure 2.2C). Additional comparisons of overall exposure are provided in Figure S3.

Across all constructs, the ACD is the most protected region, displaying the lowest fractional D-uptake values. The only substantial perturbations within the ACD observed across constructs are near the NTR-ACD boundaries (84-100 for B1, 64-80 for B5): this region is more exposed in B151 compared to WT-HSPB5 (Figure 2.2C) and more protected in B515 compared to WT-HSPB1 (Figure 2.2D). The affected residues include those that form the β3-strand of the ACD β-sandwich (PDB: 4MJH, PDB: 2N0K). In some solved ACD structures, an additional β-strand ("β2") formed by residues at the C-terminal end of the NTR pairs with β3-strand (17, 44). Reduced protection of β3 in B151 suggests an incompatibility between the β2-forming sequence of HSPB1 and the β3 strand of HSPB5. Conversely, increased protection in B515 suggests that some region of the HSPB5 NTR interacts with the β3-strand of HSPB1 ACD.

CTRs exposure is insensitive to ACD identity. The CTRs in HSPB1 and HSPB5 display high deuterium uptake at 4 seconds, consistent with their known disorder and accessibility in oligomers. Coverage across the CTRs was insufficient to allow more detailed analysis due to limited redundancy and resolution (SI Figure 4).

NTR accessibility correlates with chaperone activity. Comparison of NTRs in their native context shows that HSPB1 NTR is substantially more solvent-exposed than HSPB5 NTR under identical conditions, with average fractional D-uptake values exceeding 0.5 for HSPB1 and below 0.5 for HSPB5 (compare the lighter traces in Figure 2.2B and 2.2C). ACD identity strongly modulates HSPB1 NTR exposure: in the B151chimera, the HSPB1 NTR exhibits increased fractional D-uptake, consistent with the NTR being less effectively sequestered by the ACD of HSPB5 as inferred from the chaperone assay data. In contrast, HSPB5 NTR is comparatively less sensitive to ACD swapping. In the B515 chimera, we observe only modest and localized changes in fractional D-uptake values, including a small increase in protection of residues ~60-68 and

decreased protection in the vicinity of residues 35-48. Notably, B151, the chimera with the most prominent chaperone activity, displays the highest overall NTR exposure, and B515, which displays slightly lower chaperone activity than the WT-HSPB5, has a modest decrease in D-uptake primarily in a single region, the "Boundary" region that links the NTR to the ACD. (Figure 2.2C and Figure 2.3B).

2.2.3: Subregion-specific differences in NTR sequestration between HSPB1 and HSPB5

Previous studies showed that HSPB1 and HSPB5 oligomers exhibit bimodal HDX behavior across their NTRs, reflecting conformational heterogeneity within quasi-ordered regions (21). Bimodal exchange indicates the presence of at least two distinct populations—more protected (slower exchanging) and more solvent-exposed (faster exchanging)—that correspond to sequestered versus exposed states. Here we analyze previously defined NTR subregions (Figure 2.3A) in WT and ACD-swapped constructs. Although the roles of all subregions are not fully understood, several are known contributors to oligomer organization through their interactions with the ACD. The distal region engages the ACD edge groove, while the conserved and boundary regions interact with the ACD central groove. The Long Hydrophobic region has been implicated in modulating chaperone activity against γD-crystallin, whereas the function of the aromatic region remains unclear. Thus, The NTR subregions carry 1) structural roles (via sequestration within the oligomer) and 2) encode elements of chaperone function. HDX-MS provides a direct readout of the "structural" reorganization within oligomers that arises from differences in how each ACD variant sequesters the NTR. In the next sections we will describe structural changes in each subregion caused by ACD-swaps.

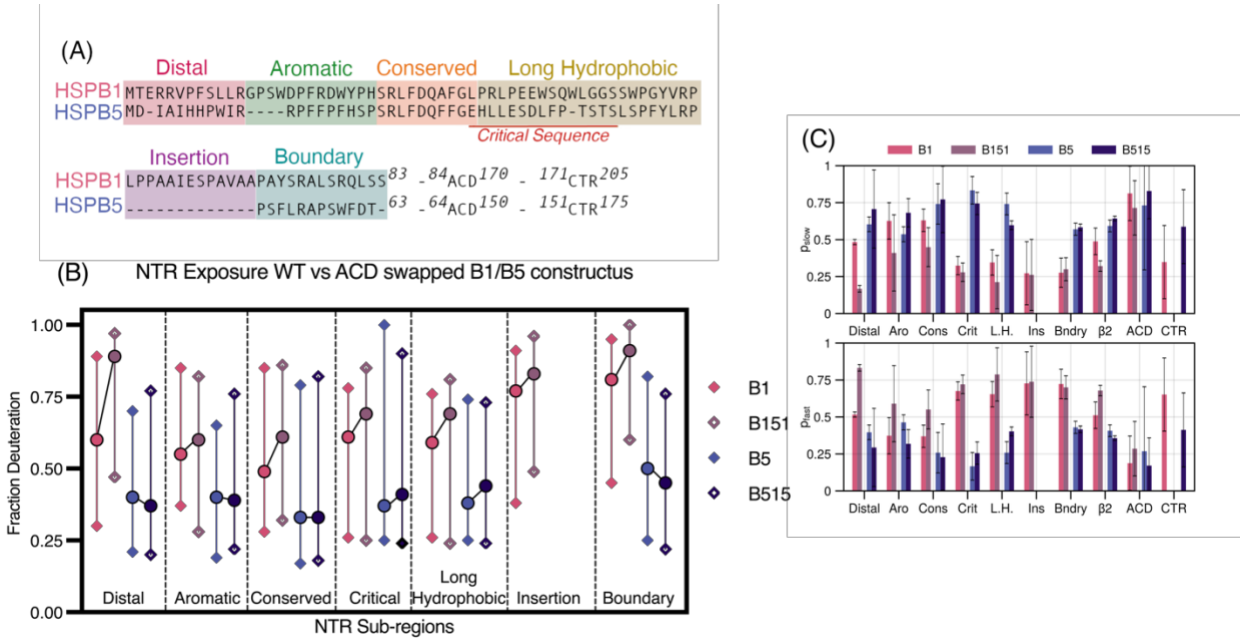

Figure 2.3. Comparison of the NTRs by subregion. (A) Sequence alignment of HSPB1 and HSPB5 NTR residues. The NTRs of HSPB1 and HSPB5 are divided into 5-6 short subregions, following Clouser 2019 nomenclature for HSPB1. All peptide data was aggregated to obtain near-residue-level fractional deuterium-uptake values, followed by bimodal analysis using the pyHXExpress workflow (44). Average fractional D-uptake for each NTR-subregion, calculated from the centroids of unimodal fits, is shown as circles (○). Deuteration levels of the two populations (slow and fast states) determined from bimodal analysis are plotted as diamonds (◇) in the corresponding color scheme. (C) Relative populations of the slow (p_{slow}) and fast (p_{fast}) exchange modes for each NTR-subregion, as well as for the ACD and CTR are shown.

Across all four constructs, most NTR subregions display bimodal behavior, consistent with earlier reports. For each subregion, we extracted: 1) fractional D-uptake values for the slow- and fast-exchanging modes (diamond markers in Figure 2.3B), and 2) the relative populations of

these modes (p_{slow} and p_{fast}, where ($p_{slow} + p_{fast} = 1.0$)). Average D-uptake values from unimodal fits are also presented in Figure 2.3B and SI Figure 4.

Overall, the most profound differences observed between a WT oligomer and its ACD-swapped counterpart are for HSPB1 and B151. In B151, multiple NTR subregions show substantial increases in the population of fast-exchanging species, indicating increased numbers of exposed regions in the oligomeric ensemble. As well, the slower-exchanging population of the Distal and Boundary regions, known to be involved in key NTR-ACD interactions, show increased fractional D-uptake values. Hence, when the HSPB1 NTR is scaffolded by the HSPB5 ACD, not only are exposed conformations more highly populated, but the slower-exchanging population is less well-sequestered. By comparison, the HSPB5 NTR is much less sensitive to the ACD identity, with B515 exhibiting only subtle changes in bimodal distribution metrics.

Distal and Boundary regions are most sensitive to ACD identity. The Distal region displays the largest ACD-dependent effects. In B151, the fractional D-uptake value of the slower-exchanging population increases from ~0.3 to ~0.47 (Figure 2.3A) accompanied by a smaller increase in uptake for the fast population. Partitioning between the two states shifts dramatically, from approximately equal populations in WT-HSPB1 to a majority of the Distal region occupying solvent-exposed states in B151. Thus, a larger fraction of the HSPB1 Distal subregion is exposed in the context of HDPB5's ACD and the protected population is less well sequestered.

A similar trend is observed for the Boundary region at the C-terminal end of the NTR. In HSPB1 constructs, the unimodal fractional D-uptake increases from 0.81 to 0.91 upon ACD swap. In contrast, it decreases from 0.5 to 0.45 when the ACD is swapped in HSPB5. The differences in HSPB1's Boundary subregion arise primarily from increased D-uptake of the slower-exchanging population, rather than a change in the partitioning between populations,

indicating that the slower-exchanging state of the HSPB1 Boundary region is less well sequestered by the HSPB5 ACD.

Both the Distal and Boundary regions mediate key NTR-ACD interactions. The Distal region contains an "IxI" motif that inserts into the ACD Edge groove: HSPB5 carries a canonical ^{3}IAI motif and HSPB1 contains a non-canonical sequence of alternating hydrophobic residues, ^{6}VPFSL. The HDX results imply that this non-canonical motif is not well accommodated by the HSPB5 Edge groove. In contrast, the more conventional ^{3}IAI motif in HSPB5 is effectively sequestered by the HSPB1 ACD.

The Boundary region can form a β2 strand that aligns antiparallel to the β3 strand of the ACD at the dimer interface. Upon ACD swapping, deuteration patterns diverge: the Boundary region becomes more exposed in B151 but modestly gains protection in B515. While it is difficult to rationalize the behavior in specific structural terms, we note that the HDX trends of higher/lower Boundary region exposure correlate with higher/lower tau chaperone activity.

Aromatic and conserved regions respond differently to ACD swapping. The Aromatic subregions which to date has no defined function, are affected by ACD identity but respond in distinct ways. In B151, the population of fast-exchanging peptides increases, while the slow mode takes up deuterium even more slowly. In B515, the population of exposed Aromatic region is decreased, while the fast-exchanging population takes up deuterium faster. Thus, a larger fraction of Aromatic regions is exposed in B151 than in WT HSPB1 oligomers and a smaller fraction is exposed in B515 than in WT HSPB5.

In both WT oligomers, the Conserved region which binds to the ACD Central (dimer interface) groove is the most protected region of the NTR and a majority of conserved regions are sequestered ($p_{slow} > 0.5$). In B151, the partitioning is altered, with more than half populating

more exposed states, indicating less effective sequestration of the HSPB1 Conserved region by HSPB5 ACD.

HSPB1-specific Insertion subregion is largely insensitive to ACD identity. The Insertion region, unique to HSPB1, is mostly exposed, with only 26% sequestered. While its partitioning does not change in the context of the HSPB5 ACD, the sequestered population has a higher fractional D-uptake value, indicating it is less accommodated by the heterologous ACD.

2.2.4: Contributions of HSPB1 and HSPB5 NTR subregions in the delay of tau aggregation.

The subregion-specific differences in NTR exposure observed by HDX-MS prompted us to ask whether exposure of particular NTR elements correlates with the ability to delay tau aggregation. To identify NTR subregions that contribute to tau chaperone activity, we generated a panel of subregion chimeras between HSPB1 and HSPB5 by swapping a single previously defined NTR subregion (Figure 2.3A). For each chimera, tau chaperone activity and oligomer size distributions were measured at pH 7.5 and pH 6.5. Chaperone activity is reported as the fold-change in T_{50} relative to T_{50} for tau alone ("T_{50} fold-change"), with values for WT and the ACD-swaps, B151 and B515, included as reference points (Figure 2.4A). This approach allowed us to assess the contributions of individual NTR elements within the oligomeric contexts imposed by each sHSP.

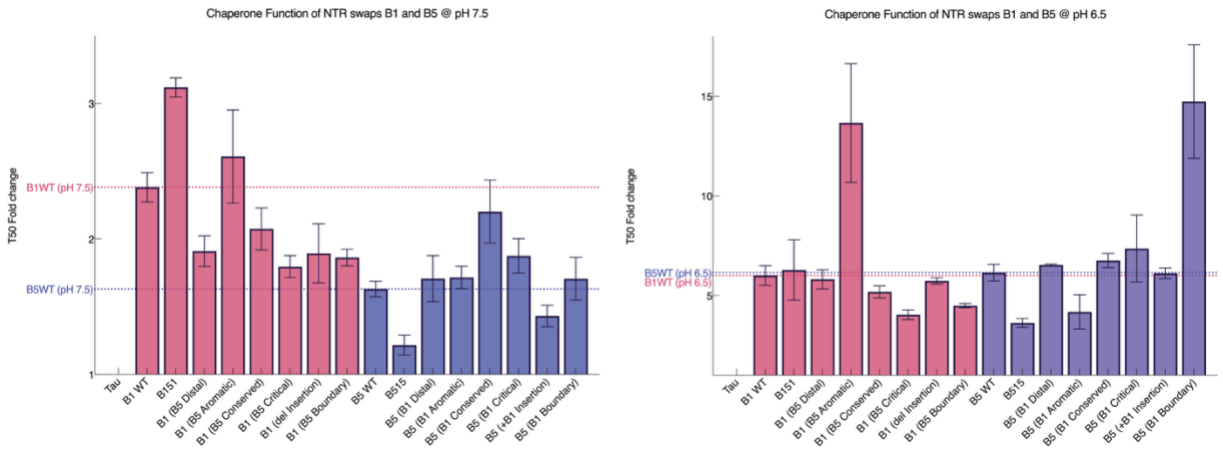

Figure 2.4. Effects of swapping individual subregions between HSPB1 and HSPB5. (A) Effects of swapping individual NTR sub-regions between HSPB1 and HSPB5 on tau chaperone activity. T_{50} fold change values for NTR sub-region swapped constructs of HSPB1 and HSPB5 constructs for assays performed at pH 7.5 (Left) and at pH 6.5 (Right). Bar graphs represent the average T_{50} values, with dotted lines representing the average T_{50} of HSPB1 and HSPB5 wild-types. T_{50} values for samples containing HSPB1 or HSPB5 were normalized to T_{50} of tau-only controls from the corresponding assays. Error bars indicate the SEM of T_{50} values calculated from 2-3 independent assays, with each assay containing 4-6 replicates.

Subregion contributions under basal conditions. At pH 7.5, WT-HSPB1 is an effective chaperone and B151 is further activated. Among the subregion swaps in the HSPB1 context, the chimera containing the Aromatic region of HSPB5 ("HSPB1-(HSPB5 Aromatic)") uniquely exhibited enhanced activity relative to WT-HSPB1. All other NTR subregion swaps resulted in reduced activity, yielding T_{50} fold-change lower than WT-HSPB1.

At pH 7.5, WT-HSPB5 has only modest activity and swapping the ACD (B515) further decreases activity. Among the NTR subregion swaps, both the Conserved and Critical regions

enhance activity, although neither restored activity to the level of HSPB1. Notably, the Conserved regions of HSPB5 and HSPB1 differ by only two amino acid differences, yet this minimal difference is sufficient to tune chaperone activity. This parallels previous findings in which three amino-acid substitutions distinguish the chaperone activities of HSPB5 and lens-specific sHSP, HSPB4 towards a lens client protein, gD-crystallin (46).

Subregion contributions under activating conditions. At pH 6.5, both wild-type HSPB1 and HSPB5 are activated and exhibit comparable chaperone function, providing a baseline for evaluating the effects of subregion swaps. Despite already being in activated states, both proteins are further activated by specific swaps (Figure 2.4). The most pronounced effects arise from the Aromatic and Boundary regions, followed by the Critical and Conserved regions, with only weak or no effects in the Distal or Insertion region.

Aromatic and Boundary regions dominate tau chaperoning activity. The Aromatic and Boundary swaps produce the strongest effects and these are reciprocal between the two analogous chimeras. HSPB1-(HSPB5 Aromatic) shows enhanced activity, while HSPB5-(HSPB1 Aromatic) has reduced activity. These results indicate that HSPB5's Aromatic region carries intrinsic tau chaperone activity that can be transferred across oligomeric contexts. Consistent with this interpretation, the Aromatic swap is the only one that decreases HSPB5 activity under conditions where HPSB5 is activated. Furthermore, installation of the Aromatic region of HSPB5 into HSPB1 greatly enhances its activity. Altogether, the observations strongly point to a direct participation of the HSPB5 Aromatic subregion in tau chaperoning function.

A similar reciprocal pattern is observed for the Boundary subregion. HSPB5-(HSPB1 Boundary) has greatly enhanced activity, whereas HSPB1-(HSPB5 Boundary) has slightly reduced activity. Together with the HDX-MS data (above), these findings suggest that the

HSPB1 boundary region, particularly when less sequestered, contributes directly to tau chaperoning. Swapping either the Critical or Conserved regions also shift activity in opposite directions, but with only modest effects. In contrast, Distal region swaps have no measurable effect, despite the large ACD-dependent effects observed by HDX at basal condition. The lack of direct involvement of the Distal subregion in tau chaperoning is consistent with previous observations (33). The results show that it is not exposure of a subregion *per se* that leads to chaperone activity and that the nature/identity of the subregion matters.

2.2.5: Oligomeric ensemble sizes of HSPB1 and HSPB5 constructs do not directly correlate with chaperone activities.

sHSPs oligomer size distributions are sensitive to environmental conditions, post-translational modifications, and mutations (47-49) and have been proposed to influence chaperone function. To investigate possible correlations between chaperone function and oligomer size, we compared the molecular weight distributions of WT and chimeric oligomers using mass photometry.

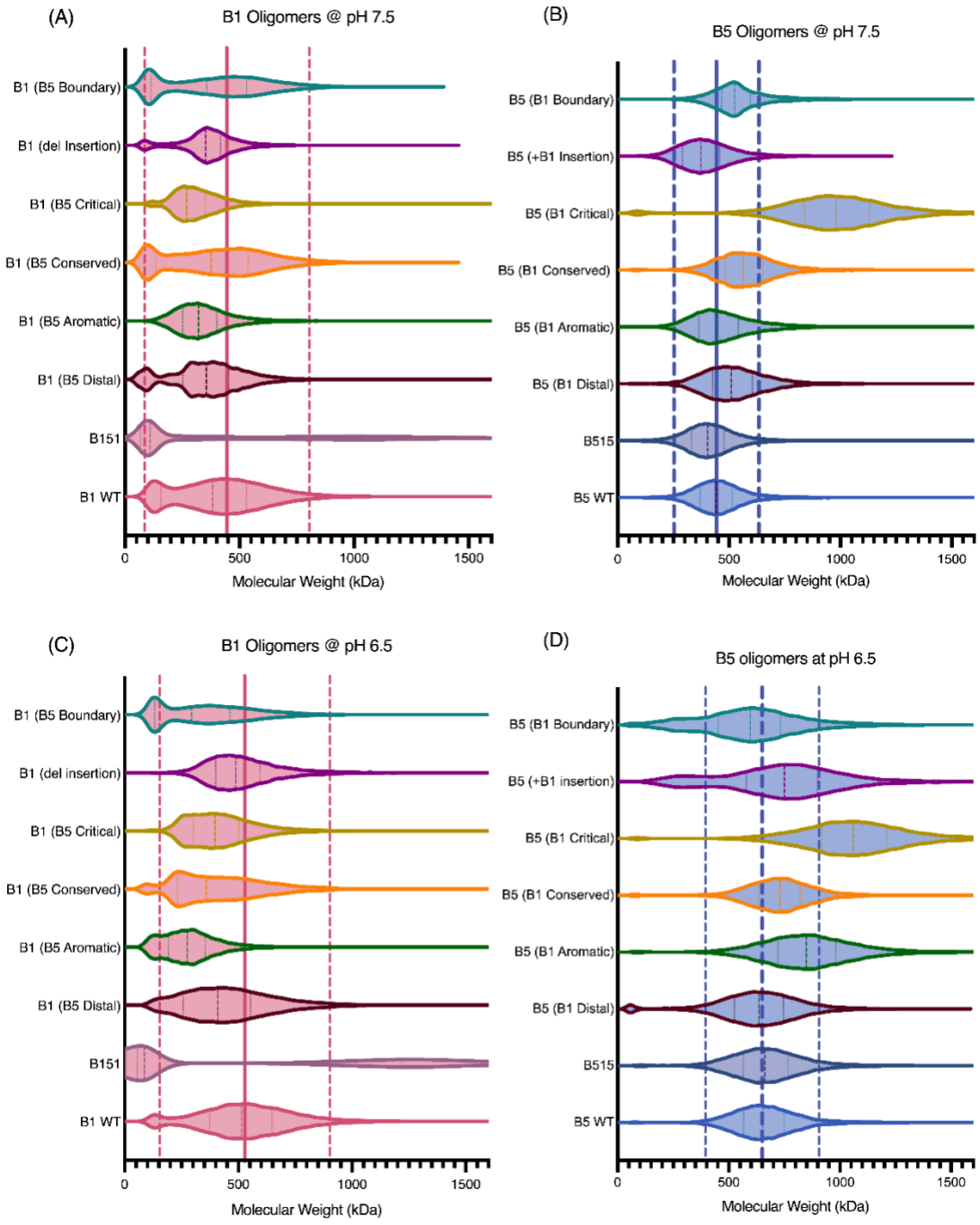

Figure 2.5: Effects of subregion swaps on oligomeric size. The molecular weight distributions of HSPB1 and HSPB5 constructs are measured by Mass Photometry. Each measurement is conducted at 1 μM final total concentration of sHSP using dilution-free measurements. The samples are incubated for 3 hours at 37 °C at the final concentration in PBS under reducing

condition at the appropriate pH. The mass photometer is calibrated using beta-amylase prior to the measurements. Solid line is drawn at the calculated average molecular weight of the large oligomers, with the dashed lines placed at ± 2 standard deviations from the mean.

Baseline oligomeric distributions at pH 7.5. At pH 7.5, where HSPB1 is the more active chaperone, HSPB1 oligomers are markedly more polydisperse than those of HSPB5 (Figure 2.5A & B). HSPB1 displays a bimodal distribution of large oligomers (Average molecular weight 406 kDa or ~20mers) and smaller species including tetramers. In contrast, HSPB5 forms a single, relatively narrow distribution centered around 443 kDa, with no detectable species below ~250 kDa. These differences suggest weaker inter-subunit interactions within HSPB1 homo-oligomers compared to those of HSPB5.

Effects of NTR subregion swaps at pH 7.5. To determine whether NTR swaps influence oligomerization, we examined the size distributions of all NTR-swap chimeras at pH 7.5. HSPB5 constructs were largely insensitive to NTR subregion swaps, with the exception of the Critical subregion swap, which results in a pronounced increase in ensemble size (WT = 443kDa vs. critical swap = 978kDa). In contrast, HSPB1 constructs were highly sensitive, with the relative populations of the smaller and larger-sized species changing in virtually every case. Aromatic and Critical swaps increase the population of larger oligomers, while Distal, Conserved, and Boundary swaps favor smaller species. Notably, replacing HSPB1's Aromatic region with that of HSPB5 yielded a unimodal distribution resembling that of WT-HSPB5.

pH-dependent effects at pH 6.5. Both WT oligomers display a pH-dependent increase in oligomeric size, forming larger species at pH 6.5. Under these activating conditions, HSPB5 constructs become more sensitive to changes within the NTR. Critical and Aromatic swaps shift

distributions to higher molecular weight, while Boundary and Insertion swaps favor smaller oligomeric species. Notably, introduction of the unique Insertion region or the Boundary region of HSPB1 into HSPB5 broadens the size distributions, producing profiles more characteristic of HSPB1 oligomers. In contrast, HSPB1 constructs at pH 6.5 show changes in both ensemble shape and molecular weight distribution, with no consistent trend across swaps.

Lack of correlation between oligomeric size and activity. Several prior studies have proposed a relationship between sHSP oligomer size and chaperone activity (48, 50). While isolated observations in our dataset could be interpreted as supporting such a correlation—for example B151 exhibits both enhanced activity and smaller oligomers relative to WT-HSPB1—analysis across the full dataset of constructs and conditions reveals no consistent relationship between oligomer size or polydispersity and tau chaperone activity.

2.3: Discussion

Our results demonstrate that HSPB1 and HSPB5 suppress tau aggregation through distinct, sequence-encoded strategies that are implemented by differential exposure of their N-terminal regions (NTRs). This divergence reflects a broader principle of sHSP function: chaperone activity is governed not simply by the presence of functional domains, but by how intrinsically disordered regions are scaffolded, sequestered, and released within dynamic oligomeric assemblies.

Division of labor between HSPB1 and HSPB5

HSPB1 suppresses tau aggregation under basal conditions, whereas HSPB5 requires stress-induced activation such as lowered pH to become effective. As both proteins are constitutively expressed in neurons, this behavior suggests a functional division of labor. HSPB1 may provide

continuous, long-term protection against tau misfolding, while HSPB5 functions as a rapidly deployable reserve that is mobilized under acute stress. Upon activation, HSPB5 becomes as effective as HSPB1, transiently boosting cellular protection when proteotoxic stress escalates.

Sequence-encoded NTR accessibility

These functional differences arise largely from intrinsic properties of the NTRs. HSPB5's NTR is more hydrophobic and histidine-rich, favoring sequestration at neutral pH and conferring sensitivity across a physiologically relevant pH range. In contrast, HSPB1's more polar NTR is less sequestered under basal conditions. Importantly, these properties are retained in NTR-ACD chimeras, demonstrating that solvent accessibility is encoded primarily in NTR sequence rather than imposed by ACD identity.

NTR-ACD interactions tune activation

The observations from the ACD-swaps can be rationalized in terms of known NTR-ACD intra-subunit interactions that can tune NTR accessibility and activity.

The Distal region of HSPB1, containing a non-canonical "IxI" motif (^{6}VPFSL) shows balanced exposure in its native context but becomes predominantly exposed when paired with the HSPB5 ACD. This suggests that the HSPB1 ACD edge groove has evolved to accommodate its unusual Distal "IxI" motif, whereas the HSPB5 ACD does not. On the other hand, the canonical IxI motif in the HSPB5 Distal sub-region (^{3}IAI) is efficiently sequestered by both ACD edge grooves. This difference likely promotes greater NTR release and thus activity in HSPB1 under basal conditions, while HSPB5's knob-into-hole IxI interaction enables sequestration until stress triggers activation. Notably, the same ACD grooves that bind NTR motifs also engage co-chaperones and clients, including tau, pointing to shared mechanisms for activation.

A second regulatory layer involves the Boundary region, which can form an additional β-strand (β2) by pairing with the ACD β3 strand. Disrupted pairing in chimeras correlates with increased NTR exposure and enhanced activity, suggesting that HSPB1 and HSPB5 NTR-ACD boundary may exist in different conformations at basal state: HSPB1 NTR boundary sub-region is mostly pointing away from the ACD, thereby enhancing overall NTR exposure, whereas HSPB5's β2 strand patches with the ACD's β3 strand, thus decreasing overall exposure of HSPB5 NTRs. Such subtle changes in NTR-ACD interactions can tune exposure within the oligomers, and thus activity of HSPB1 and HSPB5.

Modular determinants of tau specificity

Sub-region swaps reveal that tau chaperone activity is not evenly distributed across the NTR but rather is concentrated in specific subregions. Notably, installation of the Aromatic region of HSPB5 (^{12}RPFFPFHSP^{20}) into HSPB1 greatly enhanced tau chaperone activity while replacement of that sequence with the HSPB1 Aromatic sequence led to a loss of chaperone activity in HSPB5 (Figure 2.4). Installation of the HSPB1 Boundary region (^{71}PAYSRALSRQLSS^{83}) into HSPB5 led to a similar enhancement of its activity and the reciprocal swap led to decreased activity. These effects are most apparent under activating conditions at pH 6.5, when NTRs are more exposed.

Although these regions differ substantially in sequence composition, both may function either as direct tau-binding sites or as regulatory hubs that integrate environmental signals. The Aromatic region of HSPB5 has a His residue that could enable pH-dependent activation and both the Aromatic and Boundary regions contain the phosphorylation sites that activate HSPB1 and HSPB5 (S15, S78, S82 in HSPB1; S19, S59 in HSPB5). Notably, across the ten human sHSPs, phosphorylation sites cluster in the Boundary and Aromatic regions, suggesting that the positions

and properties of these subregions within otherwise variable NTRs have conserved modulatory mechanisms.

Our findings support a modular model in which different NTR sub-regions confer specificity toward distinct aggregation pathways. The Aromatic region of HSPB5 governs tau aggregation suppression, whereas the Critical region of HSPB5 drives protection of γD-crystallin aggregation in the eye lens (47). Tau and γD-crystallin undergo different aggregation pathways, forming fibrils and amorphous aggregates, respectively. We propose that the ability to engage different types of clients and their early-aggregating species may therefore arise from a diversity of sequences (subregions) within sHSP NTRs that can be reconfigured to meet a variety of cellular conditions and clients.

Disease relevance

This framework also provides insight into disease mutations. Prior HDX-MS studies of HSPB1 disease variants show altered exposure across multiple NTR sub-regions, with a shared increase in Boundary region accessibility (21). These mutations may therefore dysregulate a key structural control point that links oligomer architecture to chaperone output. The formation of hetero-oligomers between HSPB1 and HSPB5 (51-53) further suggests that cells may dynamically tune NTR accessibility in response to client load or stress.

2.4: Conclusions

In summary, our data define a mechanism in which sHSP chaperone activity emerges from dynamic, modular exposure of NTR sub-regions embedded within a quasi-ordered oligomeric network. Sequence-encoded stress sensors and ACD-mediated scaffolding jointly determine which regions are exposed, when, and to what extent. This model explains how sHSPs achieve

both client specificity and environmental responsiveness, and why certain clients may be preferentially protected under defined cellular conditions. More broadly, it identifies NTR-ACD interactions and NTR sub-regions as promising targets for therapeutic strategies aimed at modulating sHSP function in neurodegenerative disease.

2.5: Materials and methods.

Protein expression and purification

Tau4RD was expressed in *Escherichia coli* BL21 DE3 cells (New England BioLabs (NEB)). The cells were grown at 37 ºC until reaching an OD_{600} of 0.6-0.8, then induced overnight with 1 mM IPTG with the temperature adjusted to 16 ºC. Cells were harvested by centrifugation and resuspended in 50 mM Tris-base, 500 mM NaCl, 10 mM Imidazole (Buffer A). Cells were lysed by a homogenizer after adding DNase, RNase, PMSF, and HIS-protease inhibitor. The lysed cells were centrifuged then the lysate was filtered (0.45 μM) and applied to HisTrap column equilibrated in Buffer A. Bound proteins were eluted by Nickel elution buffer (Buffer A + 250 mM Imidazole). HIS-TEV protease was added to elutant and dialyzed overnight in Buffer A with 2 mM DTT added. Dialyzed protein was reapplied to HisTrap column to collect the protein without the His-tag to be concentrated to ~6 mL. The concentrated protein was injected 2mL at a time on sdx200 column in final buffer containing 25 mM NaPi, 100 mM NaCl, 0.5 mM EDTA, 2 mM. Fractions containing the protein was pooled and concentrated with a 3,000 kDa Molecular Weight Cut Off (MWCO) Amicon Ultra Centrifugal Filter.

HSPB1 and HSPB5 constructs were expressed in *Escherichia coli* BL21 DE3 cells (New England BioLabs (NEB)). The cells were grown at 37 ºC until reaching an OD_{600} of 0.6-0.8, then induced overnight with 500 μM IPTG with the temperature adjusted to 22 ºC. Cells were

harvested by centrifugation and resuspended in lysis buffer (20 mM Tris-base, 100 mM NaCl, 1 mM EDTA, pH 7.5). Cells were lysed by a homogenizer in presence of DNase, RNase, lysozyme, and protease-inhibitor. HSPB1 purification was performed by Ni-NTA, following the tau purification protocol, but the tag cleavage was performed with SENP1. Following dialysis and tag-cleavage, HSPB1 sample was desalted into 20mM Tris Buffer at pH 8.0 using a 5mL HiTrap Desalting column, then loaded on to a 5 mL HiTrap Q High Performance column and eluted over a 100 mL gradient into the same buffer containing 1 M NaCl. The sample was then concentrated using a 10,000 kDa MWCO Amicon Ultra Centrifugal Filter before size exclusion chromatography. HSPB5 purification protocol was followed as described previously (46).

Fibril formation assays

Fibrilization assay of Tau was performed on a low-binding 96-well plate using a CLARIOstar microplate reader. Each reaction contained 200 μL of sample with 5 μM Tau4RD, 1 mg/mL polyphosphate, 130 μM Thioflavin T (ThT), and 1.25 μM of chaperones in 25 mM NaPi, 20 mM NaCl, 0.5 mM EDTA, and 5 mM DTT buffer. The plate reader was shaken for 1 minute prior to fluorescent measurement at 440 nm excitation with 485 nm emission every 2.5 minutes. The enhanced dynamic range setting was applied to sample measurements. Each condition was performed in 4-6 replicates. Samples containing either HSPB1 or HSPB5 were pre-incubated in buffer and ThT for 3 hours at the same assay setting to let the oligomers and ThT come to an equilibrium on the plate reader. Tau4RD and polyphosphate were added after 3 hours to initiate the aggregation reaction.

Hydrogen-deuterium exchange mass spectrometry

All samples were incubated at 37 °C for 3 hours in water-based buffer and then cooled to room temperature before undergoing deuterium exchange. HSPB1 and HSPB5 constructs (0.04

mg/mL) were incubated at room temperature in 85% D_2O-based PBS pH 7.5 buffer for 4 seconds. Fully deuterated samples were made by incubating protein in 85% D_2O + 6 M guanidium-hydrochloride buffer at 90 °C for 30 mins. Exchange was quenched by addition of ice-cold quench buffer (1.6% formic acid) and samples were flash frozen in liquid nitrogen. Samples were automatically thawed, digested by immobilized Nepenthesin-2, and injected on a Waters Synapt G2-Si instrument using a setup built in house around the LEAP PAL system (54). HSPB5 peptides were identified by MS/MS on a Thermo Orbitrap Fusion Tribrid instrument and MS^E on a Waters Synapt G2-Si followed by data analysis using ProteinProspector (UCSF) or ProteinLynx Global SERVER (Waters). The quality of peptides were assessed in HDExaminer 3.0 (Sierra Analytics). All peptide data was aggregated to achieve near-residue level resolution, and the fractional deuterium uptake was analyzed following pyHXExpress workflow for unimodal and multimodal analysis (44).

Mass Photometry

All samples were incubated at 37 ºC for 3 hours in phosphate-based buffer (25 mM NaPi, 150 mM NaCl, 0.5 mM EDTA, 5 mM DTT at a pH of either 6.5 or 7.5) at a final concentration of 1 µM. Prior to sample preparation and incubation, the buffers were filtered using 3 kDa Millipore Amicon Ultracentrifugal filter. A Refeyn TwoMP mass photometer (Refeyn Ltd., UK) was used to analyze the sHSP samples. Beta-amylase was used to calibrate for molecular weights by assigning 56 kDa monomeric peak, 112 kDa dimeric peak, and 224 kDa tetrameric peaks. For sHSP measurements, 20 µL of 1 µM total protein sample was directly added to the coverslip using dilution free measurement. Each measurement was recorded over two minutes and fit to a Gaussian curve fit in Prism 10 (GraphPad Software, Boston, MA) for molecular weight determination of oligomeric species present.

References

1. Creekmore BC, Watanabe R, Lee EB (2024) Neurodegenerative Disease Tauopathies. Annual Review of Pathology; 19: 345–370.
2. Drubin DG, Kirschner MW (1986) Tau protein function in living cells. Journal of Cell Biology; 103(6): 2739–2746.
3. Goedert M, Spillantini MG, Jakes R, Rutherford D, Crowther RA (1989) Multiple isoforms of human microtubule-associated protein tau: Sequences and localization in neurofibrillary tangles of Alzheimer's disease. Neuron; 3(4): 519–526.
4. Lee VMY, Balin BJ, Otvos L, Trojanowski JQ (1991) A68: A Major Subunit of Paired Helical Filaments and Derivatized Forms of Normal Tau. Science; 251(4994): 675–678.
5. Jeganathan S, von Bergen M, Mandelkow EM, Mandelkow E (2008) The natively unfolded character of tau and its aggregation to Alzheimer-like paired helical filaments. Biochemistry; 47(40): 10526–10539.
6. Mandelkow EM, Mandelkow E (2012) Biochemistry and Cell Biology of Tau Protein in Neurofibrillary Degeneration. Cold Spring Harbor Perspectives in Medicine; 2(7): a006247.
7. Fitzpatrick AWP, Falcon B, He S, Murzin AG, Murshudov G, Garringer H J, Crowther RA, Ghetti B, Goedert M, Scheres SHW (2017) Cryo-EM structures of tau filaments from Alzheimer's disease. Nature; 547(7662): 185–190.
8. Haslbeck M, Franzmann T, Weinfurtner D, Buchner J (2005) Some like it hot: The structure and function of small heat-shock proteins. Nature Structural & Molecular Biology; 12(10): 842–846.

9. Hartl FU, Bracher A, Hayer-Hartl M (2011) Molecular chaperones in protein folding and proteostasis. Nature; 475(7356): 324–332.
10. Treweek TM, Meehan S, Ecroyd H, Carver J A (2015) Small heat-shock proteins: Important players in regulating cellular proteostasis. Cellular and Molecular Life Sciences; 72(3): 429–451.
11. Delbecq SP, Klevit RE (2019) HSPB5 engages multiple states of a destabilized client to enhance chaperone activity in a stress-dependent manner. Journal of Biological Chemistry; 294(9): 3261–3270.
12. Gonçalves CC, Sharon I, Schmeing TM, Ramos CHI, Young JC (2021) The chaperone HSPB1 prepares protein aggregates for resolubilization by HSP70. Scientific Reports; 11(1): 17139.
13. Reinle K, Mogk A, Bukau B (2022) The Diverse Functions of Small Heat Shock Proteins in the Proteostasis Network. Journal of Molecular Biology; 434(1): 167157.
14. Mymrikov EV, Daake M, Richter B, Haslbeck M, Buchner J (2017) The Chaperone Activity and Substrate Spectrum of Human Small Heat Shock Proteins. Journal of Biological Chemistry; 292(2): 672–684.
15. Banzet N, Richaud C, Deveaux Y, Kazmaier M, Gagnon J, Triantaphylidès C (1998) Accumulation of small heat shock proteins, including mitochondrial HSP22, induced by oxidative stress and adaptive response in tomato cells. The Plant Journal; 13(4): 519–527.
16. Hayes D, Napoli V, Mazurkie A, Stafford WF, Graceffa P (2009) Phosphorylation Dependence of Hsp27 Multimeric Size and Molecular Chaperone Function. Journal of Biological Chemistry; 284(28): 18801–18807.

17. Rajagopal P, Tse E, Borst AJ, Delbecq SP, Shi L, Southworth DR, Klevit RE (2015) A conserved histidine modulates HSPB5 structure to trigger chaperone activity in response to stress-related acidosis. eLife; 4: e07304.
18. Makley LN, Johnson OT, Ghanakota P, Rauch JN, Osborn D, Wu TS, Cierpicki T, Carlson HA, Gestwicki JE (2021) Chemical validation of a druggable site on Hsp27/HSPB1 using in silico solvent mapping and biophysical methods. Bioorganic & Medicinal Chemistry; 34: 115990.
19. Peters C, Haslbeck M, Buchner J (2024) Catchers of folding gone awry: A tale of small heat shock proteins. Trends in Biochemical Sciences; 49(12): 1063–1078.
20. Delbecq SP, Rosenbaum JC, Klevit RE (2015) A Mechanism of Subunit Recruitment in Human Small Heat Shock Protein Oligomers. Biochemistry; 54(28): 4276–4284.
21. Clouser AF, Baughman HE, Basanta B, Guttman M, Nath A, Klevit RE (2019) Interplay of disordered and ordered regions of a human small heat shock protein yields an ensemble of 'quasi-ordered' states. eLife; 8: e50259.
22. Rauch JN, Tse E, Freilich R, Mok SA, Makley LN, Southworth DR, Gestwicki JE (2017) BAG3 Is a Modular, Scaffolding Protein that physically Links Heat Shock Protein 70 (Hsp70) to the Small Heat Shock Proteins. Journal of Molecular Biology; 429(1): 128–141.
23. Baughman HER, Clouser AF, Klevit RE, Nath A (2018) HspB1 and Hsc70 chaperones engage distinct tau species and have different inhibitory effects on amyloid formation. Journal of Biological Chemistry; 293(8): 2687–2700.

24. Freilich R, Betegon M, Tse E, Mok SA, Julien O, Agard DA, Southworth DR, Takeuchi K, Gestwicki JE (2018) Competing protein-protein interactions regulate binding of Hsp27 to its client protein tau. Nature Communications; 9(1): 4563.
25. Klevit RE (2020) Peeking from behind the veil of enigma: Emerging insights on small heat shock protein structure and function. Cell Stress and Chaperones; 25(4): 573–580.
26. Bartelt-Kirbach B, Slowik A, Beyer C, Golenhofen N (2017) Upregulation and phosphorylation of HspB1/Hsp25 and HspB5/αB-crystallin after transient middle cerebral artery occlusion in rats. Cell Stress and Chaperones; 22(4): 653–663.
27. Nemes Z, Devreese B, Steinert PM, Beeumen JV, Fésüs L (2004) Cross-linking of ubiquitin, HSP27, parkin and α-synuclein by γ-glutamyl-ε-lysine bonds in Alzheimer's neurofibrillary tangles. The FASEB Journal; 18(10): 1135–1137.
28. Shimura H, Miura-Shimura Y, Kosik KS (2004) Binding of tau to heat shock protein 27 leads to decreased concentration of hyperphosphorylated tau and enhanced cell survival. The Journal of Biological Chemistry; 279(17): 17957–17962.
29. Björkdahl C, Sjögren MJ, Zhou X, Concha H, Avila J, Winblad B, Pei JJ (2008) Small heat shock proteins Hsp27 or alphaB-crystallin and the protein components of neurofibrillary tangles: Tau and neurofilaments. Journal of Neuroscience Research; 86(6): 1343–1352.
30. Sahara, N, Maeda S, Yoshiike Y, Mizoroki T, Yamashita S, Murayama M, Park JM, Saito Y, Murayama S, Takashima A (2007) Molecular chaperone-mediated tau protein metabolism counteracts the formation of granular tau oligomers in human brain. Journal of Neuroscience Research; 85(14): 3098–3108.

31. Abisambra JF, Blair LJ, Hill SE, Jones JR, Kraft C, Rogers J, Koren J, Jinwal UK, Lawson L, Johnson AG, Wilcock D, O'Leary JC, Jansen-West K, Muschol M, Golde TE, Weeber EJ, Banko J, Dickey CA (2010) Phosphorylation Dynamics Regulate Hsp27-Mediated Rescue of Neuronal Plasticity Deficits in Tau Transgenic Mice. Journal of Neuroscience; 30(46): 15374–15382.
32. Hampton DW, Amor S, Story D, Torvell M, Bsibsi M, van Noort JM, Chandran S (2020) HspB5 Activates a Neuroprotective Glial Cell Response in Experimental Tauopathy. Frontiers in Neuroscience; 14.
33. Baughman HER, Pham THT, Adams CS, Nath A, Klevit RE (2020) Release of a disordered domain enhances HspB1 chaperone activity toward tau. Proceedings of the National Academy of Sciences; 117(6): 2923–2929.
34. Janowska MK, Baughman HE, Woods CN, Klevit RE (2019. Mechanisms of small heat shock proteins. Cold Spring Harbor Perspectives in Biology; 11(10): a034025.
35. King ME, Gamblin TC, Kuret J, Binder LI (2000) Differential assembly of human tau isoforms in the presence of arachidonic acid. Journal of Neurochemistry; 74(4): 1749–1757.
36. Barghorn S, Davies P, Mandelkow E (2004) Tau Paired Helical Filaments from Alzheimer's Disease Brain and Assembled in Vitro Are Based on β-Structure in the Core Domain. Biochemistry; 43(6): 1694–1703.
37. Ramachandran G, Udgaonkar JB (2011) Understanding the Kinetic Roles of the Inducer Heparin and of Rod-like Protofibrils during Amyloid Fibril Formation by Tau Protein. Journal of Biological Chemistry; 286(45): 38948–38959.

38. Lindahl U, Kjellén L (2013) Pathophysiology of heparan sulphate: Many diseases, few drugs. Journal of Internal Medicine; 273(6): 555–571.

39. Xu, D, Esko JD (2014) Demystifying Heparan Sulfate–Protein Interactions. Annual Review of Biochemistry; 83(Volume 83, 2014): 129–157.

40. Gray MJ, Jakob U (2015) Oxidative stress protection by polyphosphate—New roles for an old player. Current Opinion in Microbiology; 24: 1–6.

41. Lempart J, Jakob U (2019) Role of Polyphosphate in Amyloidogenic Processes. Cold Spring Harbor Perspectives in Biology; 11(5): a034041.

42. Hagihara H, Shoji H, Hattori S, Sala G, Takamiya Y, Tanaka M, Ihara M, Shibutani M, Hatada I, Hori K, Hoshino M, Nakao A, Mori Y, Okabe S, Matsushita M, Urbach A, Katayama Y, Matsumoto A, Nakayama KI, Miyakawa T (2024) Large-scale animal model study uncovers altered brain pH and lactate levels as a transdiagnostic endophenotype of neuropsychiatric disorders involving cognitive impairment. eLife; 12: RP89376.

43. Woods CN, Janowska MK, Ulmer LD, Kaur Sidhu J, Stone N L, James EI, Guttman M, Bush MF, Klevit RE (2025) Activation mechanism of small heat shock protein HSPB5 revealed by disease-associated mutants. Proceedings of the National Academy of Sciences; 122(20): e2425061122.

44. Tuttle LM, Klevit RE, Guttman M (2025) A framework for automated multimodal HDX-MS analysis. bioRxiv (pre-print): 10.1101/2025.03.13.643099

45. Hochberg GKA, Ecroyd H, Liu C, Cox D, Cascio D, Sawaya MR, Collier MP, Stroud J, Carver JA, Baldwin AJ, Robinson CV, Eisenberg DS, Benesch JLP, Laganowsky A (2014) The structured core domain of αB-crystallin can prevent amyloid fibrillation and

associated toxicity. Proceedings of the National Academy of Sciences; 111(16): E1562–E1570.

46. Woods CN, Ulmer LD, Guttman M, Bush MF, Klevit RE (2023) Disordered region encodes α-crystallin chaperone activity toward lens client γD-crystallin. Proceedings of the National Academy of Sciences; 120(6): e2213765120.
47. Jehle S, Vollmar BS, Bardiaux B, Dove KK, Rajagopal P, Gonen T, Oschkinat H, Klevit RE (2011) N-terminal domain of αB-crystallin provides a conformational switch for multimerization and structural heterogeneity. Proceedings of the National Academy of Sciences; 108(16): 6409–6414.
48. Peschek J, Braun N, Rohrberg J, Back KC, Kriehuber T, Kastenmüller A, Weinkauf S, Buchner J (2013) Regulated structural transitions unleash the chaperone activity of αB-crystallin. Proceedings of the National Academy of Sciences; 110(40): E3780–E3789.
49. Berkeley RF, Plonski AP, Phan TM, Grohe K, Becker L, Wegner S, Herzik MA, Mittal J, Debelouchina GT (2025) Capturing the Conformational Heterogeneity of HSPB1 Chaperone Oligomers at Atomic Resolution. Journal of the American Chemical Society; 147(18): 15181–15194.
50. Jovcevski B, Kelly MA, Rote AP, Berg T, Gastall HY, Benesch JLP, Aquilina JA, Ecroyd H (2015) Phosphomimics Destabilize Hsp27 Oligomeric Assemblies and Enhance Chaperone Activity. Chemistry & Biology; 22(2): 186–195.
51. Aquilina JA, Shrestha S, Morris AM, Ecroyd H (2013) Structural and Functional Aspects of Hetero-oligomers Formed by the Small Heat Shock Proteins αB-Crystallin and HSP27 . Journal of Biological Chemistry; 288(19): 13602–13609.

52. Mymrikov EV, Riedl M, Peters C, Weinkauf S, Haslbeck M, Buchner J (2020) Regulation of small heat-shock proteins by hetero-oligomer formation. Journal of Biological Chemistry; 295(1): 158–169.
53. Shatov VM, Muranova LK, Zamotina MA, Sluchanko NN, Gusev NB (2023) α-Crystallin Domains of Five Human Small Heat Shock Proteins (sHsps) Differ in Dimer Stabilities and Ability to Incorporate Themselves into Oligomers of Full-Length sHsps. International Journal of Molecular Sciences; 24(2).
54. Watson MJ, Harkewicz R, Hodge EA, Vorauer C, Palmer J, Lee KK, Guttman M. 2021. Simple Platform for Automating Decoupled LC3MS Analysis of Hydrogen/Deuterium Exchange Samples. Journal of the American Society for Mass Spectrometry; 32:5973600.

3. Perturbation of the sHSP quasi-ordered network by altering NTR-ACD interactions

3.1 Introduction

Small heat shock (sHSP) oligomers are assembled not by a single rigid interface, but by multitudes of dynamic contacts distributed across all three domains: the disordered NTR, the structured ACD, and the short disordered CTR. Together, these interactions produce "quasi-order" assemblies that are heterogeneous and dynamic, yet not random in which binding is governed by sequence features, preferred orientations, and competition for binding sites (1). The ACD is the only folded domain of sHSPs and serves as a central interaction hub. Within an ACD dimer, three prominent binding grooves are defined: one central groove formed at the dimer interface and two edge grooves (one per ACD monomer). These binding grooves act as scaffolds for both inter-and intra-molecular interactions, leading to higher-ordered oligomerization of sHSP as well binding clients and co-chaperones (2). Moreover, occupancy of these binding grooves is often mediated by short "IxI" motifs, making the ACD groove key nodes in the quasi-order network (Figure 3.1).

One of the well characterized ACD-mediated interactions involves CTR "IxI" motifs, which bind to the ACD edge groove and promote oligomerization (3-4). In sHSPs lacking an IxI motif in the CTR such as HSPB6, ability to form higher-order oligomers is diminished (5). Both HSPB1 and HSPB5 contain CTR IxI motifs, but their sequences differ: HSPB1 has a non-canonical motif (ITIPV), whereas HSPB5 contains a more canonical IxI motif (IPI). Similar IxI motifs are also present within the long disordered NTR of sHSPs, and these motifs can compete for the same edge groove. In HSPB1, NTR IxI motif is non-canonical and consists of alternating hydrophobic residues (VPFSL), whereas HSPB5 again contains a more canonical motif (IAI). Beyond the interactions within the sHSP oligomers, IxI motifs are also present in clients and co-

chaperones, including tau and Bag3, and these motifs have been shown to engage the ACD edge groove (6-7). Thus, the edge groove can accommodate multiple binders, not limited to sHSP protomers, and is important for sHSP oligomerization and client/co-chaperone engagement (Figure 3.1).

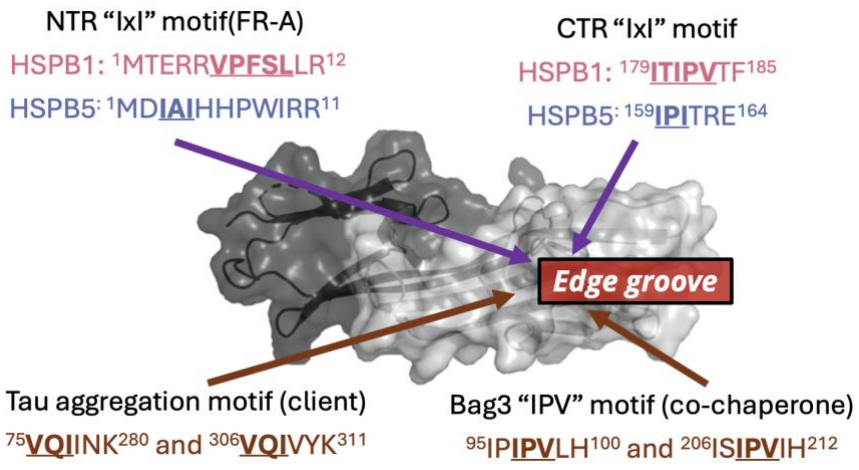

Figure 3.1: ACD edge groove mediated knob-into-hole interactions by "IxI" motif of binding partners. ACD structure (PDB: 4MJH) shows edge groove binding site where interaction of multiple binding partners has been observed. Binding partners (HSPB1, HSPB5, Tau, and Bag3 proteins) "IxI" containing motif is shown, with the motif sequence underlined.

Other than edge groove binding, the ACD dimer interface (central groove) is a prominent binding site for the NTR. Current experimental data (HDX-MS and NMR) indicates that the primary binder to this region is the conserved NTR sub-region FR-C (1,8). Further, local unfolding of residues within ACD dimer interface has been observed in HSPB1, and release of the resulting ACD monomer has been proposed to correlate with increased chaperone activity (9-11). In addition to FR-C, FR-E at the C-terminal end of the NTR has been shown to fill in parts

of the dimer interface (1,8). FR-E holds phosphorylation sites and has been implicated in delaying tau aggregation *in vitro* (12). These observations highlight the central groove as another important regulatory site that can influence both oligomer architecture and function.

In addition to groove-mediated binding, the highly disordered and interactive NTR also engages additional ACD surfaces and loops outside the defined grooves (1). NTR-NTR interactions are also prominent in both HSPB1 and HSPB5 and are thought to contribute to the dynamics and organization of sHSP oligomers (13-15). Together, these contacts form a quasi-order network in which multiple transient interactions coexist, compete, and redistribute depending on sequence, domain accessibility and environmental conditions.

In Chapter 2, several key NTR-ACD interactions in HSPB1 and HSPB5 were identified as major determinants of both oligomer organization and tau chaperone function. Building on this framework, Chapter 3 tests how disrupting specific nodes within this quasi-order network alters sHSP structure, oligomerization, and tau chaperone function. The same experimental approaches used in Chapter 2 are applied here to delineate these effects, including HDX-MS to monitor local structure, ThT tau aggregation assays to quantify chaperone function, and mass photometry to assess oligomer size distributions. Three different perturbation strategies are explored. First (Chapter 3.2.1), HSPB1 disease-associated mutations in the NTR are examined to probe how a single mutation within the NTR alters the entire sHSP dynamics. Second (Chapter 3.2.2), an ACD “bump” mutation is introduced to disrupt edge groove binding and test how loss of this binding site on the ACD template reshapes oligomers organization and quasi-order network. Finally (Chapter 3.2.3), hetero-oligomerization between HSPB1 and HSPB5 is investigated as a biologically relevant mechanism for modulating interactions, accessibility of

binders, and activity. Together, these experiments aim to refine a mechanistic model for how sHSPs encode functional organization through a dynamic but defined interaction network.

3.2 Results

3.2.1 B1 NTR Disease Mutation

Previous work from our lab used HDX-MS to examine how HSPB1 disease-association mutations in three key NTR sub-regions in FR-C, FR-D, and FR-E regions (G34R, P39L, G84R) alter local structure and dynamics (Figure 3.2). The disease mutant in FR-C (G34R) showed largest perturbation in the region where the mutation is introduced as well deprotection at the NTR-ACD boundary (residues 80-100). G84R also showed increased deuteration in the region of the mutation within the boundary sequence, as well as FR-C. P39L, a disease mutant in FR-D was the only disease mutant tested where overall protection increased, except in FR-E where it becomes slightly more exposed. Although each mutation led to varying effects on NTR dynamics and accessibility, a shared trend emerged: the boundary region (FR-E) shows increased exposure in all three mutants. This observation is consistent with results from Chapter 2, where increased exposure of the boundary region (FR-E) was correlated with enhanced HSPB1 chaperone function toward tau aggregation.

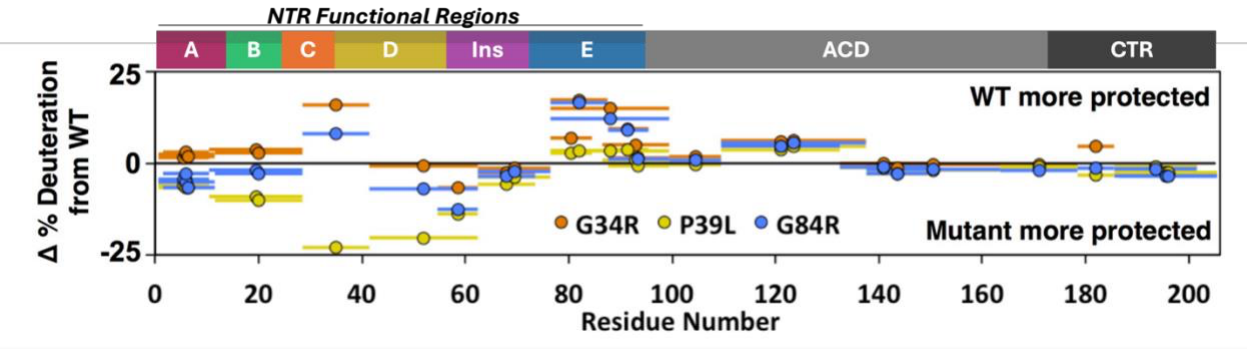

Figure 3.2: HDX-MS analysis of HSPB1 disease mutations, compared to HSPB1-WT at 3-second early timepoint. The deuteration difference from HSPB1-WT for each disease mutant is shown for each peptide. (Data from Clouser 2019)

No functional assays were reported for HSPB1 disease associated mutations in (Clouser 2019), so I tested whether the increased exposure of FR-E in the HSPB1 disease mutants also translates to increased chaperone function using *in vitro* ThT tau aggregation assay (Figure 3.3A). All three mutations increased overall chaperone activity relative to HSPB1-WT, but each led to distinct aggregation kinetics. G34R in FR-C did not alter its T50 vastly, yet it consistently reduced the final ThT fluorescence plateau across all aggregation assays with G34R. A reduced ThT plateau signal suggests decreased total fibril formation, including aggregated tau and co-aggregated HSPB1 species. G34R also showed widespread NTR deprotection by HDX-MS, except for peptides in FR-D, suggesting higher overall NTR accessibility that may suppress tau aggregation.

Both P39L and G84R showed three different phases in the aggregation kinetics: 1) the lag phase is delayed and the slope of elongation rate is also decreased, 2) after ~500minutes, the elongation rate increased and led to rapid formation of aggregates, 3) a plateau is reached within

the next 200 minutes. Such multi-phase behavior is consistent with a model in which these mutants delay nucleus formation but are less effective at suppressing aggregation once fibril elongation begins. Among all three mutants tested, only P39L produced higher level of ThT-binding species at the end of the reaction that exceeds WT, inferring co-aggregation of tau with HSPB1 oligomers. Additional experiments to quantify soluble and insoluble materials at the end of aggregation (e.g., SDS-PAGE) would help clarify the correlation of ThT signal and co-aggregation. Such mechanism of action aligns with prior work (7), which proposed that HSPB1 delays tau aggregation by maintaining tau in a soluble, monomeric state for longer durations.

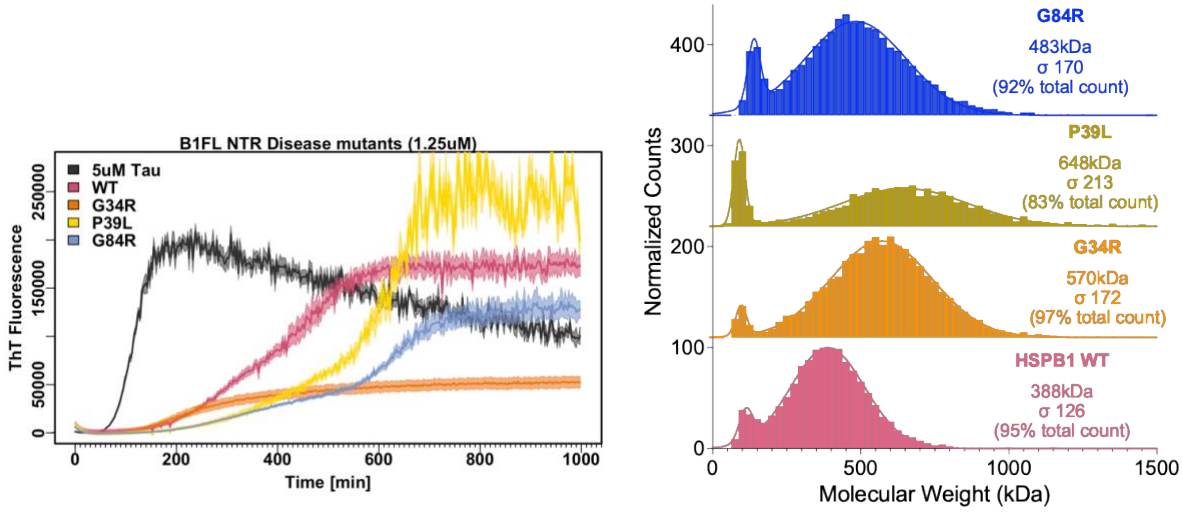

Figure 3.3: Effects of HSPB1 disease association mutation on chaperone function and oligomer size distribution. (A) In vitro aggregation assay of tau in presence of HSPB1 disease mutants. Reactions are induced by 1mg/mL polyphosphate at pH 7.5; 37°C with 5μM Tau4RD with 1.25μM sHSP. ThT fluorescence values are recorded every 2.5minutes while agitating prior to each measurement. (B) Molecular weight distribution of HSPB1 WT and disease mutant oligomers, measured by mass photometer. Each measurement is at 1μM final concentration of HSPB1 monomer in aggregation buffer with 20mM NaCl concentration under reducing

condition. The counts were recorded for two minutes using buffer-free method on mass photometer. The molecular weight distribution is calculated by fitting the normalized counts to Gaussian model with two populations.

Despite varied effects in local structure and activity, mass photometry revealed that G34R and G84R largely preserved WT-like oligomer distribution (Figure 3.3B). The molecular weight distributions of both G34R and G84R maintained the typical HSPB1 bimodal distribution with slightly higher average molecular weights and polydispersity (i.e. increased σ) in both populations. On the other hand, P39L destabilized the larger oligomeric population, increasing the average molecular weight by ~12 subunits with a much broader polydispersity. The increased oligomer heterogeneity may contribute to P39L's apparent propensity to co-aggregate with tau, as the oligomers may be less stable. Importantly, as shown in Chapter 2, oligomer size distribution alone does not directly predict chaperone activity, and that local structural accessibility within the NTR, particularly in FR-E, play a more dominant regulatory role in tuning HSPB1 chaperone function.

B1NTR Disease	Activity	Molecular Weight	Sub-regions with inc. exposure	Sub-regions with dec. exposure	Sub-regions with no change
G34R	↑	570kDa +/- 172 (97%)	FR-A, FR-B, FR-C, **FR-E**	Start of insertion	FR-D, Insertion
P39L	↑	648kDa +/- 213 (83%)	**FR-E**	FR-A, FR-B FR-C, FR-D, start of insertion	Insertion
G84R	↑	483kDa +/- 170	FR-C, **FR-E**	FR-A, FR-B, start of insertion	Insertion

Table 3.1: Summary of observations from HDX-MS, aggregation assay, and mass photometry for HSPB1 disease mutations tested compared to the HSPB1-WT.

The increased exposure of the FR-E across all three HSPB1 disease mutations could reflect a reduced secondary structure at this site. Some of the residues in the boundary region can form a β-strand structure, termed β2 and when engaged to β3 of the ACD, β2 will comprise part of the Central Groove at the dimer interface, altering its shape and properties. ACD-only structures that include parts of the boundary β2 residues (PDB:4NJH and 2N3J; 16-17) show β2 to exist in two different conformations (Figure 3.4): 1) a protected conformation in which β2 forms β-sheet interactions with ACD β3, and 2) an "open" conformation in which β2 extends away from the ACD instead of engaging β3 strand (Figure 3.4). A shift toward the open conformation, or lack of secondary structure formation in turn would lead to more accessible NTR, specifically in the boundary sequence to chaperone tau aggregation. In support of this model, residues corresponding the ACD β3 also experienced increased deuterium uptake across all three mutants. In both G34R and G84R, FR-C also showed increased D-uptake. As previously stated, NTR sequence in the FR-C binds to the ACD central groove that is also occupied by β2/3 in protected conformation. These paired changes in exposure suggest lack of β2/3 engagement, thus a shift toward an "open" conformation associated with increased chaperone activity.

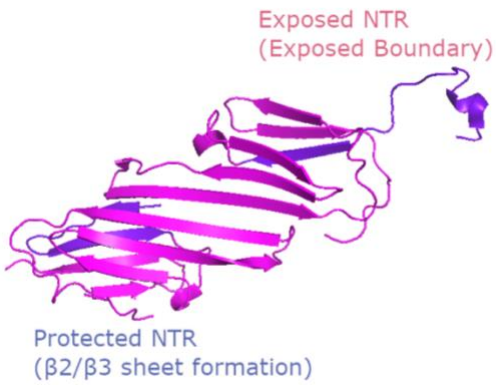

Figure 3.4: Pymol structure of one ACD monomer each from PDB: 4MJH and PDB:2N3J. In the NMR structure (PDB: 2N3J), boundary regions are pointing away from the ACD in the "open" boundary region conformation (Right). In the crystal structure (PDB: 4MJH), β2 and β3 residues are engaged in β-sheet structure formation, leading to "protected" boundary.

In contrast, P39L show increased deuterium uptake in the NTR boundary without a paired increase in FR-C exposure, as observed for G34R or G84R. This implies that P39L mutation may impose a different structural rearrangement that does not primarily operate through changes in β2/3 interaction. However, it is important to note that substitution of proline with leucine at site 39 may increase local helical propensity and reduce deuterium uptake through altered backbone dynamics.

These results further reinforce the boundary region (FR-E) as a critical regulatory element for HSPB1 chaperone activity toward tau. G34R and G84R, which directly or indirectly perturb boundary β2/3 engagement, appear to follow the mechanism proposed in Chapter 2 in which boundary exposure modulates NTR accessibility and activity. Although P39L does not show the same paired FR-C/FR-E exposure pattern, it still enhances FR-E exposure and overall

activity. Additional analysis on P39L HSPB1 oligomers also points to altered subunit exchange rate, increased local secondary (helical and/or β-sheet) structure and assembly that is unique to P39L (Clouser 2019; thesis), thus further investigation is needed to better understand the effects P39L mutation on HSPB1 oligomers.

3.2.2 The disruption of NTR-ACD interaction by a "Bump" mutation

The bump mutation was designed previously by our lab (18) to study the role of ACD edge grooves in sHSP oligomerization. The ACD edge groove is created by β4 and β8 strands of the structured ACD, creating a binding site for hydrophobic moieties through hydrophobic-hydrophobic interactions (Figure 3.5). In particular, the edge grooves bind "IxI" motifs, originally thought to involve two Ile residues but now known more generally as sequences with alternating hydrophobic residues. These interactions occur in both the CTR and NTR of sHSPs (5,7,19) and are thought to mediate inter-subunit interactions that contribute to oligomer assembly. Edge groove binding can be disrupted by introducing a bump mutation at a highly conserved Serine in β8 (S155Q in B1, S135Q in B5), where a bulkier glutamine sterically occludes the groove, thus preventing binding partners from engaging the site (2). Such binding partners are not limited to its inter-/intra-sHSP protomers but also include clients with hydrophobic patches and co-chaperones (Figure 3.5). As a result, the bump mutation serves as a useful tool to interrogate how ACD edge groove interactions influence oligomer structure and chaperone function.

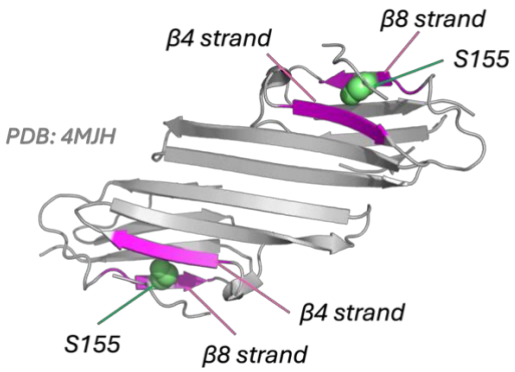

Figure 3.5: Pymol structure of HSPB1ACD (PDB: 4MJH) that shows edge grooves created by β4 and β8 strands (pink) and the conserved Serine 155 that is mutated to Glutamate (S155Q) in bump mutation.

The edge groove was initially considered a potential target site for therapeutics by modulating sHSP activity (20-21). However, experimental data indicate that binding does not directly translate to chaperone function. Previous work demonstrated that tau binds both to the ACD edge groove and to sites within the NTR of HSPB1 through IxI motifs (Figure 3.1). However, only interactions involving the NTR lead to productive chaperone activity, whereas ACD binding is uncorrelated with chaperone function (20-21). Introducing the bump mutation to abrogate binding to the ACD edge groove led to enhanced chaperone activity of HSPB1 toward tau. This leads to a mechanism in which release of the disordered NTR from ACD edge groove binding enhances chaperone activity toward tau. In this model, blocking the edge groove prevents sequestration of distal NTR, thereby increasing the accessibility of NTR regions responsible for client engagement (Figure 3.6). However, not much is understood about what this "release of NTR" means. Specifically, it is unclear whether the bump mutation causes the NTR to become globally exposed, or instead triggers more localized reorganization while keeping

other oligomeric organization intact. In this sub-chapter, I attempt to address two key questions that remain: 1) Is bump activation a general mechanism shared across sHSPs? 2) How does abrogating the edge groove reorganize oligomer structure and local dynamics?

Figure 3.6: A cartoon representation of how the bump mutation is predicted to change sHSP structure and their NTR accessibility. Upon the addition of the bump mutation, NTRs bound to the ACD edge groove become unbound, or released. The cartoon specifically represents intra-dimer interaction for simplicity, but inter-dimer interactions exit within oligomers.

First, I confirmed that tau binds specifically to the ACD edge groove in both HSPB1 and HSPB5, indicating conserved client binding site in these two proteins (Figure 3.7). By NMR, ^{15}N-labeled ACD constructs of HSPB1 and HSPB5 both showed specific chemical shift perturbations in residues associated with the edge groove. This binding is abrogated upon introducing a bump mutation to each ACD (S155Q for B1, S135Q for B5), further confirming the edge groove to be a binding site for client tau.

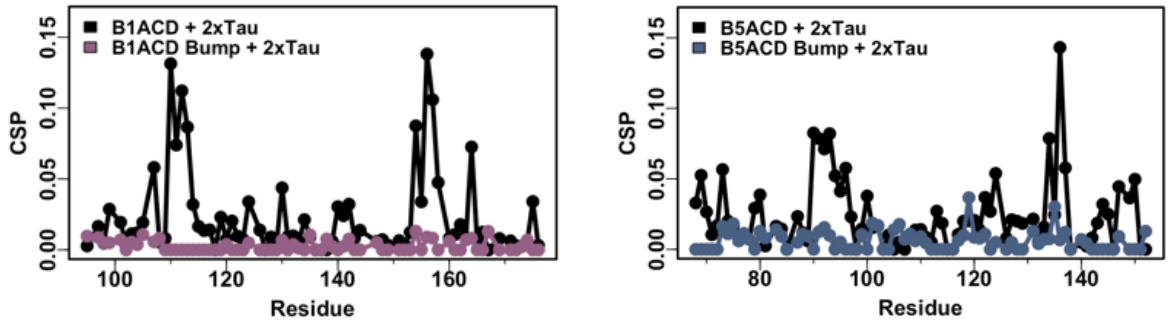

Figure 3.7: (NMR) Chemical shift perturbations (CSPs) observed in HSQC spectrum of 200µM N^{15}-labeld B1ACD and B5ACD in presence of 400µM Tau4RD are shown in black. CSPs for N^{15}-labed Bump constructs for 200µM B1ACD and B5ACD in presence of 400µM Tau is shown in pink (B1ACD Bump) and blue (B5ACD Bump)

In addition to the analogous client binding site, the introduction of the bump mutation had similar effects on the chaperone function of HSPB1 and HSPB5. The bump mutation enhanced the ability of both proteins to delay tau aggregation (Figure 3.8; left). The bump mutation was also introduced into ACD-swapped constructs (B151 and B515) to test whether the effect is generalizable across different NTR-ACD parings. Similar to the WT proteins, the bump mutation significantly enhanced activity in both chimeras (Figure 3.8; right). In B151, tau aggregation was prevented for over 16 hours (the timescale of our in vitro assay), and in B515, the T_{50} value increased by ~4.5 hours (Figure 3.8; bottom panels). The increased chaperone activities by bump are consistent with the prevailing model that blocking the edge groove disrupts distal NTR sequestration and increases accessibility of chaperone-active NTR elements.

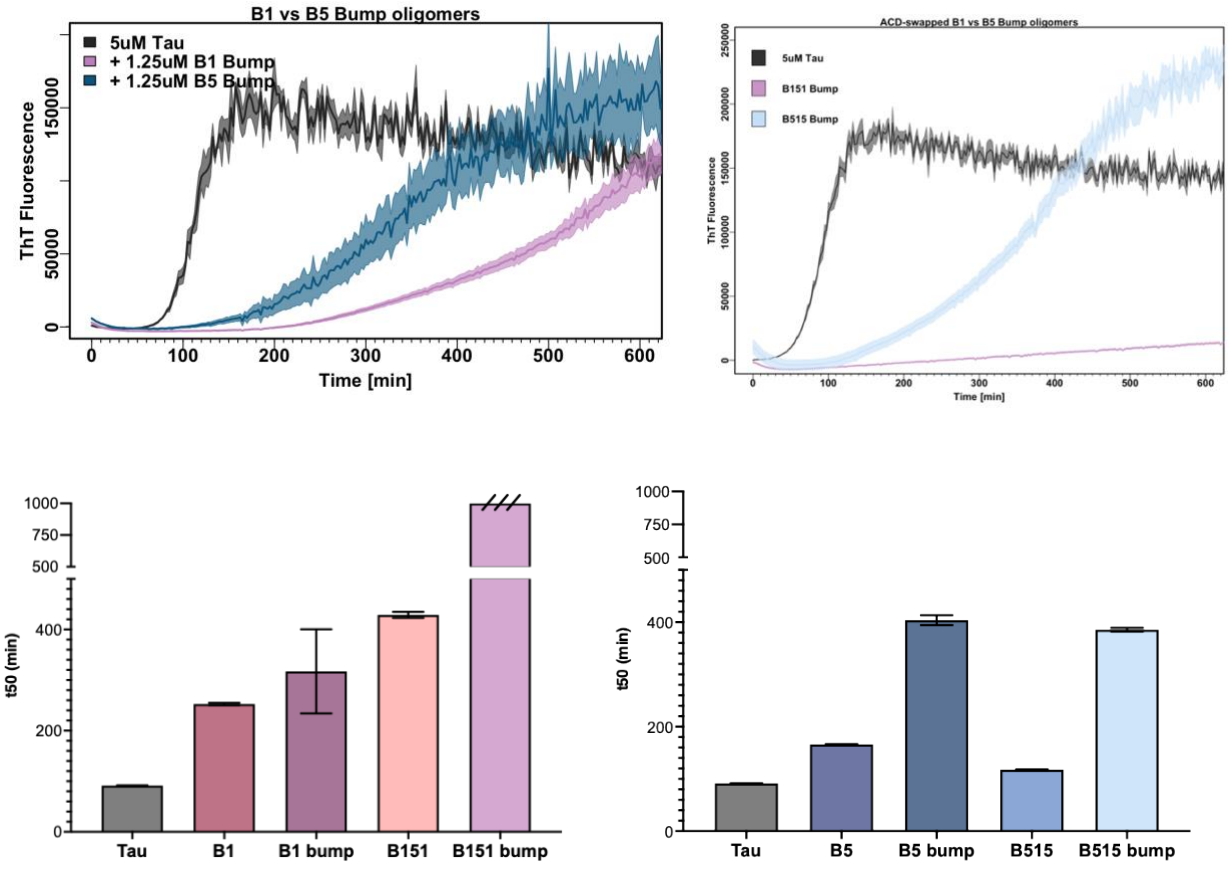

Figure 3.8: in vitro tau aggregation in presence of HSPB1 and HSPB5 bump mutants. Top panels represent tau aggregation in presence of HSPB1 and HSPB5 bump mutants (Left) and their ACD-swapped bumps. Bottom panel shows the same data, analyzed by their T50 values in comparison with their WT-counterparts. All assays are conducted using 5μM Tau with 1.25μM sHSP at 37°C at pH 7.5.

To assess changes in overall oligomer distributions, sHSP molecular weight distributions were measured using mass photometry (MP). MP reports the molecular weight distribution of heterogenous protein assemblies in solution (More detail in Chapter 4). Measurements were performed at 1μM of total protein concentration in PBS at pH 7.5. It is important to note that

sHSPs are sensitive to buffer conditions, including ionic strengths in the buffer (salt concentration) and pH. Disruption of the edge groove can have at least two consequences for oligomerization: 1) loss of CTR-IxI binding and 2) loss of NTR IxI binding. The bump mutation caused a notable shift in HSPB1 oligomer organization, reducing polydispersity and resulting in a narrower molecular weight distribution (Figure 3.9; left). This shift likely reflects disruption of the edge groove mediated interactions that contribute to recruitment and stabilization of larger oligomers. In contrast, the HSPB5 oligomer distribution was largely unaffected by the bump mutation, though it became slightly more heterogeneous based on an increased σ value (Figure 3.9; right). The effects of the bump mutation in the ACD-swapped constructs followed trends observed in their NTR identity. B515 remained in uniform oligomer distribution and was unaffected by the bump mutation. In B151, the bump mutation led to disassembly of the large oligomer population and instead showed an increase in the proportion of smaller oligomeric species (population 1 in B151 and B151 Bump). Overall, these MP results indicate that the bump mutation has different effects on HSBP1 and HSPB5 oligomer assemblies: the oligomer state of HSPB5 constructs were less impacted by domain swaps or bump mutation, while HSPB1's ability to form larger oligomers is diminished, suggesting that its oligomerization depends more on edge groove interactions. They also shed light on fundamental differences in the HSPB1 and HSPB5 NTRs: HSPB5 NTRs holistically drive oligomerization and no specific interactions with the ACD are primary drivers, whereas HSPB1 oligomerization is more dependent on having access to the edge groove.

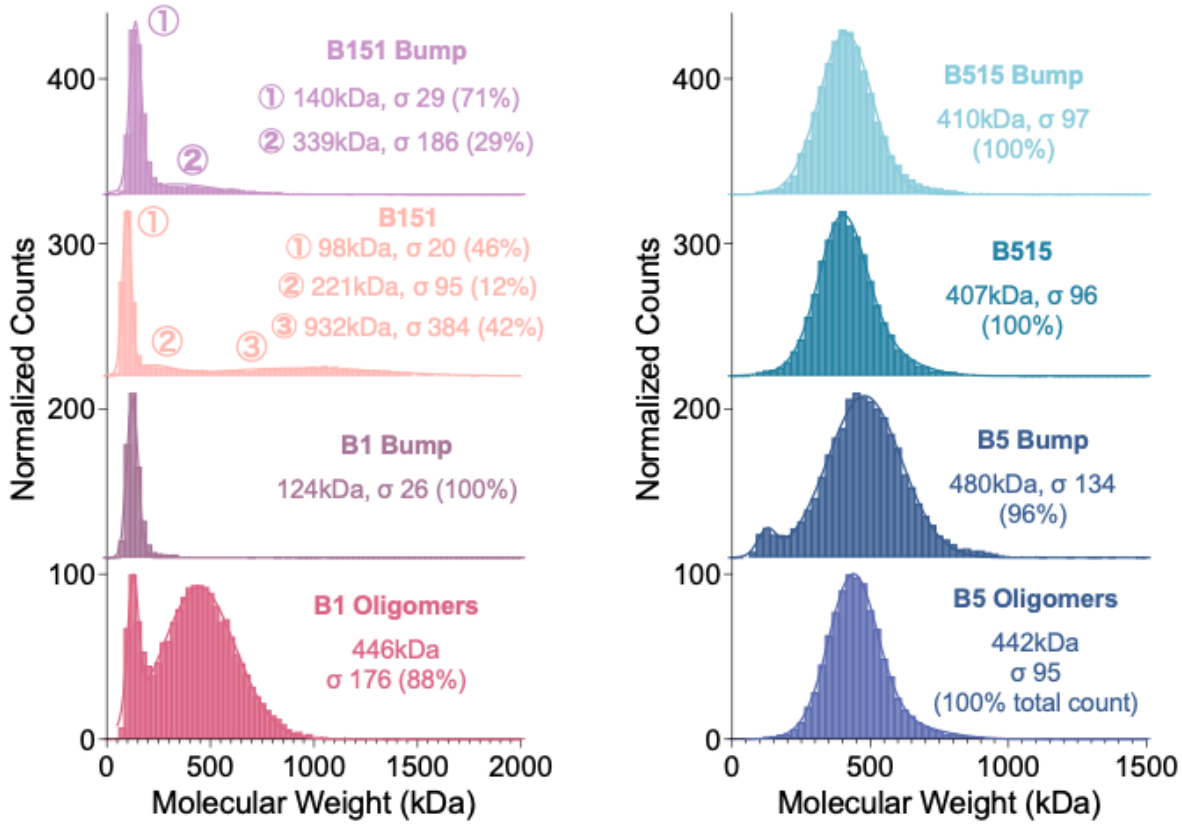

Figure 3.9: Molecular weight distribution of HSPB1 and HSPB5 WT vs bump mutant oligomers measured by mass photometry. HSPB1 constructs on the right; HSPB5 constructs on the left for comparison .Measurements were performed using the dilution-free method in PBS pH 7.5 buffer at 1μM sHSP.

To gain deeper structural insight into how the bump mutation alters local structures, we performed HDX-MS at 4-second time-point for both WT- and ACD-swapped constructs of HSPB1 and HSPB5. Analysis was performed based using fractional deuteration (fractional uptake relative to the theoretical maximum number of total deuterons). Across all constructs, overall HDX-MS patterns were consistent with expected domain architecture: a protected

structured ACD (slow exchange), a highly solvent exposed CTR (fast exchange), and NTR showed sub-region-specific behavior (Figure 3.10). Despite the substantial functional changes observed in tau aggregation assays, HDX-MS perturbations were relatively subtle overall. Still, statistically significant (p=0.05) changes in peptide deuteration were observed in specific regions. To better define the effects, a summary of regions with statistically significant changes upon bump mutation is displayed in Table 3.2. Fractional deuterium uptake is defined relative to the theoretical maximum number of total deuterons. Color indicates magnitude of deprotection: red, changes in uptake from control (Δuptake) >0.5; light orange, Δuptake≤0.5; blank cells indicate no statistically significant change.

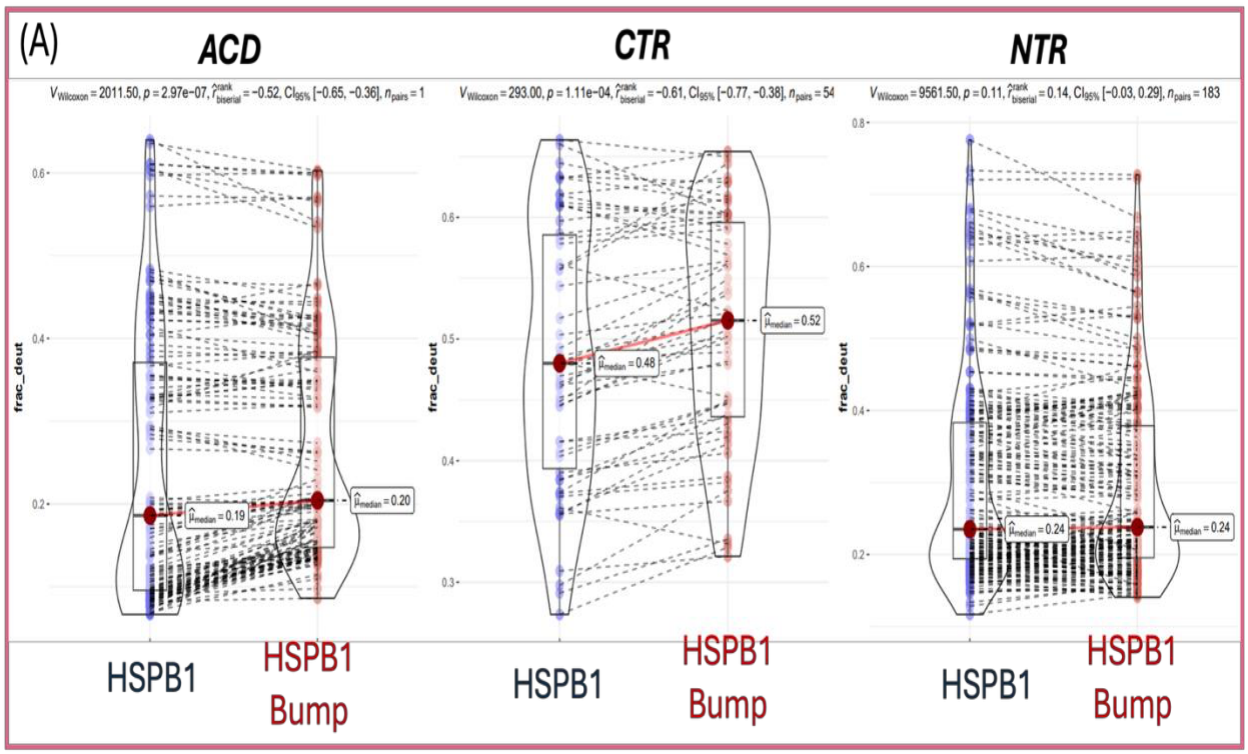

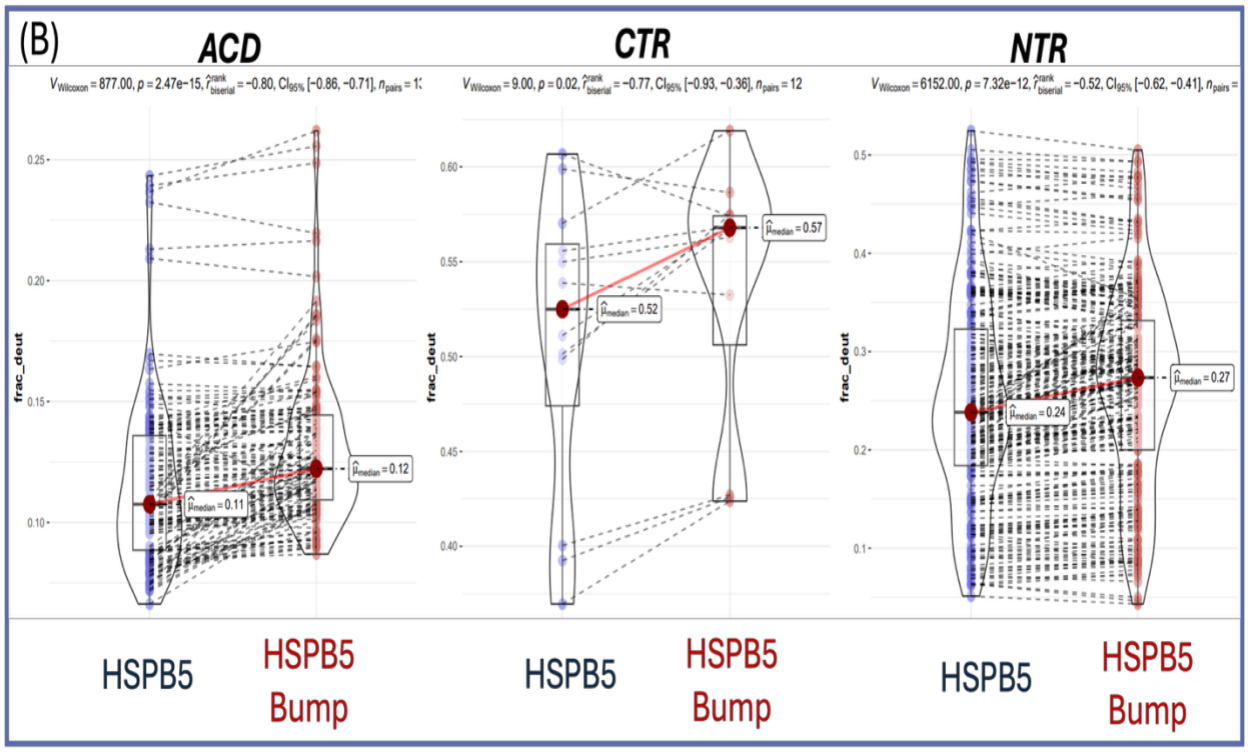
(B)
ACD
CTR
NTR
frac_deut
HSPB5
HSPB5 Bump
HSPB5
HSPB5 Bump
HSPB5
HSPB5 Bump

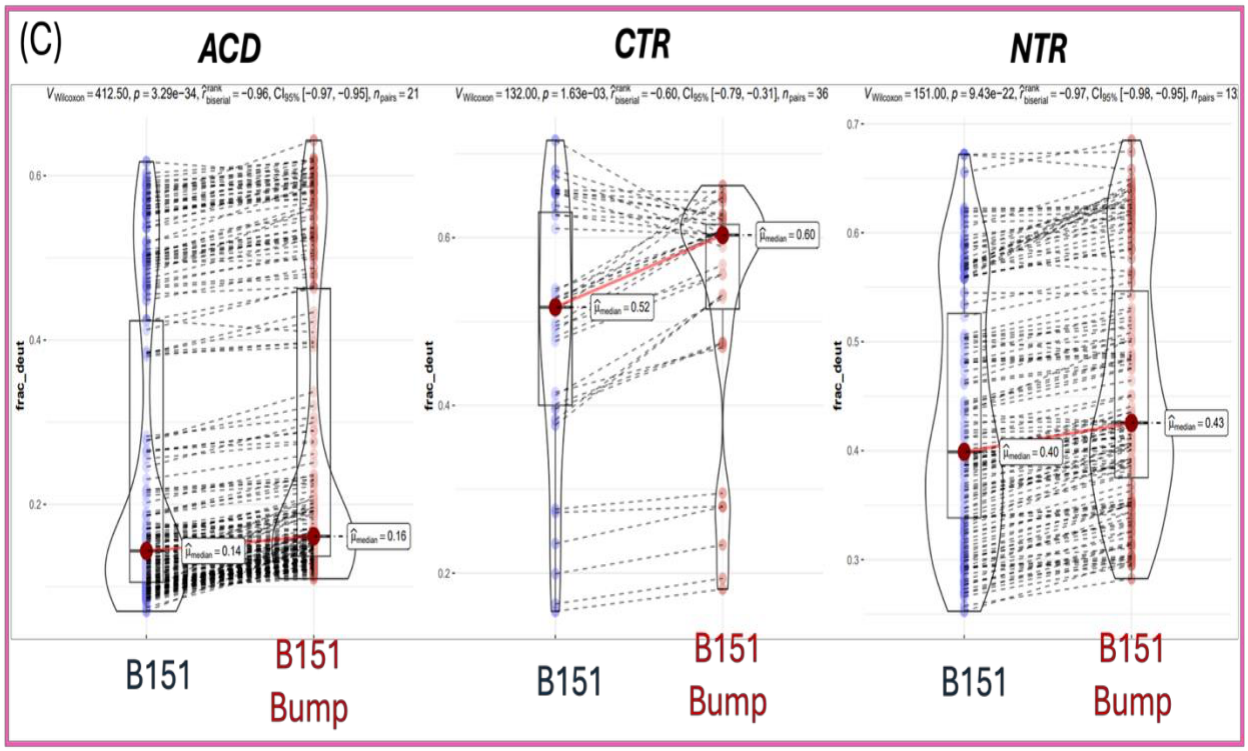
(C)
ACD
CTR
NTR
frac_deut
B151
B151 Bump
B151
B151 Bump
B151
B151 Bump

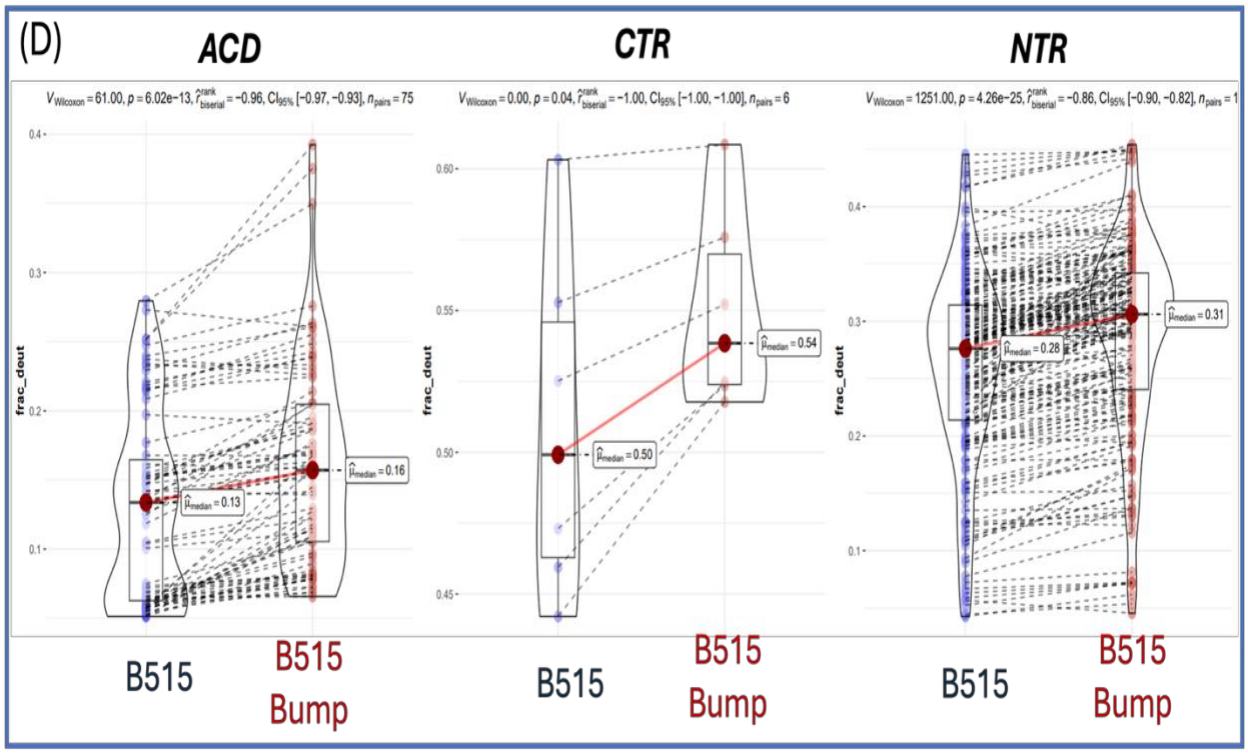

Figure 3.10: Paired HDX-MS peptide analysis for bump mutant constructs of HSPB1 and HSPB5, categorized by their domains. The same peptides are matched from paired dataset with WT constructs shown in blue with their respective bump pair in red. The median value of each domain and its shift in the bump mutant is indicated with red lines.

	FR-A	FR -B	FR -C	FR -D	Insertion	FR -E	β3, β4, loop3/4	β5	Dimer Interface	Loop 7/8	β8/9	Loop 9/CTR
HSPB1 Bump												
HSPB5 Bump					NA							
B151 Bump												
B515 Bump					NA							

Table 3.2: Summary of specific NTR, ACD, or CTR subregions that experience statistically significant differences in peptide deuteriation. Color indicates magnitude of deprotection: red, changes in uptake from control (Δ fractional uptake) >0.5; light orange, Δuptake≤0.5; blank cells indicate no statistically significant change.

The CTR becomes more exposed upon bump mutation in all constructs

The interaction between the CTR IXI motif and the ACD edge groove is a well-studied mechanism for subunit recruitment in sHSPs (19). Disrupting the edge groove by bump mutation would be predicted to reduce CTR sequestration and increase CTR accessibility in solution according to our model. Indeed, the bump mutation increased deuterium uptake in CTR peptides across all four constructs. Average fractional D_2O uptake (fD-uptake) increased by ~0.04 in HSPB1 CTR peptides, and ~0.05 in HSPB5 CTR peptides. Similar CTR exposure changes were also observed in both ACD-swapped constructs. While these changes appear small, most of the CTR is already highly exposed even in WT oligomers, so large shifts are not expected. This strongly supports a common mechanism in which the bump mutation disrupts CTR IxI binding to the ACD edge groove, thus releasing the CTR.

Effects of bump mutation on ACD and NTR local structure.

In contrast to the CTR that showed a consistent pattern across constructs, NTR perturbations differed between HSPB1 and HSPB5. HSPB1 exhibited no statistically significant changes in NTR upon bump mutation, whereas HSPB5, B151 and B515 (B5-containing constructs) showed increased deuterium uptake in all NTR sub-regions except FR-C. FR-C is conserved throughout sHSP, and FR-C interaction with the dimer interface is presumably maintained regardless of bump mutation. In HSPB5 and B515, the largest deprotection was seen in the FR-A and FR-B. Deprotection in this region suggests altered interaction between HSPB5 NTR IxI motif and the ACD edge groove due to the bump mutation. In addition, FR-D which contains “critical residues”, implicated in modulating HSPB5 chaperone function, showed increased exposure in HSPB5 and B5 containing chimeras (B151 and B515).

In addition to NTR effects, the bump mutation increased overall deuterium uptake in the ACD for all constructs. In HSPB1, the bump mutation caused deprotection at ACD residues 95-126 and 142-154. These residues encompass β3, loop3/4, β5, and loop7/8. A similar pattern is observed in B151 bump, where residues 90-124 corresponding to β3, loop3/4, and β5 become more exposed. In HSPB5 constructs, only ACD residues 72-92 increased fD-uptake in HSPB5-Bump, but B515-Bump led to increased exposure throughout the ACD. In all constructs, shared deprotection mapped to β3, loop3/4, and β4. This region has been implicated in regulating NTR accessibility (12), and in HSPB1 specifically, loop3/4 has been shown to interact with NTR FR-B residues in NMR experiments (1). Furthermore, deprotection was also observed in the NTR FR-E region in HSPB5 containing constructs, consistent with altered β-sheet interaction (β2/β3) at the NTR-ACD boundary as described in Chapter 2. In addition to perturbation in the early ACD residues, adjacent β5 residues in all constructs except HSPB5 become deprotected. Overall, the bump mutation alters both NTR and ACD local structure and increases accessibility within oligomers. Moreover, these data suggest that the HSPB5NTR engages more strongly and/or more frequently in interactions that depend on the ACD edge groove, whereas solvent exposed HSPB1 NTR may be interacting with its edge groove more transiently under these conditions.

Our initial model (Figure 3.6) predicted that abrogating edge groove interaction would lead to complete release of the NTR but instead, the structural effects appear more subtle and specific. Results here support a refined model in which the bump mutation disrupts specific edge groove dependent interactions, particularly those involving IxI motifs, leading to partial release of distal NTR regions rather than complete NTR dissociation from the ACD. In HSPB5, this partial release is detectable by HDX-MS at early time points, whereas in HSPB1, NTR changes may be too subtle to resolve at a single early time point. Additionally, previous HDX-MS

analyses of HSPB1 and HSPB5 revealed bimodality in several NTR regions, including FR-A (1,12,23). Analysis by average fractional uptake method instead of bimodal analysis may obscure population-specific changes (i.e. bound vs unbound NTR states). It is also noteworthy that bump mutation caused shared increased D-uptake in early ACD sequence even at the 4-second time point. Because the ACD is typically well protected and often requires longer exchange with deuterons to resolve changes. This suggests that bump mutation can rapidly influence local structure and/or dynamics of distal NTR, ACD, and CTR IxI motif.

3.2.3 Hetero-oligomerization of HSPB1 and HSPB5

The heterogeneity of small heat shock proteins (sHSPs) extends beyond the formation of homo-oligomeric assemblies. In addition to forming distinct homo-oligomers, HSPB1 and HSPB5 are co-localized and co-expressed in cells (24-28), including in neurons, and have been shown to spontaneously hetero-oligomerize *in vitr*o (29-30). Both proteins are present not only in normal tissues but also in pathological tissues from patients with neurodegenerative diseases (31-33). This suggests functional cooperation between these two sHSPs under physiological and stress conditions. However, the structural organization and functional consequences of HSPB1-HSPB5 hetero-oligomerization remain poorly defined. In this section, I characterize hetero-oligomeric species formed by HSPB1 and HSPB5 *in vitro*, and examine how hetero-oligomerization alters their assembly, activity, accessibility, and molecular interactions underlying these effects.

Interaction of HSPB1 and HSPB5 produce hetero-oligomers in vitro with distinct features

To characterize hetero-oligomerization of HSPB1 and HSPB5 *in vitro*, we examined whether mixing these two proteins results in assemblies that are distinct from their respective homo-oligomers. We employed two complementary, label-free, solution-based techniques: analytical sizing exclusion chromatography using a Superose 6 10/300 GL column (aSEC) and mass photometry (MP). While both methods report on oligomer size and heterogeneity, they probe different physical properties of the sample and operate at different concentration ranges, which is particularly relevant given the concentration dependence of HSPB1 oligomers. Analytical SEC separates samples based on hydrodynamic radius as they move through porous polymer beads. Mass photometer outputs molecular mass distributions of individual particles in solution using interferometric light scattering of single molecules that bind to a glass surface. Together, these techniques provide orthogonal views of oligomer size, mass, and polydispersity.

Intriguingly, aSEC elution profile and MP measurements produced apparently conflicting results. By aSEC, the elution profile of a HSPB1-HSPB5 mixture does resemble the predicted profile for two non-interacting species. Paradoxically, the elution profile appears to resemble that of HSPB5 homo-oligomers (Figure 3.11A). MP similarly shows that a 1:1 mixture assembles into a distribution more similar to HSPB5 (Figure 3.11B). This discrepancy in oligomer size between aSEC and MP could be due to differences in their interactions with the aSEC resin. Additionally, aSEC involves dilution of samples as they pass through the resin (~10-fold), whereas MP does not. I hypothesize that the HSPB5-like elution profile observed by aSEC arises from increased exposure of disordered B5NTRs or CTRs, which may interact with the resin as it passes through the column. Furthermore, HSPB1-HSPB5 mixtures were analyzed across varying stoichiometric ratios. MP measurements showed that increasing HSPB1 content resulted in larger

average MW and increased polydispersity, whereas increasing HSPB5 content reduced both parameters, while still yielding assemblies larger than HSPB5 homo-oligomers (Figure 3.11B). This continuous, ratio-dependent shift in MW and heterogeneity supports the conclusion that HSBP1-HSPB5 assemblies represent a unique class of oligomers, distinct from either homo-oligomer species.

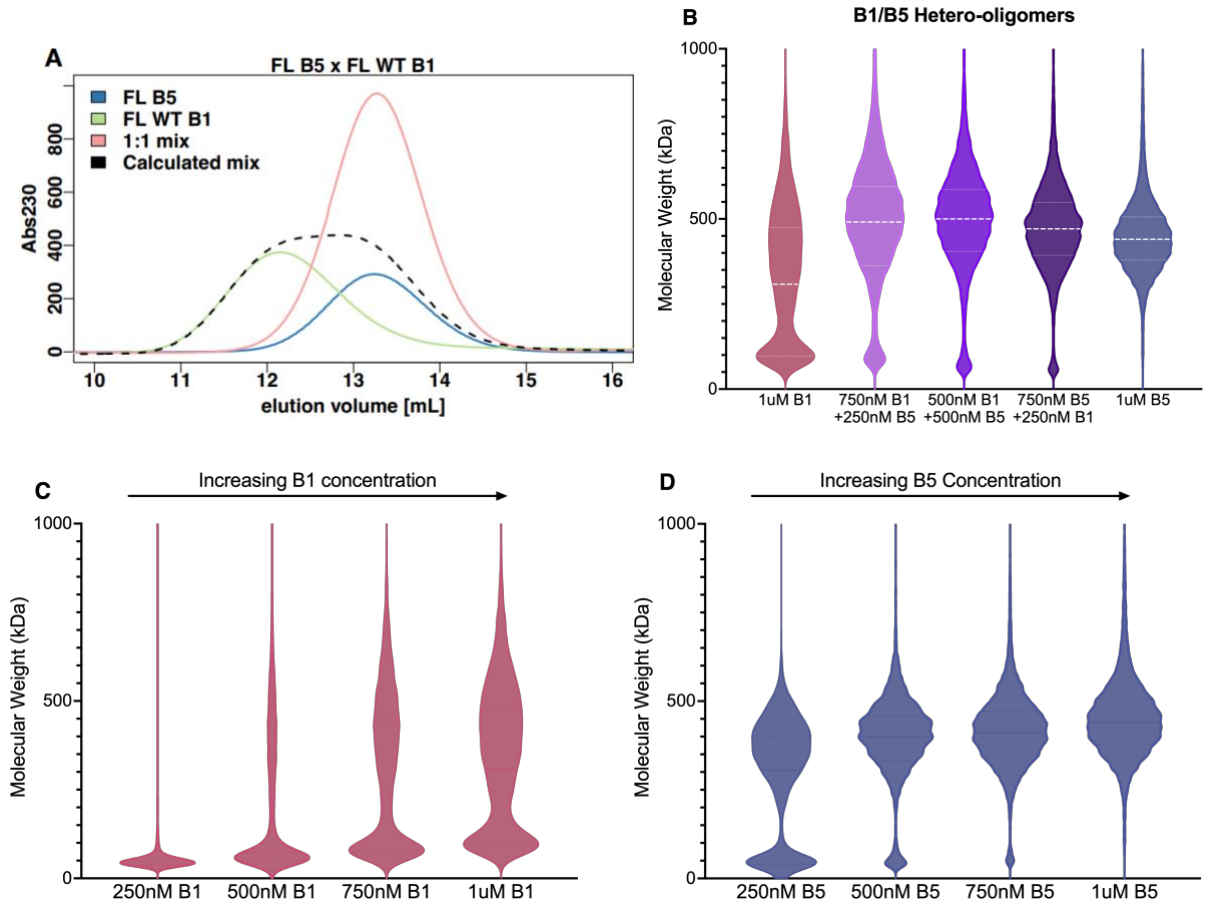

Figure 3.11: Oligomer size and distribution of HSPB1-HSPB5 hetero-oligomers. (A) Analytical sizing exclusion chromatography with GE Superose 6 10/30L of HSPB1, HSPB5 homo- and heter-oligomers. 200µM of each sHSP is injected at pH 7.5. B) Molecular weight distribution of sHSP hetero- and homo-oligomers of HSPB1 and HSPB5 measured by mass photometry. Mixture of HSPB1 and HSPB5 led to formation of distinct species that is more heterogeneous and

polydisperse compared to their homo-oligomers. They are also ratio depended, where polydispersity and size increased with increasing HSPB1 content. Controls of concentrations of HSPB1 (C) and HSPB5 (D) tested are shown on the bottom panels for each concentration range. Measurements are performed at total protein concentration of 1μM by dilution-free method at pH 7.5 in PBS post 3 hour incubation at the final concentration.

Activity of HSPB1-HSPB5 hetero-oligomers toward tau aggregation

Given the clear evidence of hetero-oligomerization, we wondered how chaperone function of both HSPB1 and HSPB5 is affected by hetero-oligomerization. For some sHSP pairings, such as HSPB4-HSPB5 in the eye lens, hetero-oligomer stoichiometries are well defined *in vivo* (34). However, the relative abundance and stoichiometry of HSPB1-HSPB5 hetero-oligomers in cells are not well established and likely change in response to changing cellular conditions. To capture a range of potential assemblies, we tested equimolar ratio (1:1), as well as 3-fold excess of either HSPB1 or HSPB5 for tau aggregation assays. In the range of concentrations tested (2.5μM – 0.625μM sHSP for 5μM Tau), chaperone activities of HSPB1 and HSPB5 homo-oligomers showed only minimal changes in chaperone activity with increasing sHSP concentration (Figure 3.12; bottom). When HSPB1 and HSPB5 were mixed at a 1:1 ratio, the overall chaperone activity was intermediate between that of the two homo-oligomers. Increasing the proportion of either HSPB1 or HSPB5 shifted activity toward that of the dominant species (Figure 3.12; top). These results suggest that hetero-oligomerization partially attenuates HSPB1 chaperone activity for tau while simultaneously enhancing HSPB5 activity. In other words, parts of HSPB1's tau chaperoning function appear to be shielded by the presence of HSPB5, whereas HSPB5 becomes activated through association with HSPB1. This tunability of

chaperone function through hetero-oligomerization provides a potential mechanism by which cells fine-tune sHSP in response to cellular stress.

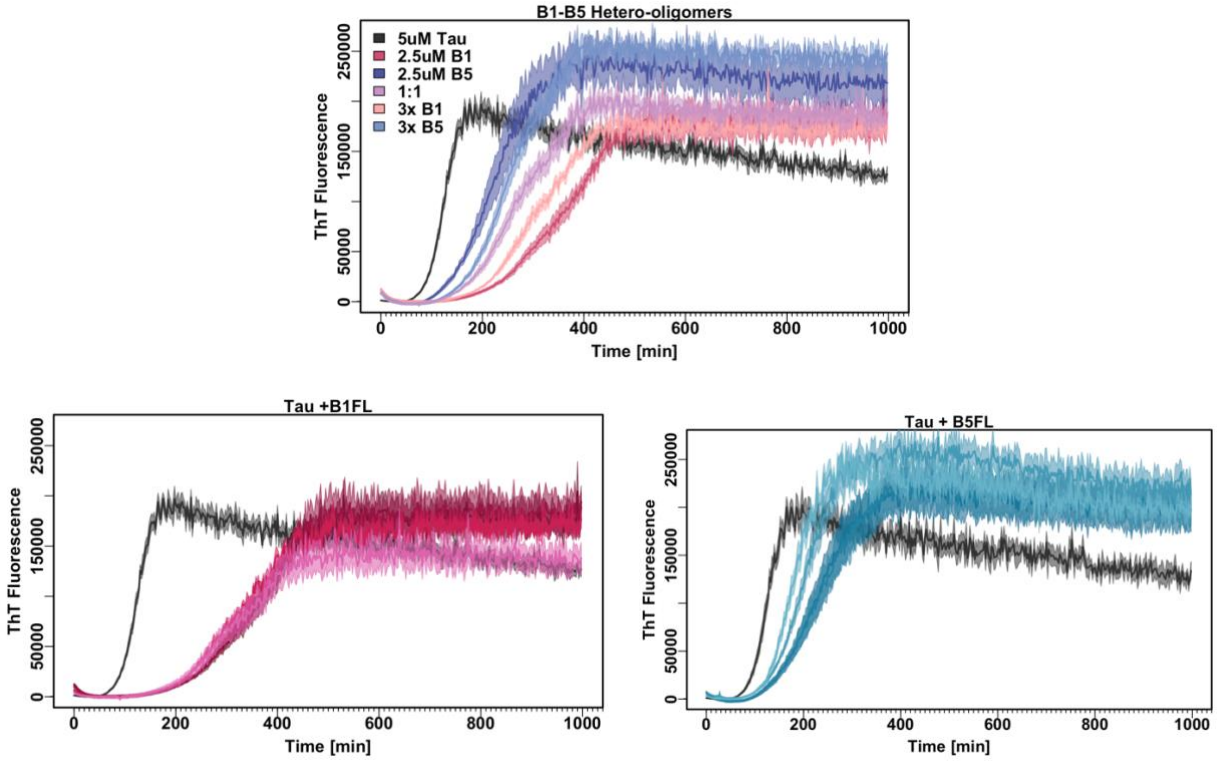

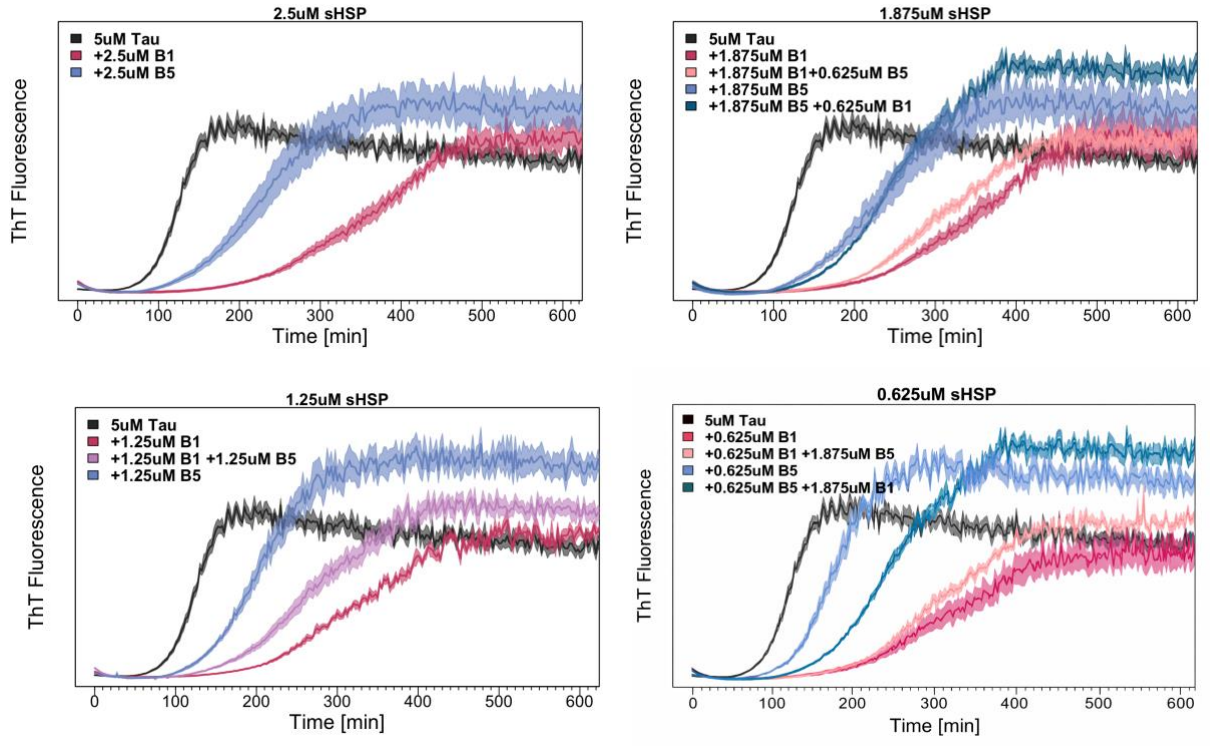

Figure 3.12: Chaperone function of HSPB1-HSPB5 hetero-oligomers toward in vitro tau aggregation. Top) Comparison of HSPB1 and HSPB5 hetero-oligomer mixtures. All mixtures contained total sHSP of 2.5μM with 5μM tau aggregation reaction. 1:1 equal ratio mixture is at 1.25μM:1.25μM; 3:1 mixture used 1.875μM:0.625μM concentration. Bottom) Chaperone function of HSPB1 and HSPB5 homo-oligomers at the same concentration range tested. Darker shade indicates higher concentration in both panels with tested concentration of 2.5μM, 1.875μM, 1.25μM, and 0.625μM sHSP concentration. The chaperone functions at each concentration are also shown.

Hetero-oligomerization alters NTR accessibility in HSPB1 and HSPB5

We next investigated how hetero-oligomerization alters the accessibility of specific NTR subregions in HSPB1 and HSPB5. In both HSPB1 and HSPB5 homo-oligomers, NTR

accessibility is regulated by networks of NTR-ACD interactions within the oligomer, controlling exposure of functional regions involved in client binding. To our surprise, hetero-oligomerization produced reciprocal global effects on the two proteins. Overall NTR exposure decreased in HSPB1, whereas NTR exposure increased in HSPB5 (Figure 3.13A). Under basal conditions, HSPB1 NTRs are generally more solvent exposed and accessible to tau, while HSPB5 NTRs are more sequestered (12,14). The reversal of this trend in hetero-oligomers suggests that reorganization of intermolecular interactions within the mixed oligomers redistributes NTR accessibility.

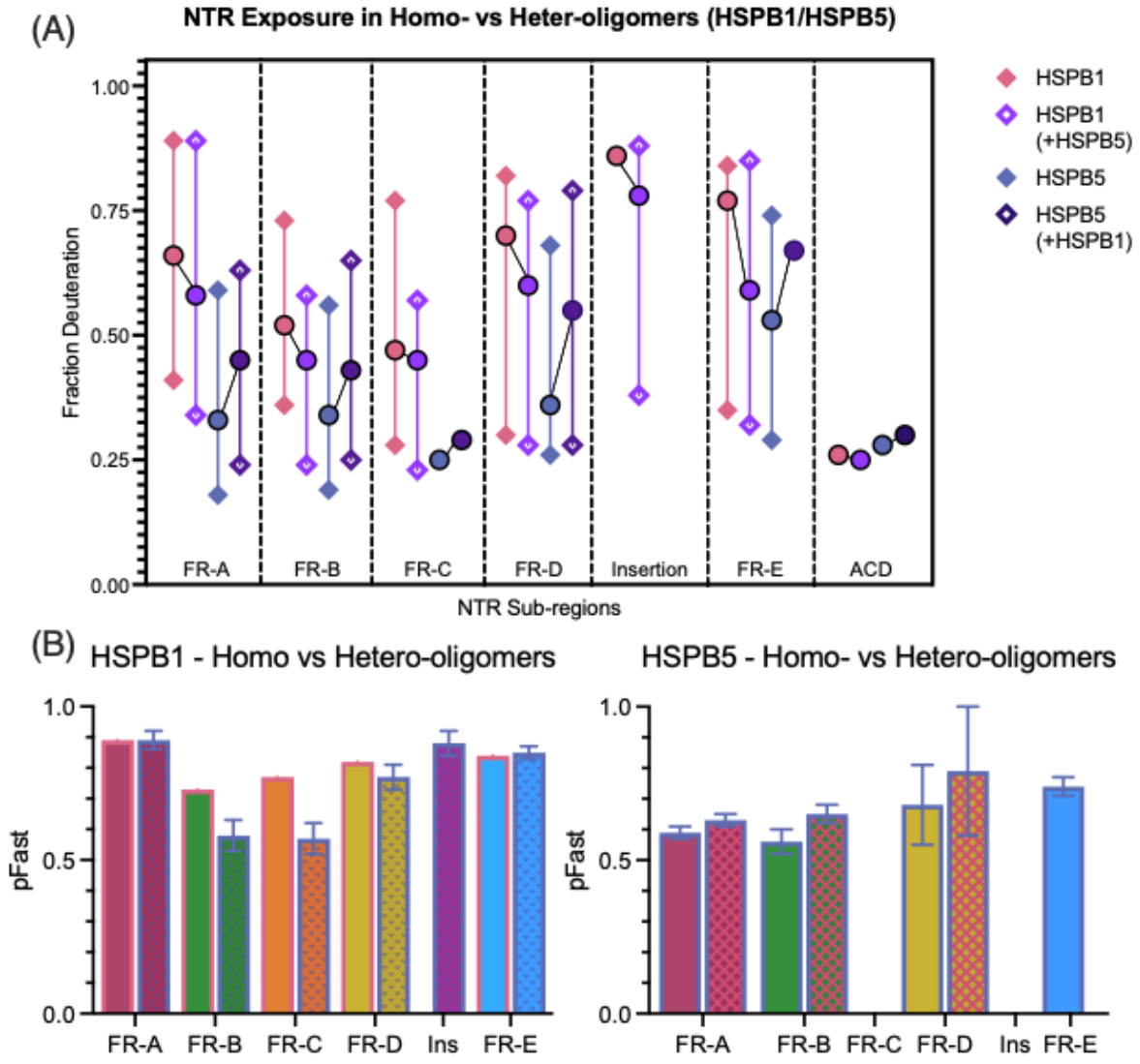

Figure 3.13: NTR sub-region Exposure by HDX-MS at 5-second time point. All peptide data was aggregated to obtain near-residue-level fractional deuterium-uptake values, followed by bimodal analysis using the pyHXExpress workflow (35). (A) Average fractional D-uptake for each NTR-subregion, calculated from the centroids of unimodal fits, is shown as circles (○). Deuteration levels of the two populations (slow and fast states) determined from bimodal analysis are plotted as diamonds (◇) in the corresponding color scheme. Homo-oligomers are shown as pink for HSPB1-WT; blue for HSPB5-WT; and the hetero-oligomers shown in different shades of purple.

Comparisons are made for each NTR-subregions between the HSPB1 or HSPB5 peptides in homo- vs hetero-oligomer context. (B) Relative populations of the slow (p_{slow}) exchange modes for each NTR-subregion are shown are shown for HSPB1 (left) and HSPB5 (right), comparing homo- and hetero-oligomer conditions.

To quantify these effects of hetero-oligomerization of HSPB1 and HSPB5 on specific NTR sub-regions, the peptide data for each sub-region were aggregated to obtain average fractional deuteration-uptake (fD-uptake) for each NTR subregion (Figure 3.13A). All NTR subregions exhibited reciprocal behavior upon hetero-oligomerization: HSPB1 became more protected, while HSPB5 became more exposed.

FR-A and FR-B showed similar magnitudes of reciprocal change in fD-uptake. In HSPB1, fD-uptake decreased from 0.66 to 0.58 in FR-A and 0.52 to 0.48 in FR-B. In contrast, HSPB5 exhibited increased fD-uptake (0.33 to 0.45 in FR-A; 0.34 to 0.43 in FR-B). FR-A contains the "IxI" motif, which mediates binding to the ACD edge groove and scaffolds the NTRs in the oligomer in both proteins. The reciprocal pattern observed here suggests that HSPB1 and HSPB5 compete for edge groove interactions, with HSPB1 gaining access to HSPB5 ACD binding sites previously occupied by HSPB5 NTR. Both FR-A and FR-B peptides display bimodality attributed to existence of two states: a solvent exposed (fast-exchange) state and a more protected (slow-exchange) species, presumably reflecting differences in ACD binding. In HSPB1, there is no substantial change in distribution of bound/unbound states between homo- and hetero-oligomers. On the contrary, HSPB5 has a higher population of protected species in homo-oligomers but shifted toward approximately having higher population of unprotected species upon hetero-oligomerization (Figure 3.13B).

FR-C corresponds to the conserved NTR sequence capable of binding the ACD dimer interface. FR-C showed the least perturbation within the NTRs for both proteins, indicating that this region remains largely protected and scaffolded in both homo- and hetero-oligomers. HSPB5 FR-C is the most well-protected region across all mixtures and remained unimodal (i.e. essentially all is highly protected).

FR-D exhibited the largest deprotection in HSPB5, with fD-uptake increasing from 0.36 to 0.55, while HSPB1 became more protected (0.70 to 0.60). This region of HSPB5 has been implicated in holding chaperone function for another client gamma-D, highlighting how hetero-oligomerization can expose functionally relevant regions by reorganizing oligomeric interactions. In line with this notion, the unprotected population of HSPB5 FR-D substantially increases upon hetero-oligomerization. In HSPB1, an insertion sequence that is highly solvent exposed by HDX-MS also became more protected in hetero-oligomers (0.86 to 0.78), consistent with global HSPB1 NTR protection.

Finally, FR-E showed pronounced reciprocal changes and is the only NTR sub-region with higher average fD-uptake in HSPB5 than HSPB1. In HSPB1, FR-E shifted from predominantly fast-exchange peptides in homo-oligomers to a mixed fast/slow population, with average fD-uptake decreasing from 0.77 to 0.59, which is the largest protection change observed in HSPB1. In contrast, HSPB5 FR-E became more exposed, with fD-uptake increasing from 0.53 to 0.67 and exists as a unimodal fast-exchange state. This pattern suggests that upon hetero-oligomerization, HSPB1 FR-E forms β-sheet interaction with an ACD (Chapter 2) to gain overall NTR protection. In HSPB5, β2/β3 interactions could be out-competed by HSPB1 FR-E, leading to untethering of its NTR to become more solvent accessible. Indeed, FR-E has been proposed to act as a regulatory hub that alters NTR conformation through forming β-sheet interaction with

parts of the ACD as discussed in Chapter 2. Overall, these structural changes align well with the intermediate chaperone activity observed for hetero-oligomers in tau aggregation assay. Moreover, HSPB5 regions with proposed chaperone activity (FR-B for tau; FR-D for gamma-D) are deprotected whereas HSPB1's FR-E that's active for tau become more protected.

NTR Distal "IxI" can bind to either HSPB1 or HSPB5 ACD

To dissect the interactions governing hetero-oligomerization, we examined distal NTR-ACD interactions mediated by IxI motifs in FR-A. Peptides from HSPB1 and HSPB5 containing the FR-A IxI motif were titrated into ^{15}N-labeled ACD-only constructs of each protein and analyzed by NMR (Figure 3.14). For both ACDs, peptide addition induced chemical shift perturbations localized primarily to the edge groove. In general, addition of the HSPB5 peptide to HSPB1-ACD caused larger perturbations than addition of HSPB1 peptides. Thus, HSPB1ACD binds the HSPB1 distal peptide more weakly than the HSPB5 distal peptide. Complementary experiments performed with ^{15}N-labeled HSPB5 ACD showed that HSPB5 binds its own distal IxI motif approximately 10-fold more strongly than the HSPB1 IxI motif (data not shown). Together, these NMR results indicate that HSPB1 NTR IxI motif is a weaker binder to both ACDs, likely due to its unusual IxI sequence.

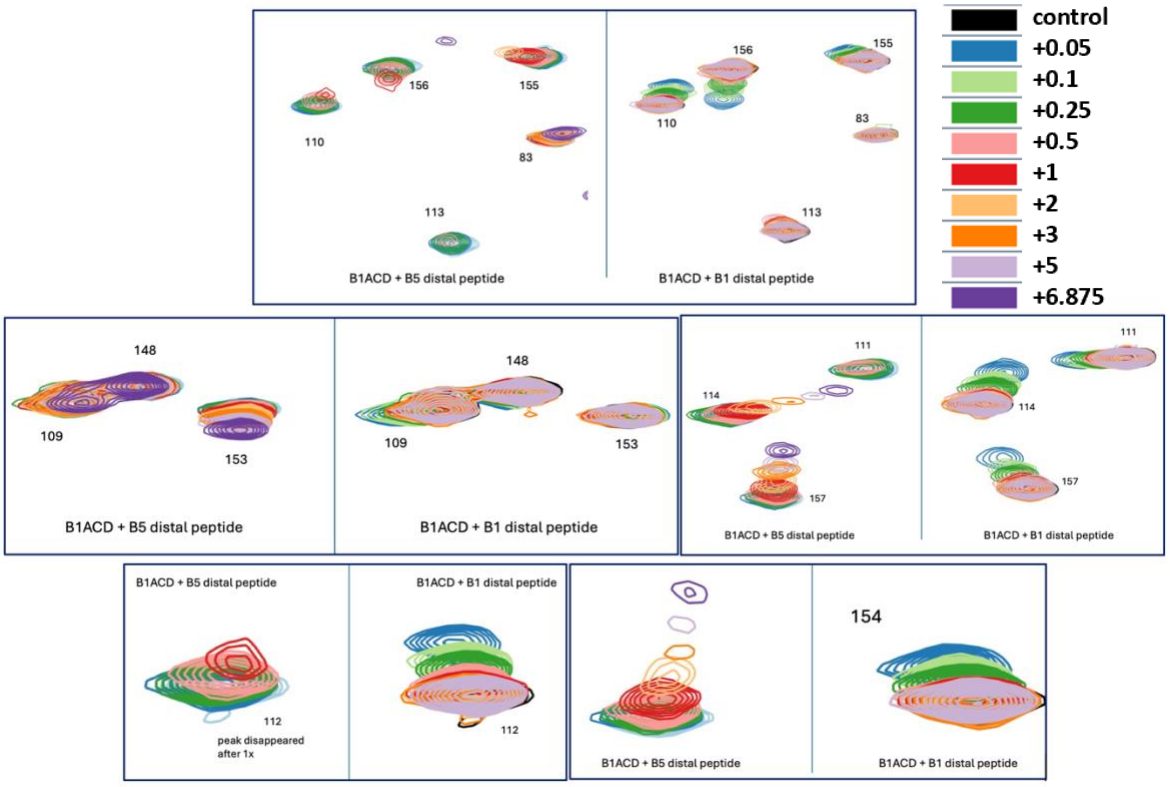

Figure 3.14: NMR distal peptide titration experiments on N15-labeld HSPB1-ACD. HSPB1-ACD residues showing chemical shift perturbation or peak disappearances are shown for addition of HSPB1 distal peptides up to 5x molar excess or HSPB5 distal peptides up to 3x molar excess, due to solubility. All experiments are performed using 200μM ACD on 500Hz Tess NMR at pH 7.5. Corresponding color legend for peptide concentration added is shown.

Bump effects on HSPB1-HSPB5 hetero-oligomers

To further probe the role of ACD edge groove binding, we applied a bump strategy presented above (Section 3.2.2) to selectively disrupt IxI-edge groove interaction. The effect of each bump mutation was evaluated by mass photometer for size and aggregation assay for activity. First, MP revealed that eliminating either edge groove alone did not dramatically disrupt

hetero-oligomer formation (Figure 3.15; left). Removing the HSBP5 edge groove slightly reduced average molecular weight and increased polydispersity, while eliminating the HSPB1 edge groove led to the formation of smaller oligomer population, but most oligomer species stayed in the larger oligomer (89% total population in large oligomer). However, simultaneously blocking both edge grooves destabilized larger oligomers, producing a smaller tetramer-like species, making up about 83% of total distribution. These results indicate that either edge groove can compensate to support hetero-oligomer assembly, but loss of both interactions compromises oligomer stability. Intriguingly, tau aggregation assays showed that hetero-oligomers lacking both edge grooves exhibited the highest chaperone activity (Figure 3.15; right). Assemblies with only one edge groove disrupted displayed intermediate activity between WT-heterooligomers and double-bump hetero-oligomers. These findings, together with HDX-MS and NMR data suggest that abrogating NTR-ACD interactions by taking away the edge groove further rearranges the oligomers, enhancing activity. Further investigation of other functional NTR sub-region binding to ACD is needed to create a full picture of sHSP interactome within hetero-oligomers.

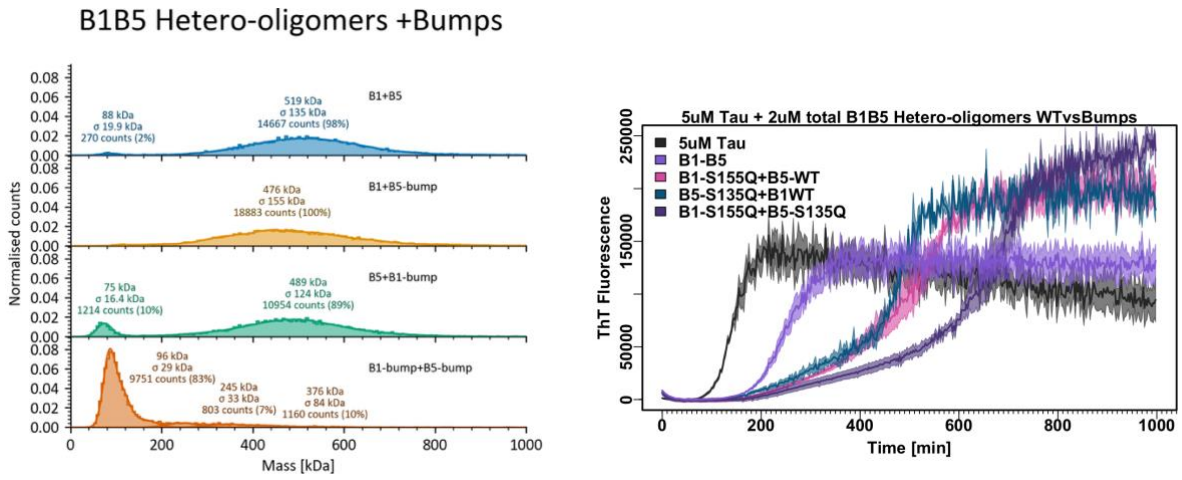

Figure 3.15: Consequences of bump mutation in HSPB1-HSPB5 hetero-oligomerization. (Left): Molecular weight distribution of HSBP1-HSPB5 hetero-oligomers mixes with WT and Bump

mutation combinations, measured by mass photometry. 1μM total sHSP is tested with equal ratio (0.5μM+0.5μM) of each species incubated for three hours prior to the measurements. (Right): in vitro tau aggregation assay in presence of HSPB1-HSPB5 hetero-oligomer bump mutants. 2μM total sHSP concentrations were added to 5μM tau aggregation assay at 37°C, induced by polyphosphate.

ACD-ACD hetero-dimerization

For both homo-oligomers, homo-dimerization of two ACD units is an important step in assembling sHSP oligomers. Previous NMR studies from our lab demonstrated that HSPB1 and HSPB5 ACDs can form hetero-dimers. Using ^{15}N-labeled HSPB5 ACD-only construct, titrating unlabeled HSPB1 ACD showed chemical shift perturbations, specifically at the dimer interface (data not shown). Thus in hetero-oligomers, three potential dimeric units exist: 1) HSPB1 homo-dimers, 2) HSPB5 homo-dimers, 3) HSPB1-HSPB5 hetero-dimers. Further investigation of affinities for homo- vs hetero-dimerization of the ACD could help parse out how by hetero-oligomerization reorganizes assembly.

NTR-NTR interactions happen between HSPB1 and HSPB5 (BPA)

In addition to interactions facilitated by ACD, NTR-NTR contacts provide another layer of complexity (34). Crosslinking experiments using BPA incorporated throughout the NTRs of HSPB1 and HSPB5 revealed additional crosslinks upon hetero-oligomerization. Further optimization is needed to better optimize reproducible crosslinks (Discussed further in chapter 4), but BPA-XL-MS analysis of hetero-dimers could further reveal key interactions within the hetero-oligomer network.

3.3 Discussion

In this chapter, NTR-ACD interactions were disrupted in several ways to better define how the quasi-order network within the sHSPs is established, maintained and modulated. Because sHSP oligomers are heterogeneous and highly dynamic, features that complicate analysis by traditional structural methods, we used a layered set of complementary approaches. Hydrogen-deuterium exchange mass spectrometry (HDX-MS) was used to assess local structural protection and dynamics, mass photometry (MP) to quantify oligomer distributions, and tau aggregation assays to evaluate how such perturbations translated into altered chaperone function. Across all perturbations tested, HSPB1 and HSPB5 responded in distinct ways, revealing both conserved and protein-specific features of their quasi-order networks.

First, HSPB1 disease-associated mutations in the NTR produced variable and site-specific consequences. Rather than globally destabilizing oligomer or uniformly increasing NTR exposure, each disease mutation altered protection patterns in a way that depended strongly on its location and interaction within the NTR. This reinforces the idea that NTR contains multiple sub-regions that participate in specific NTR-ACD interaction networks that are also interconnected.

Second, perturbation of the ACD edge groove using the bump strategy produced different effects in HSPB1 versus HSPB5. In HSPB1, abrogation of edge groove interactions destabilized the larger oligomeric species, shifting the distribution toward smaller assemblies. In contrast, HSPB5 maintained its overall oligomeric distribution despite losing the analogous groove, indicating that HSPB5 oligomers are either less reliant on edge groove binding or are stabilized through compensatory interactions like NTR-NTR, other NTR-ACD contacts, or the conserved region mainly drives oligomerization in HSPB5. In other words, the drive of HSPB5 NTR to be

sequestered is so strong that it has multiple pathways to achieve protection. Although both proteins can be activated by bump mutation, divergent effects on oligomerization highlight different intrinsic properties of HPSB1 and HSPB5. The difference in HSPB1 and HSPB5's response to bump mutation suggests that activation and oligomerization are not obligatorily linked and that two proteins employ distinct strategies for tuning oligomer architecture and activity. HDX-MS further revealed that the bump mutation exposes the CTR but does not simply "free" the NTR by removing a binding site as originally presumed (Figure 3.6). Instead, perturbations propagated into the ACD. Specifically, decreased protection was consistently observed at residues within β3/β4 and loop3/4 across all bump constructs tested. Similar to the observation of the ACD-swaps, increased exposure in FR-E could reflect reduced β2/β3 interactions at the NTR-ACD boundary (12). While further bimodal analysis or longer exchange time may be needed, the NTR also experiences deprotection, especially at the N-terminal distal end (FR-A and FR-B) in HSPB5 containing species (HSPB5 bump, B515 bump, B151 bump). However, these structural changes are modest compared to the dramatic functional effects of the bump mutation. Although many mechanistic models have emphasized the NTR, these results show the ACD-local changes can also contribute to activated response and that disrupting edge groove availability triggers rearrangement of multiple interaction nodes simultaneously. Because edge groove binding is central to the architecture of the oligomer, its perturbation likely forces redistribution of NTR and CTR interactions, changes in ACD dynamics, and altered competition for binding sites. As a result, it may be difficult to reduce the consequences of bump mutation to a single structural event given such interconnectivity within the sHSP oligomers.

In a realistic cellular context, it is unlikely that all edge grooves in oligomers would become simultaneously unavailable, as occurs with the bump mutation. Instead, edge groove

occupancy by a client protein or co-chaperone likely occurs transiently at a subset of sites. Such edge groove binding event could trigger local rearrangements and competition among potential binders. Given the transient nature of sHSP interactions with each subunit, higher affinity binding with clients or co-chaperones would be able to rearrange the oligomers. This would allow for either 1) release of subunits from the oligomers to generate more solvent-exposed active forms, as proposed in some models (9,11), and/or 2) stabilization of client binding within the oligomer through edge groove by sequestering misfolded proteins until re-folding activity by ATP-dependent chaperones.

Finally, HSPB1-HSPB5 hetero-oligomerization produced intriguing trends: the dominant effects seen at early-time point were localized within the NTRs, and these effects moved in opposite direction for the two proteins. Hetero-oligomerization of HSPB1 and HSPB5 is a biologically relevant process as two proteins are co-expressed and co-localized in cells, and they spontaneously form hetero-oligomers *in vitro*. MP and aSEC confirmed formation of a distinct hetero-oligomeric species that is larger and more polydisperse than either homo-oligomers. The distribution is dependent on stoichiometry: increasing the HSPB1 content promoted larger, more polydisperse assemblies, whereas increasing HPSB5 shifted the population to the opposite pattern. HDX-MS showed that in hetero-oligomer, the HSPB1 NTR becomes globally more protected, while the HSPB5 NTR becomes more exposed. This pattern is striking when compared to the ACD-swapped chimeras analyzed previously in Chapter 2. In the ACD-swapped constructs, introducing the HSPB5 ACD into HSPB1 scaffold increased HSPB1 NTR exposure (B151), whereas the HSPB5 NTR showed minimal perturbation in the reciprocal chimera (B515). By contrast, in the heterooligomers, the presence of additional HSPB5 subunits leads to increased protection of the HSPB1 NTR, while presence of HSPB1 drives deprotection of the

HSPB5 NTR. This discrepancy suggests that hetero-oligomerization cannot be explained solely as a simple sum of heterotypic NTR-ACD binding possibilities. Instead, it indicates that the ensemble of interactions favored in a mixed oligomers differs from what is possible in a tethered NTR-ACD chimera. In the ACD-swapped chimeras, the NTR and ACD are connected, enforcing proximity even when interactions are not optimal. In hetero-oligomers, by contrast, all binding surfaces are present and interactions are governed by competition and energetic preferences across the ensemble. In addition, hetero-oligomer mixtures allow heterotypic NTR-NTR interactions between HSPB1 and HSPB5, which is absent in the ACD-swapped oligomers. The hetero-oligomer therefore reveals which interactions are favored when the system is allowed to self-organize in its preferred fashion. Functionally, these data are consistent with hetero-oligomerization as a potential regulatory mechanism used by sHSP. In the heterooligomer context, regions previously associated with chaperone function in HSPB5 (FR-B and FR-D) become more exposed, consistent with increased activity. In contrast, HSPB1 experiences protection in its chaperone active region (FR-E), consistent with relative inhibition of HSPB1 activity. These findings suggest that mixing HSPB1 and HSPB5 could tune the balance of chaperone function in cells by redistributing exposure of specific NTR functional regions across subunits. In cells, this balance could be further modulated by PTMs, stress conditions, or dynamic exchange of subunits between hetero- and homo-oligomer pools.

Across all perturbations tested in this chapter, several consistent trends emerged that clarify conserved features of the quasi-order network. First, FR-C remained well protected, presumably by maintaining binding to the central groove. Notably, FR-C is perturbed by disease associated HSPB1 mutations: it becomes more exposed in G34 and G84 mutants and more protected in P39L. The fact that clinically relevant mutations perturb this highly conserved

interaction suggests that destabilization of the FR-C-central groove interaction may be particularly disruptive to oligomer regulation. These results suggest that FR-C and central groove binding represents one of the more stable and conserved interactions in the sHSP quasi-order network. Second, IxI mediated contacts in both the NTR (FR-A) and in the CTR were sensitive across essentially all perturbations. Rather than being static anchors, these IxI motifs appear to change binding in response to direct or allosteric changes, contributing to the plasticity of oligomer architecture. Third, exposure of FR-E and corresponding interacting ACD residues consistently correlated with changes in chaperone activity. All three disease-associated HSPB1 mutants showed increased activity accompanied by increased FR-E exposure. Similarly, most bump constructs (with the exception of HSPB1 bump) showed increased FR-E exposure, and all bump constructs showed increased exposure in the ACD residues corresponding to β3/β4 and loop3/4 region. Finally, in hetero-oligomers, FR-E exposure shifted in opposite directions for HSPB1 and HSPB5: HSPB1 FR-E became more protected and HSPB5 FR-E became solvent accessible. Together, these results suggest that FR-E accessibility may serve as structural indicator of sHSP activation across various perturbations in their oligomer network. Indeed, FR-E is a hotspot for phosphorylation sites (Table 1.11; S78 and S82 in HSPB1, S59 in HSPB5) that could modulate accessibility of this region.

Finally, these data reinforce that oligomer size alone is not well correlated with chaperone function. In multiple contexts, substantial changes in oligomer distributions occurred without proportional changes in activity, and conversely, significant changes in activity were observed without large changes in oligomer size. Thus, oligomer size is best understood as being a consequence of altered networks and accessibility of sHSP, and not a direct determinant of function. Function is instead more closely tied to which NTR and ACD residues are accessible

within the ensemble. Certain interactions, like FR-C binding to the ACD are maintained across diverse perturbations, while other regions (FR-E and IxI mediated interactions) behave as tunable nodes that shift accessibility and function. HSPB1 and HSPB5 respond differently to the same disruption (like bump) and reach distinct structural and oligomeric outcomes. These results emphasize that sHSP regulation emerges from a distributed interaction network responds to stress, mutation, PTMs, or hetero-oligomerization.

3.5 Materials and Methods

Analytical sizing exclusion chromatography (aSEC)

All aSEC experiments were performed on an GE AKTA Purifier equipped with a Superose 6 10/300 GL column and a 100 µL sample loop in MOPS 150 at pH 7.5 at room temperature (~25 °C) with samples preincubated at 37 °C for three hours.

2D NMR

NMR samples contained 200M ^{15}N-labeled ACD-only construct protein in pH 7.5 buffer containing 25 mM sodium phosphate, 150 mM sodium chloride, 2 mM DTT, and 0.5 mM EDTA. Spectra were collected at on a 500MHz Bruker magnet at 30^{o}C. Data were processed using NMRpipe and analyzed with NMRViewJ. Peak broadening was quantified by dividing the intensity of each peak in the bound spectrum by the intensity of the corresponding peak in the unbound spectrum. Chemical shift perturbations were then quantified for analysis. For tau NMR experiments, up to 400µM (2x molar ratio) of tau (K18 construct) was titrated. The distal peptides were purchased from Genscript and dissolved in NMR buffer before mixing with ^{15}N-labeld ACD for measurement.

HDX-MS, MP, and in vitro tau aggregation assays were performed as described in Chapter 2 Methods and materials section.

Author Contribution: HDX-MS of HSPB1 disease mutants (Figure 3.2) were performed by Amanda Clouser, HDX-MS of HSPB1-HSPB5 hetero-oligomers (Figure 3.13) was performed by Maria Janowska and Natalie Stone, analyzed by Lisa Tuttle. Analytical sizing experiment of HSPB1-HSPB5 (Figure 3.11A) was performed by Brian Pham. All other experiments in this chapter were performed by Mia Cervantes.

References

1. Clouser AF, Baughman HE, Basanta B, Guttman M, Nath A, Klevit RE. Interplay of disordered and ordered regions of a human small heat shock protein yields an ensemble of 'quasi-ordered'states. Elife. 2019 Oct 1;8:e50259.
2. Klevit RE. Peeking from behind the veil of enigma: emerging insights on small heat shock protein structure and function. Cell Stress and Chaperones. 2020 Jul 1;25(4):573-80.
3. Pasta SY, Raman B, Ramakrishna T, Rao CM. The IXI/V motif in the C-terminal extension of alpha-crystallins: alternative interactions and oligomeric assemblies. Mol Vis. 2004 Sep 8;10(78):655-62.

4. Studer S, Obrist M, Lentze N, Narberhaus F. A critical motif for oligomerization and chaperone activity of bacterial α-heat shock proteins. European journal of biochemistry. 2002 Jul;269(14):3578-86.

5. Janowska MK, Baughman HE, Woods CN, Klevit RE. Mechanisms of small heat shock proteins. Cold Spring Harbor perspectives in biology. 2019 Oct 1;11(10):a034025.

6. Rauch JN, Tse E, Freilich R, Mok SA, Makley LN, Southworth DR, Gestwicki JE. BAG3 is a modular, scaffolding protein that physically links heat shock protein 70 (Hsp70) to the small heat shock proteins. Journal of molecular biology. 2017 Jan 6;429(1):128-41.

7. Baughman HE, Clouser AF, Klevit RE, Nath A. HspB1 and Hsc70 chaperones engage distinct tau species and have different inhibitory effects on amyloid formation. Journal of Biological Chemistry. 2018 Feb 23;293(8):2687-700.

8. Sluchanko NN, Beelen S, Kulikova AA, Weeks SD, Antson AA, Gusev NB, Strelkov SV. Structural basis for the interaction of a human small heat shock protein with the 14-3-3 universal signaling regulator. Structure. 2017 Feb 7;25(2):305-16.

9. Alderson TR, Roche J, Gastall HY, Dias DM, Pritišanac I, Ying J, Bax A, Benesch JL, Baldwin AJ. Local unfolding of the HSP27 monomer regulates chaperone activity. Nature communications. 2019 Mar 6;10(1):1068.

10. Selig EE, Lynn RJ, Zlatic CO, Mok YF, Ecroyd H, Gooley PR, Griffin MD. The monomeric α-Crystallin domain of the small heat-shock proteins αB-Crystallin and Hsp27 binds amyloid fibril ends. Journal of Molecular Biology. 2022 Aug 30;434(16):167711.

11. Collier MP, Alderson TR, de Villiers CP, Nicholls D, Gastall HY, Allison TM, Degiacomi MT, Jiang H, Mlynek G, Fürst DO, van der Ven PF. HspB1 phosphorylation regulates its intramolecular dynamics and mechanosensitive molecular chaperone interaction with filamin C. Science Advances. 2019 May 22;5(5):eaav8421.

12. Cervantes M, Janowska MK, Tuttle LM, Nath A, Klevit RE. Function within Disorder: Small heat shock proteins use different functional regions to chaperone tau aggregation. bioRxiv. 2026:2026-01.

13. Hanazono Y, Takeda K, Oka T, Abe T, Tomonari T, Akiyama N, Aikawa Y, Yohda M, Miki K. Nonequivalence observed for the 16-meric structure of a small heat shock protein, SpHsp16. 0, from Schizosaccharomyces pombe. Structure. 2013 Feb 5;21(2):220-8.

14. Woods CN, Janowska MK, Ulmer LD, Kaur Sidhu J, Stone NL, James EI, Guttman M, Bush MF, Klevit RE. Activation mechanism of Small Heat Shock Protein HSPB5 revealed by disease-associated mutants. Proceedings of the National Academy of Sciences. 2025 May 20;122(20):e2425061122.

15. Peters C, Haslbeck M, Buchner J. Catchers of folding gone awry: a tale of small heat shock proteins. Trends in Biochemical Sciences. 2024 Dec 1;49(12):1063-78.

16. Hochberg GK, Ecroyd H, Liu C, Cox D, Cascio D, Sawaya MR, Collier MP, Stroud J, Carver JA, Baldwin AJ, Robinson CV. The structured core domain of αB-crystallin can prevent amyloid fibrillation and associated toxicity. Proceedings of the National Academy of Sciences. 2014 Apr 22;111(16):E1562-70.

17. Rajagopal P, Liu Y, Shi L, Clouser AF, Klevit RE. Structure of the α-crystallin domain from the redox-sensitive chaperone, HSPB1. Journal of biomolecular NMR. 2015 Oct;63(2):223-8.

18. Delbecq SP, Rosenbaum JC, Klevit RE. A mechanism of subunit recruitment in human small heat shock protein oligomers. Biochemistry. 2015 Jul 21;54(28):4276-84.

19. Delbecq SP, Jehle S, Klevit R. Binding determinants of the small heat shock protein, αB-crystallin: recognition of the 'IxI'motif. The EMBO Journal. 2012 Dec 12;31(24):4587-9

20. Makley LN, Johnson OT, Ghanakota P, et al. Chemical validation of a druggable site on Hsp27/HSPB1 using in silico solvent mapping and biophysical methods. Bioorg Med Chem. 2021;34:115990.

21. Freilich R, Betegon M, Tse E, Mok SA, Julien O, Agard DA, Southworth DR, Takeuchi K, Gestwicki JE. Competing protein-protein interactions regulate binding of Hsp27 to its client protein tau. Nature communications. 2018 Nov 1;9(1):4563.

22. Baughman HE, Pham TH, Adams CS, Nath A, Klevit RE. Release of a disordered domain enhances HspB1 chaperone activity toward tau. Proceedings of the National Academy of Sciences. 2020 Feb 11;117(6):2923-9.

23. Stone NL, Janowska MK, Narisawa L, Tuttle LM, Ulmer LD, Guttman M, Bush MF, Klevit RE. Disorder with consequence: Phosphorylation sites in HSPB5 yield distinct structural outcomes. bioRxiv. 2025 Oct 28:2025-10.

24. Nemes Z, Devreese B, Steinert PM, Beeumen JV, Fésüs L (2004) Cross-linking of ubiquitin, HSP27, parkin and α-synuclein by γ-glutamyl-ε-lysine bonds in Alzheimer's neurofibrillary tangles. The FASEB Journal; 18(10): 1135–1137.

25. Shimura H, Miura-Shimura Y, Kosik KS (2004) Binding of tau to heat shock protein 27 leads to decreased concentration of hyperphosphorylated tau and enhanced cell survival. The Journal of Biological Chemistry; 279(17): 17957–17962.

26. Björkdahl C, Sjögren MJ, Zhou X, Concha H, Avila J, Winblad B, Pei JJ (2008) Small heat shock proteins Hsp27 or alphaB-crystallin and the protein components of neurofibrillary tangles: Tau and neurofilaments. Journal of Neuroscience Research; 86(6): 1343–1352.

27. Sahara, N, Maeda S, Yoshiike Y, Mizoroki T, Yamashita S, Murayama M, Park JM, Saito Y, Murayama S, Takashima A (2007) Molecular chaperone-mediated tau protein metabolism counteracts the formation of granular tau oligomers in human brain. Journal of Neuroscience Research; 85(14): 3098–3108.

28. Bartelt-Kirbach B, Slowik A, Beyer C, Golenhofen N (2017) Upregulation and phosphorylation of HspB1/Hsp25 and HspB5/αB-crystallin after transient middle cerebral artery occlusion in rats. Cell Stress and Chaperones; 22(4): 653–663.

29. Mymrikov EV, Riedl M, Peters C, Weinkauf S, Haslbeck M, Buchner J. Regulation of small heat-shock proteins by hetero-oligomer formation. Journal of Biological Chemistry. 2020 Jan 3;295(1):158-69.

30. Shatov VM, Strelkov SV, Gusev NB. The heterooligomerization of human small heat shock proteins is controlled by conserved motif located in the N-terminal domain. International Journal of Molecular Sciences. 2020 Jun 15;21(12):4248.

31. Kato, K., Shinohara, H., Goto, S., Inaguma, Y., Morishita, R., and Asano, T. (1992) Copurification of small heat shock protein with B crystallin from human skeletal muscle. J. Biol. Chem. 267, 7718 –7725

32. Zantema, A., Verlaan-De Vries, M., Maasdam, D., Bol, S., and van der Eb, A. (1992) Heat shock protein 27 and B-crystallin can form a complex, which dissociates by heat shock. J. Biol. Chem. 267, 12936 –12941

33. Sakuma, K., Watanabe, K., Totsuka, T., and Kato, K. (1998) Pathological changes in levels of three small stress proteins, B crystallin, HSP 27 and p20, in the hindlimb muscles of dy mouse. Biochim. Biophys. Acta 1406, 162–168

34. Woods CN, Ulmer LD, Guttman M, Bush MF, Klevit RE. Disordered region encodes α-crystallin chaperone activity toward lens client γD-crystallin. Proceedings of the National Academy of Sciences. 2023 Feb 7;120(6):e2213765120.

35. Tuttle LM, Klevit RE, Guttman M. A framework for automated multimodal HDX-MS analysis. bioRxiv. 2025 Mar 15.

4. Method Development for sHSP Characterization

4.1 Introduction

The inherent heterogeneity and polydispersity of small heat shock proteins (sHSPs) allow them to adapt to a wide range of client proteins and cellular conditions. However, these same features make sHSPs particularly challenging to characterize using traditional structural biology approaches. As a result, alternative and complementary methods are required to probe their structure, organization, and function. sHSPs exhibit multiple layers of structural and functional complexity, each of which can be interrogated using different experimental techniques. In this chapter, I describe the development and optimization of techniques that were critical for investigating the structure and function of HSPB1 and HSPB5, as presented in Chapters 2-3. These methods enabled the analysis of sHSP behavior across different oligomeric states, activation conditions, and interactions with the client tau. Additionally, I describe different purification protocols optimized for HSPB1 to improve yield and efficiency. The combination of work outlined in this chapter provided the foundation for exploring multiple layers of HSPB1 and HSPB5 behavior that would not have been accessible using a single experimental approach.

4.2 Results

4.2.1 Method development and optimization of B1 purification protocol

When I joined the lab, the existing HSPB1 purification protocol was suboptimal and consistently yielded lower total protein than HSPB5. For example, one notable difference was the cell lysis step: HSPB1 purification relied on detergent-based lysis, whereas HSPB5 purification employed a pressure-based mechanical disruption method commonly used in our

lab. The HSPB1 purification protocol had been inherited from earlier work and had not been systematically revisited or optimized in several years.

To improve overall yield and streamline HSPB1 production, I first tested whether HSPB1 purification could be improved by adapting the HSPB5 native protein purification workflow with appropriate modifications. These modifications were guided by known differences in the biophysical properties of HSPB1 and included adjusting the total ammonium sulfate concentration used for protein precipitation, as well as optimizing the salt gradients applied during DEAE and HiTrapQ anion-exchange chromatography (Table 4.1). These adjustments led to a substantial improvement in HSPB1 yield while maintaining high purity in the final sample.

Although adapting the HSPB5 workflow improved HSPB1's yield, previous work (1) reported successful purification of HSPB1 constructs using affinity tags, which substantially reduces both the time and complexity of purification compared to our existing protocol. To take advantage of this approach, I cloned both full-length and the isolated ACD into a new expression vector, pET-24b(+), containing an N-terminal His-SUMO fusion tag, using Gibson Assembly. The His-SUMO system is widely used due to its ability to enhance protein solubility and its highly specific cleavage by the protease SENP1 (2). Importantly, this system also enables a more streamlined and user-friendly purification pipeline, which is particularly valuable for training undergraduate researchers with limited time or protein purification experience.

Using these new constructs, I developed two updated HSPB1 purification protocols: a long and a short version, summarized in Table 4.1. The long version spans 2-3 days and includes an overnight dialysis step, followed by sizing in anion-exchange buffer, anion-exchange chromatography (HiTrapQ), and final buffer exchange or overnight dialysis into the storage buffer. This "long" protocol is designed to accommodate undergraduate students with time

constraints, as daily time commitment is flexible. The short version can be completed within 1-2 days, as it omits the overnight dialysis step. Instead, samples proceed directly from SENP1 cleavage to desalting, anion-exchange chromatography, and final size-exclusion chromatography into the storage buffer. The omission of the overnight dialysis step can be justified by reports showing that SENP1 cleavage reaches maximum efficiency within 15 minutes (2), allowing for a more rapid purification workflow without compromising protein quality.

	Original version	**Short Version**	**Long version**
Vector	pET23a; pET151d	pET-24b(+)	pET-24b(+)
Growth Condition	0.5L LB + 1mM IPTG	1L LB + 0.5mM IPTG	1L LB + 0.5mM IPTG
Cell Lysis	Chemical (detergent)	French Press or homogenizer	Frech Press or homogenizer
Purification Workflow	1. Ammonium Sulfate Precipitation 2. Desalting (G25) 3. Anion-exchange (DEAE and HitrapQ) 4. Size exclusion chromatography	1. Nickel affinity chromatography 2. SENP1 tag cleavage for 15-minutes 3. Desalting (G25) 4. Anion-exchange (HitrapQ) 5. Size exclusion chromatography	1. Nickel affinity chromatography 2. Overnight dialysis SENP1 tag cleavage 3. Size exclusion chromatography 4. Anion-exchange (HitrapQ) 5. Buffer exchange or dialysis
Purification timeline	3-4 days	1-2 days	2-3 days

Table 4.1: Table organization of three different HSPB1 purification protocols. The description of both previous and new vectors and purification information are summarized. Details are shown for the original purification protocol, and the updated short and long versions.

4.2.2 Production and uses of BPA Incorporation in HSPB1 and HSPB6

The genetic code expansion system unlocks new avenues for manipulating biological system in ways that enable novel functional insights (3-4). In the Klevit lab, the noncanonical

UV-crosslinkable amino acid, p-benzoyl-L-phenylalanine (BPA) has been particularly powerful for dissecting the tangled and dynamic interactions of small heat shock proteins (5-7). Using amber codon suppression technology, BPA can be introduced at a specific residue along the sequence of sHSP. Upon UV irradiation, BPA will react to form a covalent bond if there is an interacting CH bond present in proximity (8). Subsequent analysis of crosslinked peptides via mass spectrometry allows for residue-level identification of crosslinks present within the HSPB5 oligomers. In collaboration with the Bush lab in UW Chemistry, the BPA crosslink mass spectrometry (BPA-XL-MS) workflow has been streamlined and optimized for several positions within the HSPB5 NTR, establishing this approach as a robust tool in our system (9). Previous studies using BPA-XL-MS in HSPB5 have provided critical insights into NTR-ACD interactions and client engagement, including interactions with tubulin and other substrates (5-7). The technology's capacity to resolve transient and heterogeneous contacts that are difficult to chapter using traditional structural methods highlight the unique opportunity to expand this toolkit further.

Given the demonstrated usefulness of BPA incorporation in HSPB5, I sought to expand the toolkit by generating a broader panel of BPA-containing constructs across multiple sHSPs. As described in Chapter 3.3 and in other work, hetero-oligomers form between B1, B5 and B6, and each pairing produces distinct oligomeric distributions and functional behaviors (10-12). Our lab has also collected structural information on both homo- and hetero-oligomers of these sHSP pairs using HDX-MS (Chapter 3.3). Adding complementary crosslinking data provides an additional layer of structural information, enabling a more detailed understanding of how the network of interactions within sHSPs is reorganized upon hetero-oligomerization.

To expand our BPA toolkit, I tested 9 positions in full-length HSPB1 and 4 positions in full-length HSPB6. Protein concentrations for all BPA-containing variants were quantified using BCA assays. The BPA positions, crosslinking outcomes (See Appendix SI Figure 6), and notes on protein expression and purification are summarized in Table 4.2.

BPA Mutant	Sub-region	Concentration (μM)	Crosslinked? (Y/N)	Notes
B1 T2	FR-A	67	Y	Good final product and crosslink, but too short for mass spec analysis
B1 F8	FR-A	<10	N	Not enough final product to test for crosslinks; previous F8 mutant purifications showed challenges
B1 L11	FR-A	164	Y	Good final product and crosslink
B1 W16	FR-B	240	Y	Good final product and crosslink
B1 W22	FR-B	525	Y	Good final product and crosslink
B1 F29	FR-C	NA	NA	Plasmid available for this mutant, but not yet purified or tested
B1 W42	FR-D	135	Y	Good final product and crosslink
B1 W51	FR-D	110	Y	Good final product and crosslink
B1 L77	FR-E	248	N	Multiple purification attempts, all led to unstable/cleaved final products with no UV reaction
B1 L81	FR-E	457	Y	Monomer purification product and crosslinked dimer is broad on gel
B6 W11	FR-A	415	N	Multiple purification attempts, all led to cleaved product (smaller MW) with unsuccessful crosslinking
B6 L22	FR-B	82	Y	Good final product and crosslink
B6 F29	FR-C	198	Y	Good final product and crosslink
B6 Y53	FR-D	32	Y	Very low concentration and crosslink efficiency

Table 4.2: Summary of HSPB1 and HSPB6 BPA-containing mutants. Cells shaded in pink show detail of HSPB1 BPA-containing mutants, and pale-orange show HSPB6 BPA mutants. Information on BPA position, functional region, concentration, crosslink, and purification are detailed in the table.

While further optimization will be required to achieve high confidence crosslinks for HSPB1 and HSPB6 BPA samples, initial mass spectrometry analyses performed by Lucas Narisawa (PhD student in the Bush Lab) showed a promising start. Crosslink bands on mass spec contained peptides from HSPB1 and HSPB6 with BPA incorporated, but several early challenges emerged in identifying the specific crosslinked residues. For HSPB1 BPA-XL-MS experiments, a high local density of aromatic residues led to poor proteolytic cleavage and reduced resolution in the FR-B and FR-D sub-regions. Despite these challenges, incorporation of BPAs into HSPB1 and HSPB6 broadened our experimental toolkit and allowed for asking new mechanistic questions that we could not probe previously. In the following section, I present one such example using HSPB1 BPA constructs to better characterize changes in NTR-ACD interactions upon introducing the bump mutation. The bump mutation abrogates binding to ACD edge grooves that can typically harbor sHSP protomers and clients. One of the well characterized interactions involves NTR "IxI" motif binding to the ACD edge groove as discussed in Chapter 3.

To better understand how the bump mutation affects the ACD's ability to scaffold its NTR, we quantified direct NTR-ACD interactions using 4 different BPA sites within the NTRs of HSPB1 and HSPB5. By placing BPAs at multiple NTR sites, we were able to compare crosslinking efficiencies between different NTR functional regions. Upon UV exposure, BPA forms a crosslink with interacting amino acids within ~3Å, with no specific amino acid preference, allowing for broader and unbiased coverage of crosslinks. A schematic of the experimental design is shown in Figure 4.1. Briefly, BPA-containing sHSP oligomers were UV-irradiated in the presence of isolated ACD-only constructs (WT or bump), then the new NTR-ACD crosslink is identified by SDS-PAGE. Crosslinks were quantified from three independent

SDS-PAGE images obtained from the same crosslinking reactions for each mutant. In this experiment, we quantified crosslinks formed between BPA in NTRs and ACD-only constructs (WT vs bump) to determine how the bump mutation influences NTR-ACD interaction. The crosslinks were quantified from three independent SDS-PAGE images from the same crosslink reactions for each mutant. This experimental approach allows direct comparison of how each FR in HSPB1 and HSPB5 is influenced by the bump mutation. Prior work from our lab demonstrated that recruitment of an isolated ACD dimer into sHSP oligomers occurs through two mechanisms: 1) interactions between the CTR IXI motif and the edge groove, and 2) subunit exchange into and out of oligomers through monomer exchange at the dimer interface level. Incorporation of the bump mutation significantly reduced ACD recruitment, highlighting the importance of edge groove availability for sHSP oligomerization (13).

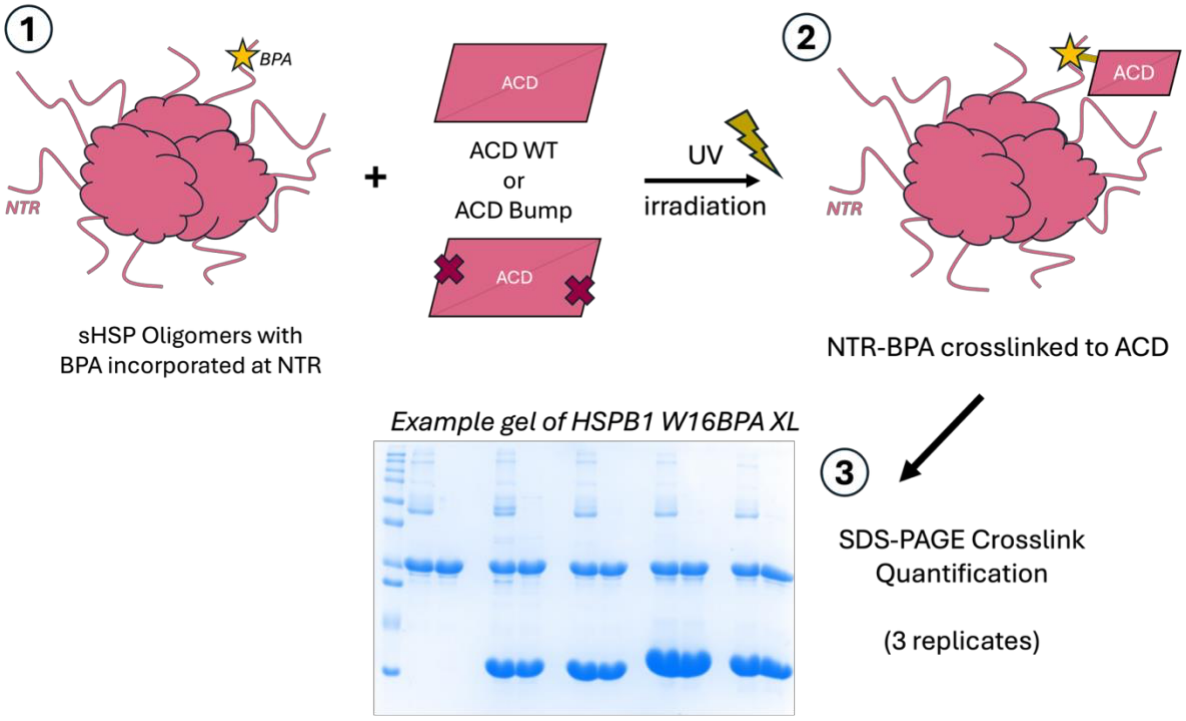

Figure 4.1 A schematic of BPA experimental set up to quantify crosslink band formed between BPA at the HSPB1 or HSPB5 NTRs with ACD -WT and -Bump. 1) A photoreactive non-canonical

amino acid, BPA is genetically incorporated throughout the NTRs of HSPB1 and HSPB5. The BPA-containing oligomers are mixed and incubated with isolated ACD (WT or Bump); 2) The mixture is exposed UV irradiation for 30 minutes so the BPA can crosslink with a nearby residue; 3) 3 independent SDS-PAGE is performed to accurately quantify a gel band corresponding to crosslinked NTR-ACD species

For HSPB1-BPA mutants, crosslink efficiency depended strongly on the BPA insertion site (Figure 4.2). HSPB1 W16-BPA (FR-B) did not show abundant crosslinking to HSPB1ACD-WT. In contrast, the two BPA sites within FR-D exhibited different crosslinking reactions: W42-BPA crosslinked substantially more efficiently than W51-BPA. Although both residues are located within FR-D, they are separated by 9 residues, which can represent a meaningful spatial separation in an intrinsically disordered region. This difference could be due to how interactive the neighboring regions of W42-BPA and W51-BPA are with the ACD. W42-BPA is positioned near the conserved region (FR-C) previously shown to bind the ACD dimer interface groove (14), which could explain its higher reactivity toward HSPB1 ACD. By contrast, W51-BPA lies closer to the insertion region that is expected to be highly solvent-exposed and does not form sustained contact with the ACD, resulting in lower crosslinking efficiency. Surprisingly, HSPB1 L81BPA (FR-E) showed the highest crosslinking efficiency across all samples tested. This suggests that FR-E boundary region forms frequent or persistent contacts with the ACD under these conditions. For HSPB5-BPA mutants, the most efficient crosslink was observed at W9-BPA (FR-A). In contrast, F28-BPA (FR-C), F48-BPA (FR-D), and F61-BPA (FR-E) all exhibited similarly low crosslinking reactivity to B5ACD-WT, with F48-BPA showing a slightly higher signal relative to the other two sites.

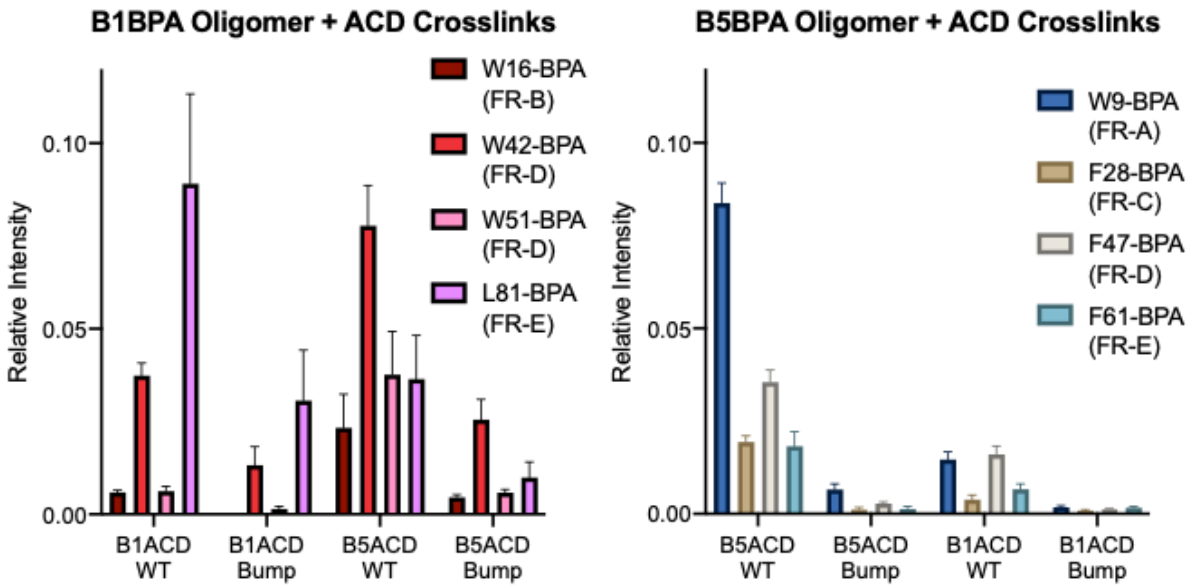

Figure 4.2: NTR-ACD BPA crosslink reactions quantified by BPA incorporated in NTR of HSPB1 (Left) and HSPB5 (Right). Each BPA-containing mutant were mixed with ACD-only constructs, both WT and Bump of each ACD. The intensity of crosslink band formed between HSPB1 or HSPB5 BPA and ACD constructs were quantified between three replicate gel samples.

To test the role of the ACD edge groove in mediating NTR-ACD interactions, we introduced the bump mutation into the ACD. Across all BPA sites tested in both HSPB1 and HSPB5, the bump mutation caused a significant decrease in the intensity of NTR-ACD crosslink bands. This broad reduction in NTR-ACD crosslinking reinforces that the bump mutation weakens NTR-ACD contacts and the availability of the edge groove is crucial for efficient subunit recruitment. Intriguingly, a subset of crosslinks persisted in the presence of the bump mutation, including HSPB1 W42-BPA and L81-BPA, and to a much lesser extent HSPB5 W9-BPA. The high reactivity of the HSPB1 L81-BPA mutant, observed for both B1ACD and bump, aligns with previous findings that the B1NTR boundary region binds the dimer interface (14).

The persistence of these signals means that some NTR-ACD interactions remain possible even when edge groove interactions are disrupted. The residual crosslinking is consistent with subunit incorporation mechanisms that are less dependent on the edge groove, such as monomer exchange.

Further, I quantified hetero-oligomer crosslinking reactions in which HSPB1-BPA variants were crosslinked to HSPB5ACD (WT or bump), and conversely HSPB5-BPA variants were crosslinked to HSPB1ACD (WT or bump). These experiments revealed striking asymmetry between HSPB1 and HSBP5. All HSPB1-BPA mutants crosslinked efficiently to HSPB5ACD, with W42-BPA producing the most abundant crosslinks. Notably, W42-BPA crosslink to HSPB5ACD was preserved even in the bump mutant, although with reduced efficiency. In contrast, HSPB5-BPA mutants exhibited substantially weaker crosslinking to HSPB1ACD compared to HSPB5ACD, and these NTR-ACD crosslinks were nearly abolished upon introduction of the bump mutation into HSPB1ACD.

Overall, all BPA sites tested in HSPB1 and HSPB5 displayed reduced crosslinking in the bump mutant, confirming that the bump mutation broadly weakens NTR-ACD interactions. This effect was more pronounced in HSPB5BPA mutants, correlating with HSPB5's greater sensitivity to activation by the bump mutation compared to HSPB1. The sensitivity and resolution of BPA crosslinking as shown here highlights the wealth of residue-level information that is accessible by BPA-XL-MS technology for heterogenous samples like sHSPs.

4.2.3. Mass Photometry Method development and optimization for sHSP

Mass photometry (MP) has emerged as a powerful technique for determining the molecular weight and distribution of biological complexes using label-free, solution-based measurements. MP captures the optical contrast generated as single molecule species in the solution bind to a glass-coverslip surface. The contrast observed is directly proportional to the mass of individual molecules, so this results in accurate molecular weight measurements even for highly heterogeneous samples (15). Historically, obtaining comparable information has been both labor and time intensive, relying on techniques such as SEC-MALS, analytical ultracentrifugation, or native mass spectrometry (15). In addition, light-scattering based techniques such as DLS are inherently biased toward larger species (16). MP bypasses many of these challenges: measurements are fast, require little sample, and are not intrinsically biased toward higher molecular weight assemblies. Several comprehensive reviews and protocols now outline best practices for MP measurements (17).

Here, I describe the method development and experimental challenges encountered in applying MP to characterize the oligomeric properties of small heat shock proteins HSPB1 and HSPB5. This work includes optimization of sample preparation, refinement of data acquisition workflows, and the establishment of a set of practical “rules” and best practices that proved essential for obtaining reproducible sHSP molecular weight distributions by MP.

The first priority was to establish consistency in preparation of core reagents, including standardizing the coverslip cleaning and buffer preparation protocol, as detailed in the Method section of Chapter 2. With these steps in place, I optimized the full MP workflow to ensure reproducibility across multiple days, protein stocks, and different users of the instrument, which were especially important considering the inherent heterogeneity of sHSP oligomers. During

these optimizations, I observed an unexpected discrepancy: measurements of HSPB1 differed between users, even when identical protein stocks at the same concentrations were used (Figure 4.3; Top left and middle). Interestingly, HSPB5 measurements were consistent across replicates under either pH conditions (Figure 4.3; Top right), indicating that the variability was specific to HSPB1 oligomers. Specifically, the average molecular weight observed in my hands was smaller (~350kDa) compared to another user's measurement of the same sample (~450kDa). Since HSPB1 oligomerization is known to be concentration dependent (18), I initially hypothesized that sample dilution during the standard MP workflow might contribute to this variability. To address this, I adopted a dilution-free MP protocol in which sHSPs were pre-incubated at the final 1μM concentration in buffer before being added directly to the sample well. While this approach improved overall reproducibility, user-to-user differences persisted, prompting investigation of other factors that might influence MP measurements.

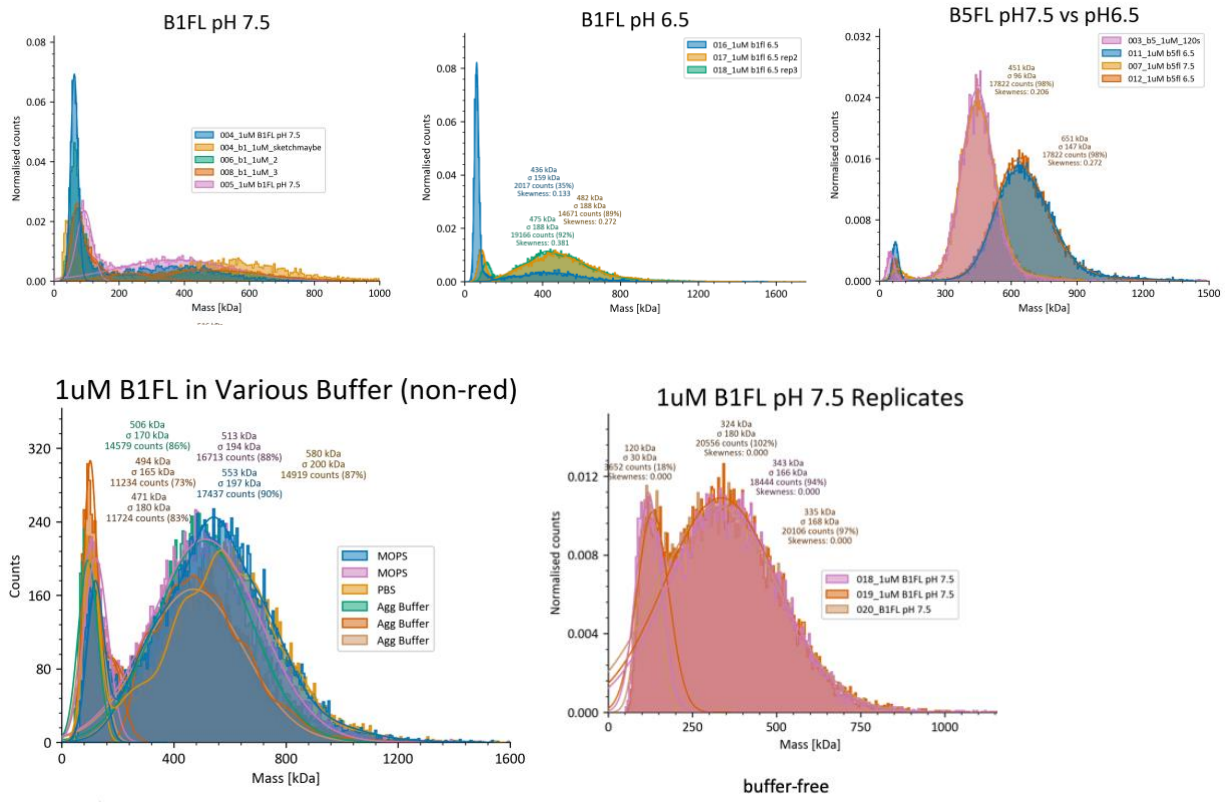

Figure 4.3: Molecular weight distribution of HSPB1 and HSPB5 oligomers under different conditions measured by mass photometry during method development. (Top) 1µM sHSP measurement of HSPB1 and HSPB5 at pH 7.5 and pH 6.5. Replicates were tested from the same sample stock, and/or solution. HSPB1 showed variability in molecular weight distribution at both pH conditions, while HSBP5 showed reproducible oligomeric distribution. (Bottom Left) 1µM HSPB1 sample equilbrated in multiple buffer conditions to evaluate the effect of buffer condition on MP measuremetns. Variable MW were seen for low salt and high salt buffers. (Bottom Right) Measuremetns of HSPB1 using the dilution-free method in the low salt buffer showed increased reprodubicility in MW distribution.

Further investigation revealed that users were preparing MP buffers with different salt concentrations, or ionic strengths. Specifically, I had been using a low-salt aggregation buffer (20mM NaCl), whereas others used PBS containing 150mM NaCl (Figure 4.3; Bottom left). To directly test whether salt concentration influenced the measurements, I incubated both HSPB1 and HSPB5 in buffers of varying ionic strength and analyzed them using the dilution-free method. As shown in Figure 4.4, only HSPB1 displayed clear shifts in overall molecular weight as a function of salt concentration. This result not only explains the variation of MW observed for HSPB1 samples but also demonstrates that HSPB1 oligomeric distributions are sensitive to ionic strength. In contrast, HSPB5 was unaffected by changes in salt concentration. HSPB1 oligomer's sensitivity to ionic strength suggests that formation of larger oligomers at higher salt concentration is hydrophobically driven, whereas HSPB5 is unaffected. Such differences highlight the differences in their NTR properties HSPB1 and HSPB5, as described in Chapter 1 and 2.

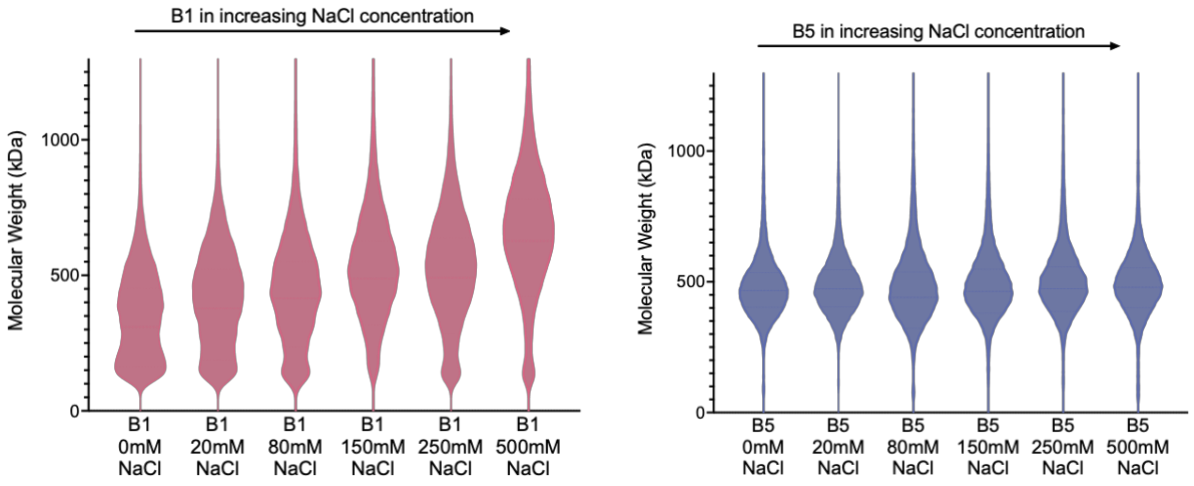

Figure 4.4: Molecular weight distribution of HSPB1 and HSPB5 oligomers under different ionic strength in the buffer measured by mass photometer. 1μM total sHSP were incubated in

phosphate-based buffer with varying NaCl salt concentrations. HSPB1 experienced sensitivity to changes in ionic strength in the buffer (left) but HSPB5 remained unchanged (Right).

Beyond static measurements, MP's capacity to be relatively high throughput enabled rapid measurements of sHSP oligomeric assemblies. One application addressed the question of how quickly HSPB1 and HSPB5 form stable homo- and hetero-oligomeric assemblies. To probe this, I prepared time-course samples in which HSPB1 and/or HSPB5 were mixed and incubated for defined time intervals prior to MP analysis. These experiments were designed to answer two questions: 1) How rapidly HSPB1 and HSPB5 homo-oligomers reach equilibrium, and 2) how quickly hetero-oligomerization occurs between HSPB1 and HSBP5.

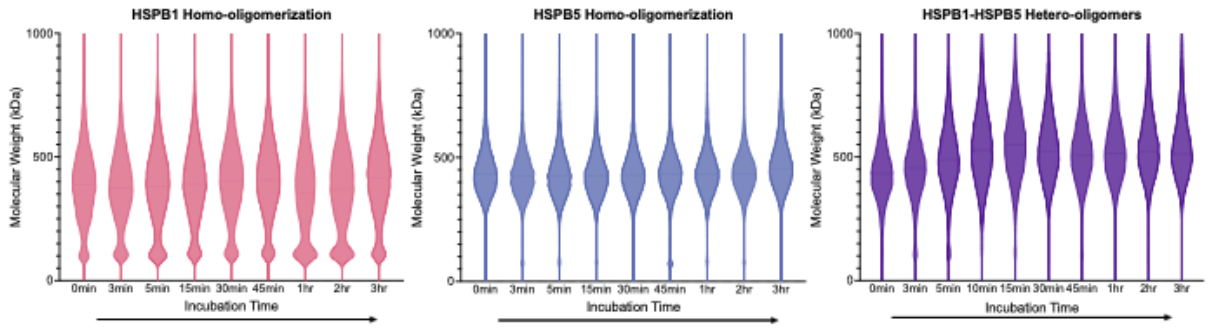

Figure 4.5: Molecular weight measurements of HSPB1 and HSPB5 homo- and hetero-oligomers over the typical 3 hour incubation time. Top: Homo-oligomers of HSPB1 (left) and HSPB5 (middle) were incubated for varying time-intervals (0min; 3min; 5mim; 10min; 15min; 30min; 45min; 1hr; 2hr; 3hr) at 37°C while shaking. Same data is shown for their hetero-oligomer assembly (right).

Under standard experimental conditions, sHSP samples are typically incubated at 37ºC for 3 hours to allow oligomer rearrangement and subunit exchange to reach equilibrium. Strikingly, MP measurements revealed that both homo- and hetero-oligomeric assemblies exhibited characteristics of near-equilibrated oligomers even prior to incubation at time = 0 (Figure 4.5). From time 0 (mixed on ice right before MP measurement), HSPB1 displayed a bimodal distribution of smaller and larger oligomers, whereas HSPB5 and HSPB1-HSBP5 hetero-oligomers were predominantly composed of large oligomer assemblies. By 30 minutes, only minimal changes in oligomeric distributions were observed, with subtle rearrangements continuing until the 3 hour time point. These data demonstrate that both homo- and hetero-oligomeric assemblies of HSPB1 and HSBP5 form rapidly and show no bias for homo- versus hetero-oligomerization. The rapid attainment of near-equilibrium oligomeric distribution suggests that oligomerization is strongly favored for both proteins. Moreover, the comparable assembly time observed for homo- and hetero-oligomer formation indicate that neither HSPB1 nor HSPB5 exhibits a strong intrinsic preference for remaining exclusively in homo-oligomeric states. Instead, their ability to readily form hetero-oligomers appears to be encoded in their biological properties, supporting the importance of their cooperative sHSP function in maintaining proteostasis under cellular stress.

4.2.4 *In vitro* tau aggregation assay development and optimization

Monitoring the *in vitro* fibrilization of tau using the amyloid-sensitive dye Thioflavin T (ThT) is one of the most widely used approaches for quantifying protein aggregation kinetics (19). Previous work established a standardized ThT assay to evaluate how HSPB1 delays the onset of tau aggregation (20). However, a major limitation of this assay was that it could only be

performed using HSPB1 dimer constructs, as native oligomeric HSPB1 produced background fluorescence due to direct interactions with ThT. While such dimeric constructs are useful for structural NMR studies, they require the introduction of multiple mutations (3 NTR phosphomimics and a GxG mutation in the CTR) and therefore may not accurately represent the sHSP species present in cells. In addition, spontaneous *in vitro* aggregation of tau is slow and typically requires a polyanion inducer to initiate aggregation. Traditionally, a sulfated polysaccharide, heparin is used to trigger *in vitro* aggregation of tau (21). However, heparin is produced in mast cells and basophils (22), raising concerns about its physiological relevance in neuronal tau aggregation. In this section, I describe a series of assay modifications implemented to address these limitations. I also discuss additional experimental capabilities enabled by the installation of a new plate reader in lab (CLARIOstar) and how these advances led to the proposal of an additional aggregation inhibition mechanism by sHSPs beyond those previously described in Chapter 2.

Optimization of a biologically relevant tau aggregation inducer, polyphosphate (pP)

My first goal was to optimize the use of a more biologically relevant inducer of tau aggregation. In place of heparin, I used polyphosphate, a polyanion with chains of phosphate groups, to induce tau aggregation. Polyphosphate is present in the cytoplasm of neurons and its levels increase with stress, thus providing a more realistic context for in vitro aggregation studies (23). Previous work has demonstrated that polyphosphate effectively induces *in vitro* tau aggregation (24). To identify the optimal assay conditions, I tested a range of polyphosphate concentrations at both pH 7.5 and pH 6.5. Since commercial polyphosphate stocks contain heterogeneous chain lengths and therefore lack a defined molecular weight, concentrations are reported in the units of mg/mL. Polyphosphate concentrations ranging from 10ng/mL and

5mg/mL were added to 5µM tau and successfully induced *in vitro* tau aggregation under both pH conditions (Figure 4.6). In the range of polyphosphate concentrations tested, polyphosphate exhibited biphasic effects on tau aggregation kinetics where mid-range concentration was optimal: at lower concentrations, polyphosphate accelerates nucleation and shortens the lag phase, whereas higher concentrations slow aggregation likely due to excessive charge screening and nonspecific interactions (23). To balance the need for a measurable lag phase that would allow for sHSP to interact with early tau aggregation species, while achieving robust fibrillization at both pH values, a final polyphosphate concentration of 1mg/mL was selected. Therefore, all subsequent aggregation assays described in my work were induced using 1mg/mL polyphosphate.

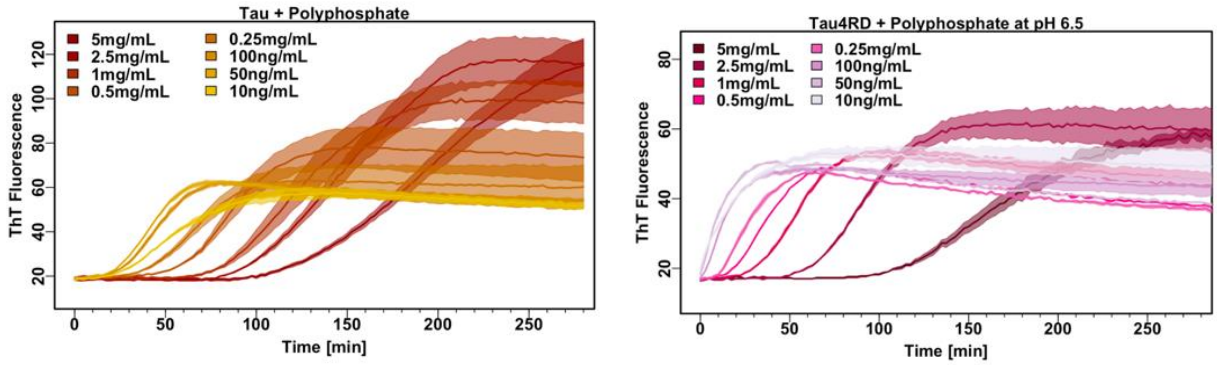

Figure 4.6: in vitro tau aggregation induced by a range of polyphosphate concentrations at pH 7.5 (Left); and pH 6.5 (Right). 5µM tau is added in a reaction at 37 °C with agitation every 2.5 minutes, with 4 replicates per condition.

In vitro tau aggregation with oligomeric HSPB1 and HSPB5

Next, I optimized the addition of oligomeric HSPB1 and HSPB5 in the ThT aggregation assay. In prior studies, only dimeric sHSP constructs were compatible with ThT measurements due to background fluorescence. This issue was resolved by pre-incubating sHSPs with ThT dye at 37^{o}C for 3 hours, directly in the sample wells, to allow the system to reach equilibrium prior to initiating tau aggregation. All assays were performed in low-binding 96-well plates to minimize nonspecific binding of sHSPs to the well surface. After the completion of each run, background fluorescence from sHSP-only controls was subtracted during data analysis to account for ThT signals from sHSP-ThT dye interactions.

Improved sensitivity with the CLAIOstar Plate Reader

Most of my early aggregation assays were performed using the Nath lab plate reader (HT Synergy). The lab later acquired a new plate reader (CLARIOstar), prompting a direct comparison of ThT fluorescence sensitivity between the two instruments. Identical assay plates were prepared on the same day and measured tau aggregation at varying concentration on both plate readers (Figure 4.7). The increased sensitivity of the CLARIOstar was immediately apparent, likely due to its ability to automatically optimize detector gain, whereas the HT Synergy plate reader required manual gain selection. As a result, CLARIOstar showed subtle differences in tau aggregation kinetics across conditions and improved reproducibility between replicates. All subsequent ThT aggregation assays were conducted using the CLARIOstar plate reader to achieve improved reproducibility and sensitivity.

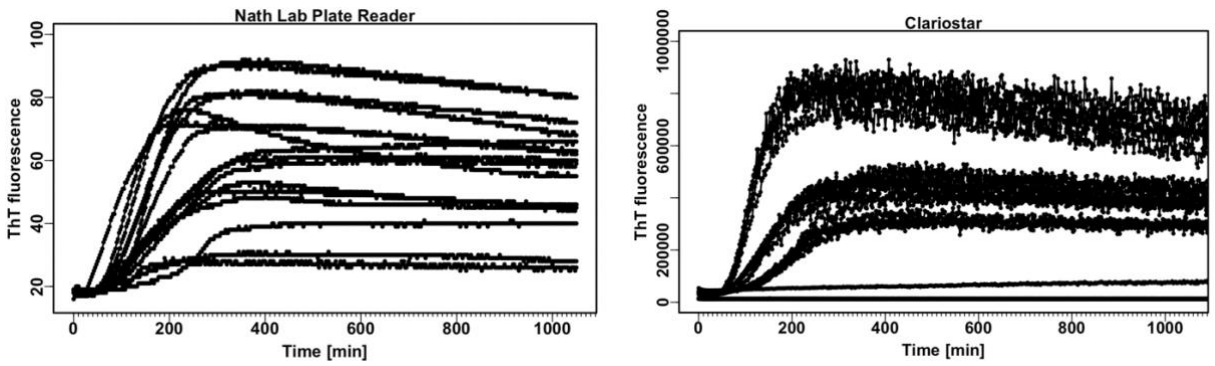

Figure 4.7: Comparison of in vitro tau aggregation performed on the HT Synergy (Left) and CLARIOstar (Right). Two duplicate plates with the same sample preparation were tested on two different instruments.

Time-resolved sHSP addition using automated injection

With the CLAIOStar plate reader system, one of the added features is the programmable auto-injection arms. This enabled time-resolved addition of sHSPs at specific time points during the aggregation reaction. While similar experiments were previously performed manually (25), manual injection is is labor-intensive and could introduce variability. The automated injection system allowed precise and reproducible addition of sHSPs at defined stages of aggregation, allowing new mechanistic questions to be asked.

Two primary technical challenges were optimized for automated injection of sHSPs. First, sHSP injection perturbed ThT fluorescence when it is added due to its interaction with ThT. This issue was addressed by including buffer-only injection controls to normalize the baseline. Second, samples were prone to evaporation during long overnight measurements because the wells needed to remain accessible to the injection arm and therefore could not be covered.

Evaporation was minimized by adding buffer to inter-well spaces and filling unused wells to reduce uneven evaporation across the plate.

ACD monomer may participate in fibril capping to suppress tau aggregation

Previous work showed that HSPB1 dimers are effective only when added during early aggregation stages, with little chaperone effect when added during elongation stage (24). To determine whether this mechanism extends to full-length oligomers of HSPB1 and HSPB5, I added each protein at multiple stages of tau aggregation using the auto-injection system. At pH 7.5, both HSPB1 and HSPB5 exhibited progressively diminished chaperone activity when added later in the reaction, with minimal effects when added during elongation (Figure 4.8; Top panels). These results are consistent with prevailing model that sHSPs primarily target early aggregation species. In contrast, under activating condition at pH 6.5, addition of either HSPB1 or HSPB5 produced substantially stronger inhibition of tau aggregation (Figure 4.8; middle panels). Remarkably, even when added during the elongation phase, both proteins significantly slowed fibril growth. This observation suggests that pH acidosis activates additional chaperone mechanism beyond early-stage sequestration by the NTRs. To distinguish whether these effects arose from altered tau aggregation kinetics at pH 6.5 versus intrinsic changes in sHSP activity, I repeated these experiments using pH-activating mutants (H124K for HSPB1 and H104K for HSPB5) at pH 7.5. This allowed testing of activated HSPB1 and HSBP5 mutants without changing tau aggregation kinetics due to lowered pH. These mutations have been structurally characterized by NMR in ACD-only constructs (26-27). Introducing these “pH mimicking “ mutations led to ACD conformational changes that are structurally equivalent to the ACD structure at pH 6.5. In both cases, the pH-mimicking mutants exhibited strong chaperone activity when added during both the lag and elongation stages of tau aggregation (Figure 4.8; bottom

panels). These results indicate that the pH activated sHSPs hold additional inhibitory effects on tau aggregation.

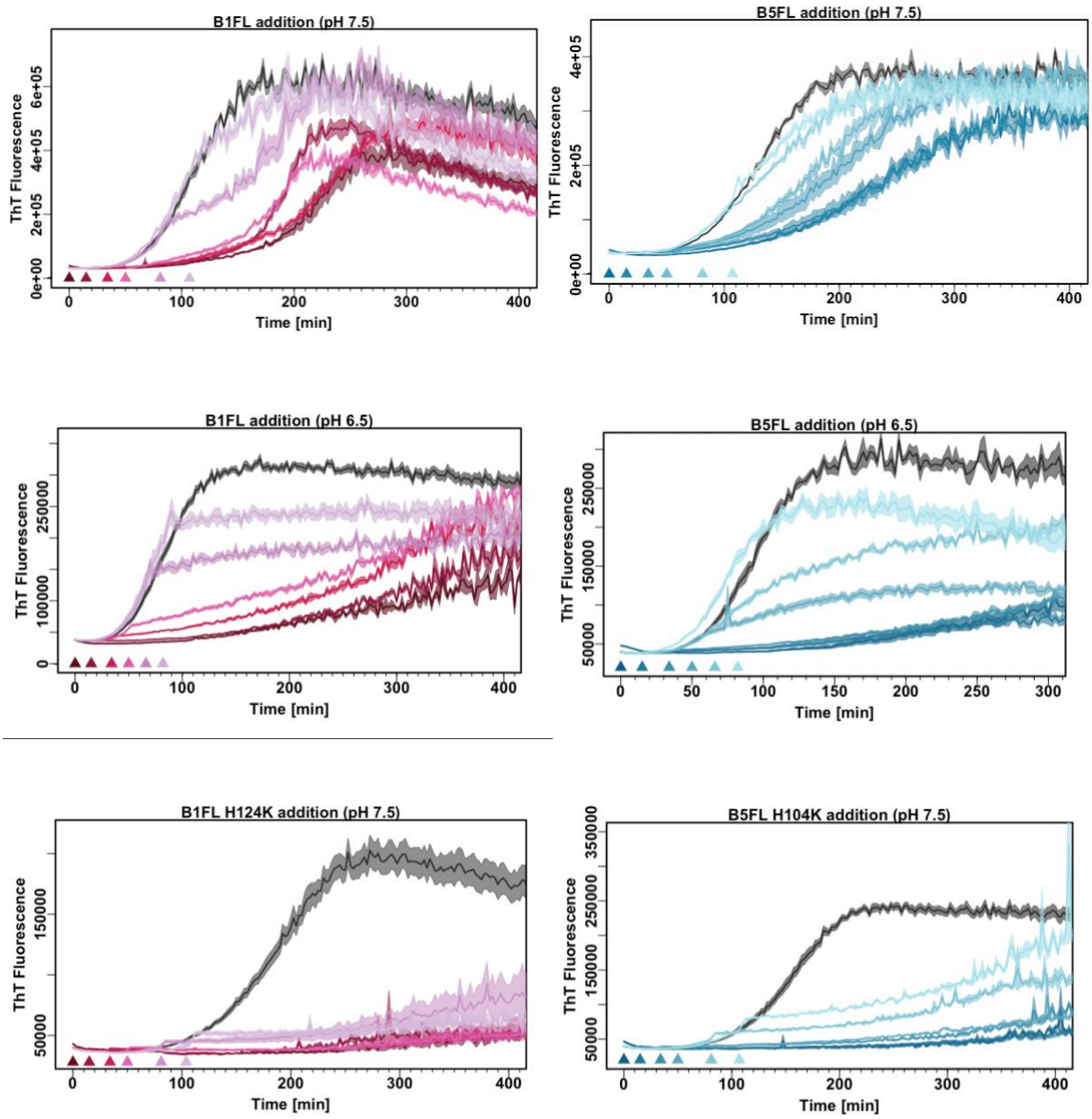

Figure 4.8: in vitro tau ThT aggregation assays using the automated injection arms for time-resolved addition of sHSP at lag and elongation phase. (Top left) WT-HSPB1 FL was added to pH 7.5 tau aggregation reaction at the start, early/late lag phase, and early/late elongation

phase. Arrows represent the time of injection of sHSP. Reactions are performed at 37 C° with 5μM Tau induced with 1mg/mL polyphosphate, with 1μM sHSP added. The equivalent results are shown for WT-HSPB5 at pH 7.5 (Top Right); WT-HSPB1 at pH 6.5 (Middle Left); WT-HSPB5 at pH 6.5 (Middle Right); HSPB1-H124K at pH 7.5 (Bottom Left); HSPB5-H104K (Bottom Right). All sHSPs injected were at 1μM monomer concentration.

Previous work (28) demonstrated that ACD-only constructs of HSPB1 and HSPB5 can exhibit chaperone activity toward model clients via a "fibril-capping" mechanism. Structural analysis has shown that acidic pH can destabilize the ACD dimer interface (29), particularly the long $\beta 6/\beta 7$ strands, promoting ACD monomerization (Figure 4.9). Such "ACD monomers" are hypothesized to bind to fibril ends through beta-sheet formation with the dimer interface. Moreover, HSPB1 contains a cysteine at its dimer interface that has been proposed to function as an oxidative switch. As shown in Chapter 2, ACD-only constructs exhibit minimal activity at pH 7.5 unless at high concentrations. To test if the ACD becomes activated under pH acidosis, ACD-only constructs were added at multiple stages throughout tau aggregation at pH 6.5. To better visualize the magnitude of ACD-dependent effects, a 1x molar ratio of ACD was used throughout tau aggregation, since the ACD effect is relatively small at concentrations compared to full-length oligomers. Under activating conditions at pH 6.5, ACD-only constructs of both HSPB1 and HSPB5 slowed elongation regardless of when they were added during the aggregation reaction (Figure 4.10). This suggests that pH activation could help expose the ACD dimer interface, enabling a fibril capping mechanism through direct interaction with growing tau fibrils. The chaperone mechanism proposed here could occur from within an oligomer and/or from dissociated subunits that recruit clients.

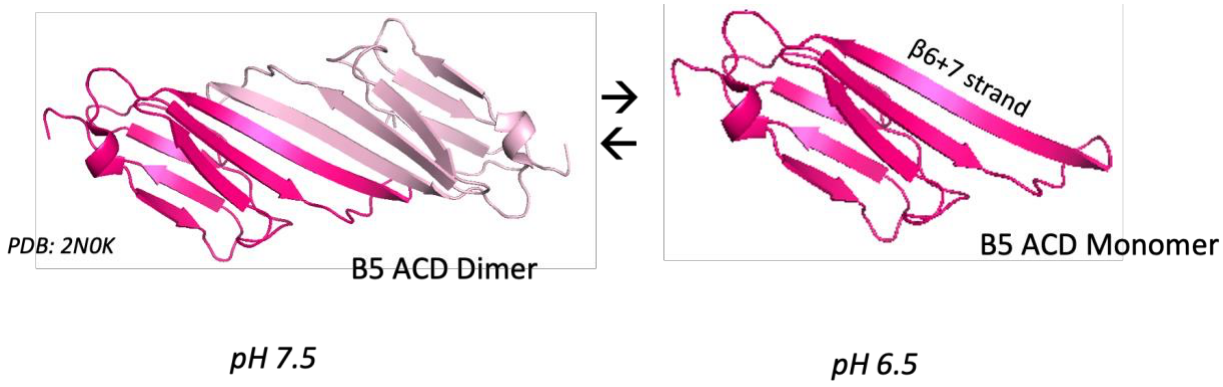

Figure 4.9: Proposed transition of ACD dimer to monomer under acidic condition. PDB:2N0K structure of HSPB5-WT ACD Dimer solved at a neutral pH condition (Left). Under activating low pH condition, it has been hypothesized that ACD can become unstable and monomerize, exposing the long β6 and β7 strands to be available to β-sheet structures of aggregation fibrils.

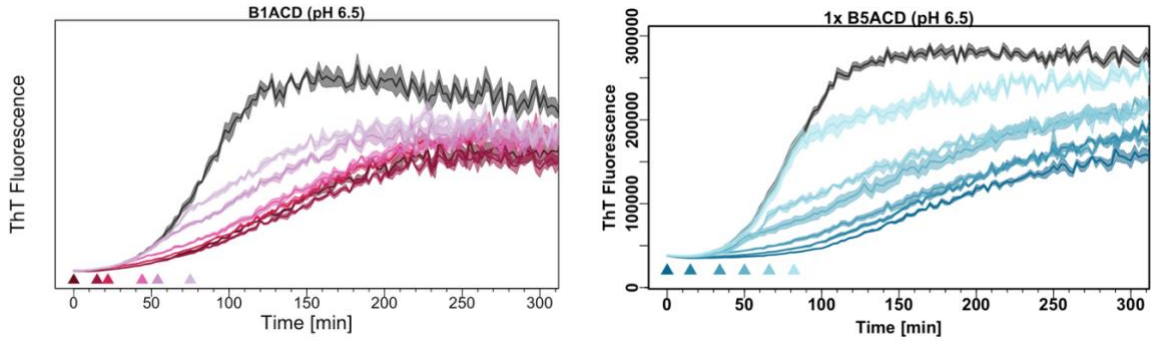

Figure 4.10: Chaperone function of ACD-only constructs added at different aggregation time points. Addition of 1x WT-HSPB1 ACD-only construct at the start, early/late lag phase, and early/late elongation phase of tau aggregation at pH 6.5 (Left). Same experiments were repeated for 1x WT-HSPB5 ACD-only construct (Right). 5μM tau aggregation is induced by polyphosphate at pH 6.5; 37°C in presence of 1x molar ratio (5μM) ACD added at varying time points.

While MP reports the heterogeneous sHSP oligomeric species, its MW detection limit is 30-40kDa, so ACD monomers are too small to be accurately measured. Instead, the elution profiles of ACD-only constructs were analyzed by analytical size-exclusion chromatography (GE Superose 6 10/300 GL) at pH 7.5 and pH 6.5 (Figure 4.11) to characterize pH-dependent shifts in ACD monomerization. Both HSPB1-ACD and HSPB5 were injected onto the column at 4 different concentrations (250μM, 100μM, 50μM, 25μM) under both pH conditions. The resulting aSEC elution profiles provide information on changes in the monomer-dimer equilibrium as a funcytion of concentration and how this equilibrium shifts with changes in pH. At pH 7.5, HSPB1 ACD showed no detectable change in elution volume as a function of ACD concentration, while the HSPB5 ACD exhibited a slight shift toward smaller size. In contrast, at pH 6.5, both HSPB1 and HSPB5 ACDs eluted as progressively smaller populations with decreasing concentration and overall, eluted at later volume compared to pH 7.5. These results suggest that acidic pH promotes dissociation of ACD dimers into monomers across the concentration range tested. This destabilization of the ACD dimer is in line with the hypothesized ACD structural rearrangement shown in Figure 4.8. The proposed fibril-capping mechanism can also be tested by quantifying tau fibrils formed in the presence or absence of activated sHSPs and comparing fibril length distributions. If fibril capping mechanism operates as predicted by the hypothesis, shorter fibrils would be expected in the presence of activated sHSPs capable of binding the β-sheet structure at fibril ends. Experiments of this type would further elucidate the diverse mechanisms by which sHSPs exert their chaperone function.

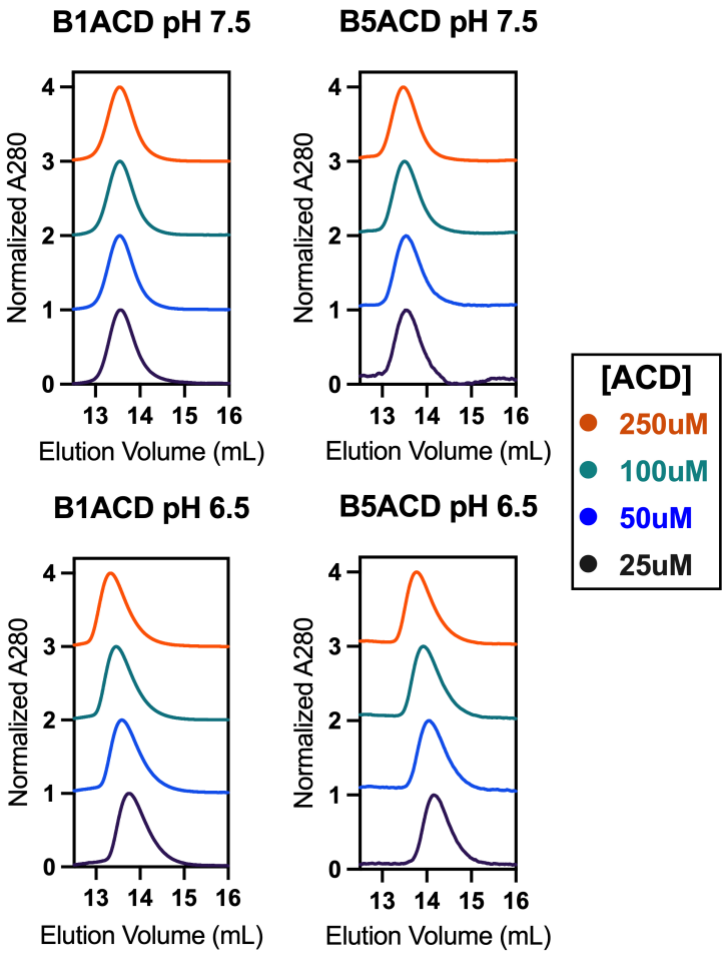

Figure 4.11: Analytical sizing elution profile for HSPB1 and HSPB5 ACD-only constructs at pH 7.5 or pH 6.5. The elution profile is shown for highest concentration at the top, with lowest concentration on the bottom. A280 absorbance were normalized for each sample and a line is draw for the lowest concentration elution peak.

Collectively, these results support a multilayered model of sHSP chaperone function. Under basal conditions, HSPB1 and HSPB5 predominantly suppress early tau aggregation through NTR-mediated interactions. Specific functional regions within the NTR (FR-E in HSPB1 and FR-B in HSPB) serve as regulatory hubs for phosphorylation and pH sensing to help

"open" chaperone function (Mechanism 1; Figure 4.12, Left). Upon activation, or during chronic stress, conformational rearrangements not only enhance NTR accessibility but also expose chaperone-active surfaces within the ACD, particularly at the dimer interface (Mechanism 2; Figure 4.12, Right). While the ACD contributes less strongly than the NTRs and require higher local concentrations, its ability to cap fibril ends provides an additional layer of protection by directly suppressing elongation. This dual targeting of both soluble and fibrillar tau species may help explain how sHSPs adapt to diverse aggregation phases and client types, including both fibrillar (tau, Aβ peptides) and amorphous substrates (gamma-D, tubulin).

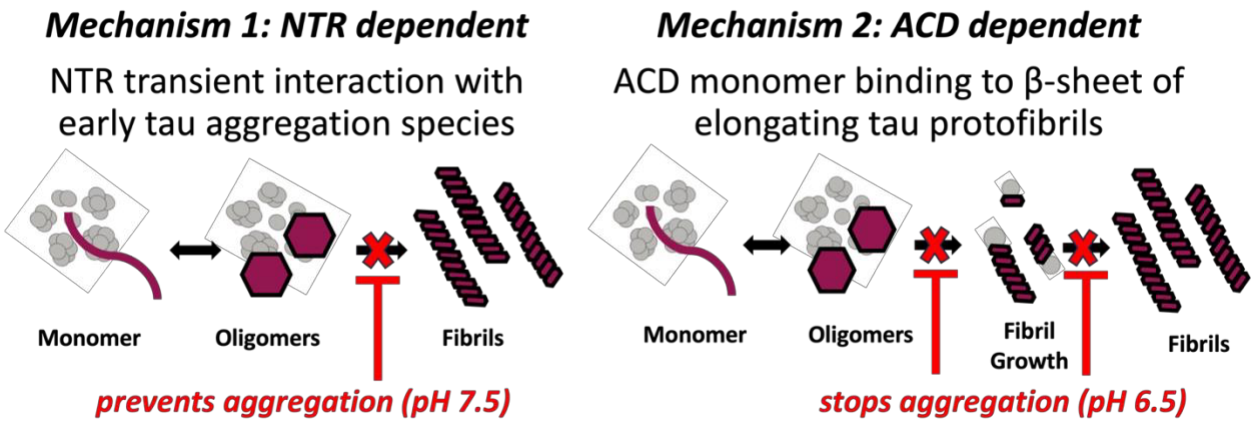

Figure 4.12: Proposed mechanisms of sHSP chaperone mechanism. (Left) Mechanism 1 prevents tau aggregation using specific NTR sub-regions. (Right) Activated chaperone function is proposed to be involved in fibril capping to suppress elongation rate in Mechanism 2.

The approaches described here were foundational for testing hypotheses throughout this thesis. The methods developed and optimized in this chapter were specifically designed to overcome key challenges posed by sHSPs, including oligomer polydispersity and heterogeneity.

These efforts will allow for future investigations that examine sHSPs from multiple perspective in a systematic manner to parse out functionally relevant interactions and structural features.

References:

1. Zhang S, Zhu Y, Lu J, Liu Z, Lobato AG, Zeng W, Liu J, Qiang J, Zeng S, Zhang Y, Liu C. Specific binding of Hsp27 and phosphorylated Tau mitigates abnormal Tau aggregation-induced pathology. Elife. 2022 Sep 1;11:e79898.
2. Xu Z, Au SW. Mapping residues of SUMO precursors essential in differential maturation by SUMO-specific protease, SENP1. Biochemical Journal. 2005 Mar 1;386(2):325-30.
3. Allen MC, Karplus PA, Mehl RA, Cooley RB. Genetic encoding of phosphorylated amino acids into proteins. Chemical reviews. 2024 May 1;124(10):6592-642.
4. Costello A, Peterson AA, Chen PH, Bagirzadeh R, Lanster DL, Badran AH. Genetic code expansion history and modern innovations. Chemical Reviews. 2024 Oct 28;124(21):11962-2005.
5. Woods CN, Ulmer LD, Guttman M, Bush MF, Klevit RE. Disordered region encodes α-crystallin chaperone activity toward lens client γD-crystallin. Proceedings of the National Academy of Sciences. 2023 Feb 7;120(6):e2213765120.
6. Woods CN, Janowska MK, Ulmer LD, Kaur Sidhu J, Stone NL, James EI, Guttman M, Bush MF, Klevit RE. Activation mechanism of Small Heat Shock Protein HSPB5 revealed by disease-associated mutants. Proceedings of the National Academy of Sciences. 2025 May 20;122(20):e2425061122.

7. Stone NL, Janowska MK, Narisawa L, Tuttle LM, Ulmer LD, Guttman M, Bush MF, Klevit RE. Disorder with consequence: Phosphorylation sites in HSPB5 yield distinct structural outcomes. bioRxiv. 2025 Oct 28:2025-10.
8. Sia Y, Pan H, Chen K, Chen Z. Structural insights into chromatin remodeling by ISWI during active ATP hydrolysis. Science. 2025 Apr 3;388(6751):eadu5654.
9. Ulmer LD, Canzani D, Woods CN, Stone NL, Janowska MK, Klevit RE, Bush MF. High-performance workflow for identifying site-specific crosslinks originating from a genetically incorporated, photoreactive amino acid. Journal of Proteome Research. 2024 Jul 5;23(8):3560-70.
10. Mymrikov EV, Riedl M, Peters C, Weinkauf S, Haslbeck M, Buchner J. Regulation of small heat-shock proteins by hetero-oligomer formation. Journal of Biological Chemistry. 2020 Jan 3;295(1):158-69.
11. Aquilina JA, Shrestha S, Morris AM, Ecroyd H. Structural and functional aspects of hetero-oligomers formed by the small heat shock proteins αB-crystallin and HSP27. Journal of biological chemistry. 2013 May 10;288(19):13602-9.
12. Heirbaut M, Lermyte F, Martin EM, Beelen S, Sobott F, Strelkov SV, Weeks SD. Specific sequences in the N-terminal domain of human small heat-shock protein HSPB6 dictate preferential hetero-oligomerization with the orthologue HSPB1. Journal of Biological Chemistry. 2017 Jun 1;292(24):9944-57.
13. Delbecq SP, Rosenbaum JC, Klevit RE. A mechanism of subunit recruitment in human small heat shock protein oligomers. Biochemistry. 2015 Jul 21;54(28):4276-84.

14. Clouser AF, Baughman HE, Basanta B, Guttman M, Nath A, Klevit RE. Interplay of disordered and ordered regions of a human small heat shock protein yields an ensemble of ‘quasi-ordered’states. Elife. 2019 Oct 1;8:e50259.
15. Asor R, Loewenthal D, van Wee R, Benesch JL, Kukura P. Mass Photometry. Annual Review of Biophysics. 2025 May 6;54(1):379-99.
16. Roy J, Marathe I, Wysocki V, Pradeep T. Observing atomically precise nanocluster aggregates in solution by mass photometry. Chemical Communications. 2024;60(52):6655-8.
17. Kratochvíl J, van Wee R, Thiele JC, Loewenthal D, Bardzil J, Iqbal K, Benesch JL, Thorpe S, Kukura P. Best practice mass photometry: a guide to optimal single-molecule mass measurement. Nature Protocols. 2025 Oct 13:1-25.
18. Berkeley RF, Plonski AP, Phan TM, Grohe K, Becker L, Wegner S, Herzik Jr MA, Mittal J, Debelouchina GT. Capturing the Conformational Heterogeneity of HSPB1 Chaperone Oligomers at Atomic Resolution. Journal of the American Chemical Society. 2025 Mar 27;147(18):15181-94.
19. Xue C, Lin TY, Chang D, Guo Z. Thioflavin T as an amyloid dye: fibril quantification, optimal concentration and effect on aggregation. Royal Society open science. 2017 Jan 4;4(1):160696.
20. Baughman HE, Pham TH, Adams CS, Nath A, Klevit RE. Release of a disordered domain enhances HspB1 chaperone activity toward tau. Proceedings of the National Academy of Sciences. 2020 Feb 11;117(6):2923-9.

21. Ramachandran G, Udgaonkar JB. Understanding the kinetic roles of the inducer heparin and of rod-like protofibrils during amyloid fibril formation by Tau protein. Journal of biological chemistry. 2011 Nov 11;286(45):38948-59.
22. Schwartz LB. Mast cells and basophils. Inflammatory mechanisms in allergic diseases. 2023 Jan 6:3-42.
23. Lempart J, Jakob U. Role of polyphosphate in amyloidogenic processes. Cold Spring Harbor perspectives in biology. 2019 May 1;11(5):a034041.
24. Wickramasinghe SP, Lempart J, Merens HE, Murphy J, Huettemann P, Jakob U, Rhoades E. Polyphosphate initiates tau aggregation through intra-and intermolecular scaffolding. Biophysical journal. 2019 Aug 20;117(4):717-28.
25. Baughman HE, Clouser AF, Klevit RE, Nath A. HspB1 and Hsc70 chaperones engage distinct tau species and have different inhibitory effects on amyloid formation. Journal of Biological Chemistry. 2018 Feb 23;293(8):2687-700.
26. Rajagopal P, Tse E, Borst AJ, Delbecq SP, Shi L, Southworth DR, Klevit RE. A conserved histidine modulates HSPB5 structure to trigger chaperone activity in response to stress-related acidosis. elife. 2015 May 11;4:e07304.
27. Clouser AF, Klevit RE. pH-dependent structural modulation is conserved in the human small heat shock protein HSBP1. Cell Stress and Chaperones. 2017 Jul 1;22(4):569-75.
28. Selig EE, Lynn RJ, Zlatic CO, Mok YF, Ecroyd H, Gooley PR, Griffin MD. The monomeric α-Crystallin domain of the small heat-shock proteins αB-Crystallin and Hsp27 binds amyloid fibril ends. Journal of Molecular Biology. 2022 Aug 30;434(16):167711.

29. Alderson TR, Roche J, Gastall HY, Dias DM, Pritišanac I, Ying J, Bax A, Benesch JL, Baldwin AJ. Local unfolding of the HSP27 monomer regulates chaperone activity. Nature communications. 2019 Mar 6;10(1):1068.

APPENDIX

Amino acid scale values:

Amino Acid	Hydrophobicity scale value
Ala	-0.500
Arg	3.000
Asn	0.200
Asp	3.000
Cys	-1.000
Gln	0.200
Glu	3.000
Gly	0.000
His	-0.500
Ile	-1.800
Leu	-1.800
Lys	3.000
Met	-1.300
Phe	-2.500
Pro	0.000
Ser	0.300
Thr	-0.400
Trp	-3.400
Tyr	-2.300
Val	-1.500

Supplementary Figure 1 (Chapter 1): Amino acid scale: Hydrophilicity used for NTR Function regions of 10 human small heat shock proteins. The values used are based on the following published work: Author(s): Hopp T.P., Woods K.R. Reference: Proc. Natl. Acad. Sci. U.S.A. 78:3824-3828(1981).

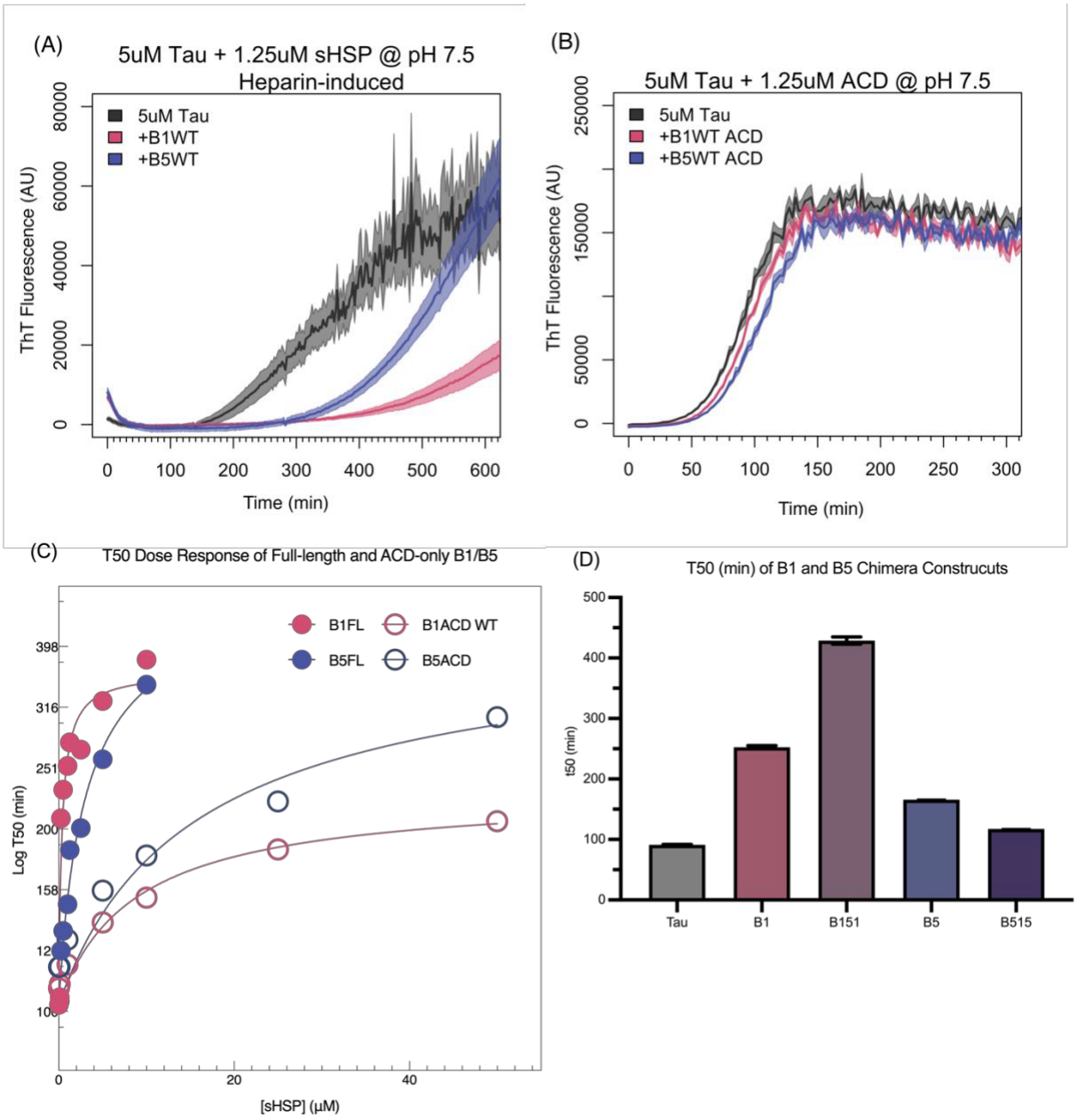

Supplemental Figure 2 (Chapter 2): A) HSPB1 and HSPB5 chaperone heparin-induced aggregation of tau. B) ACD-only constructs at the equivalent concentration at 1.25μM show no chaperone function. 5μM Tau aggregation is induced by 1mg/mL polyphosphate. C) T50 dose response curves for both Full-length and ACD-only constructs of HSPB1 and HSPB5, plotted on a log scale. Both Full-length constructs reach near saturation by 10μM or maximum concentration tested. HSPB5 ACD shows some titratable activity at high concentration, but the

chaperone activities of both ACDs are much lower compared to equivalent concentrations of their full-length counterparts. D) Calculated T50 values of HSPB1 and HSPB5 constructs chaperone activity measured by ThT assay. SEM of 6 replicates are shown as error bars.

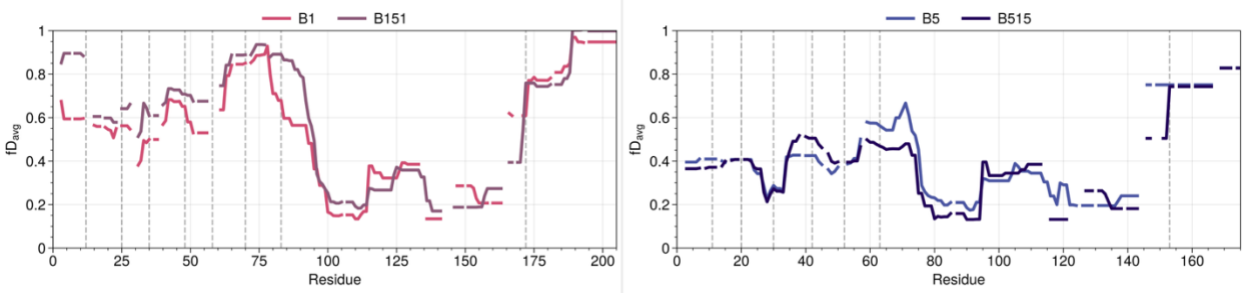

Supplemental Figure 3 (Chapter 2): HDX-MS full length comparison. Average deuteration level calculated based on unimodal analysis is shown for corresponding residues. Comparison of the full-length sequence for HSPB1-WT (pink) and B151 (purple) are shown in the Lef panel. Comparison of HSPB5-WT (blue) and B515 (dark blue) are shown in the Right panel. Dashed lines correspond to NTR sub-regions, ACD, and CTR residue boundaries.

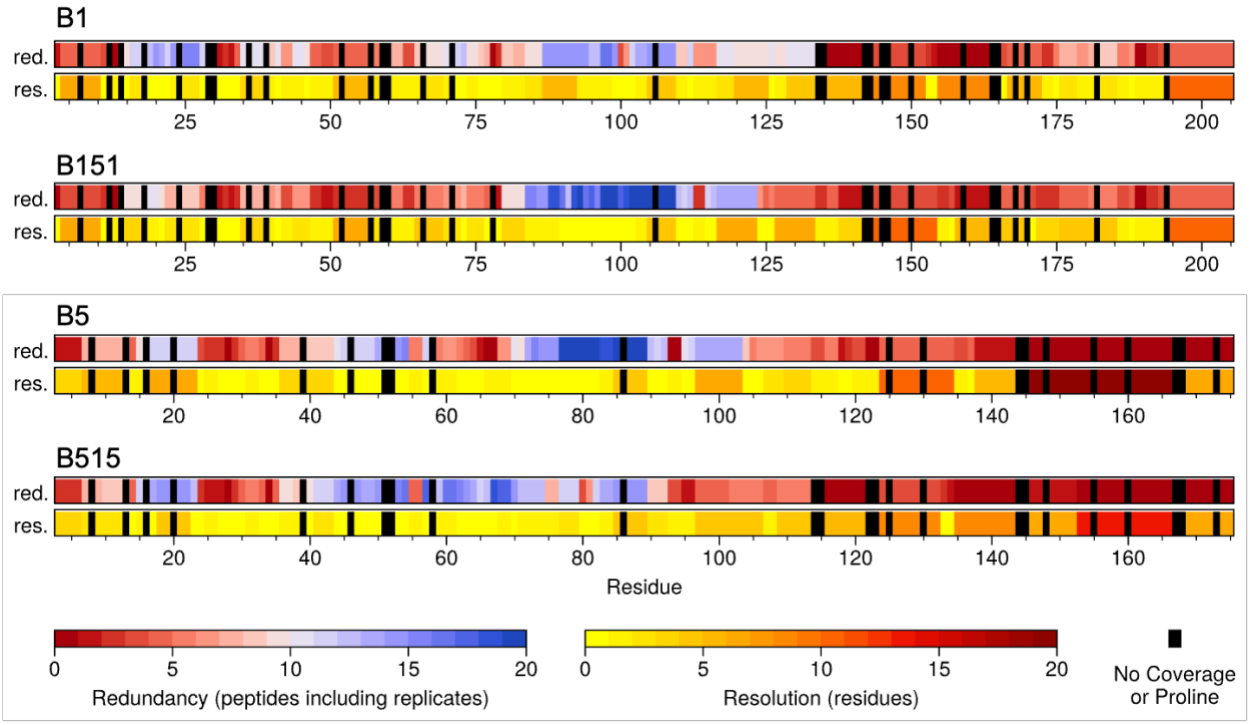

Supplemental Figure 4 (Chapter 2): HDX-MS Redundancy: The redundancy and resolution of peptides along the sequence are shown for HSPB1WT, HSPB151, HSPB5WT and HSPB515. Regions where there are no coverage or Proline residues depicted in black.

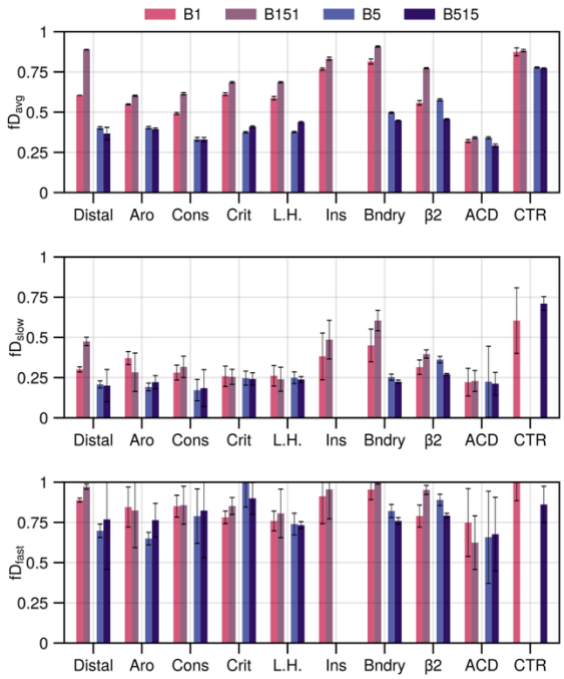

Supplemental Figure 5 (Chapter 2): Bimodal analysis of HSPB1 and HSPB5 constructs. Average fractional deuterium uptake for each NTR sub-regions, ACD, and CTR (Top). Fractional deuterium uptake for the slower exchanging population (middle) and fast exchanging population (bottom).

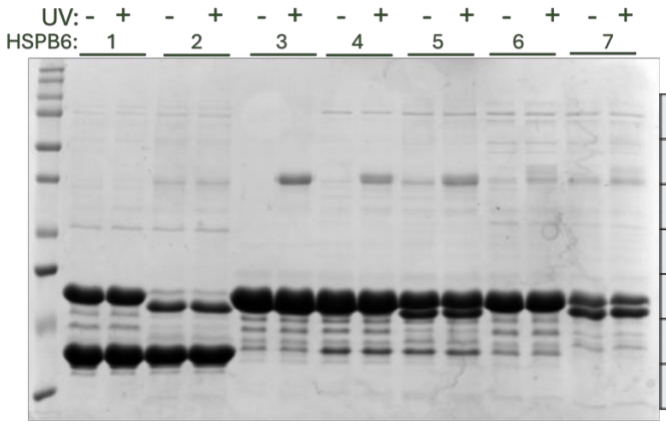

1	50μM HSPB6 W11bpa + 50μM HSPB6 WT
2	50μM HSPB6 W11bpa + 60μM HSPB3 WT
3	50μM HSPB6 Y22bpa + 50μM HSPB6 WT
4	50μM HSPB6 F29bpa + 50μM HSPB6 WT
5	50μM HSPB6 F29bpa + 60μM HSPB3 WT
6	50μM HSPB6 Y53bpa + 50μM HSPB6 WT
7	50μM HSPB6 Y53bpa + 60μM HSPB3 WT

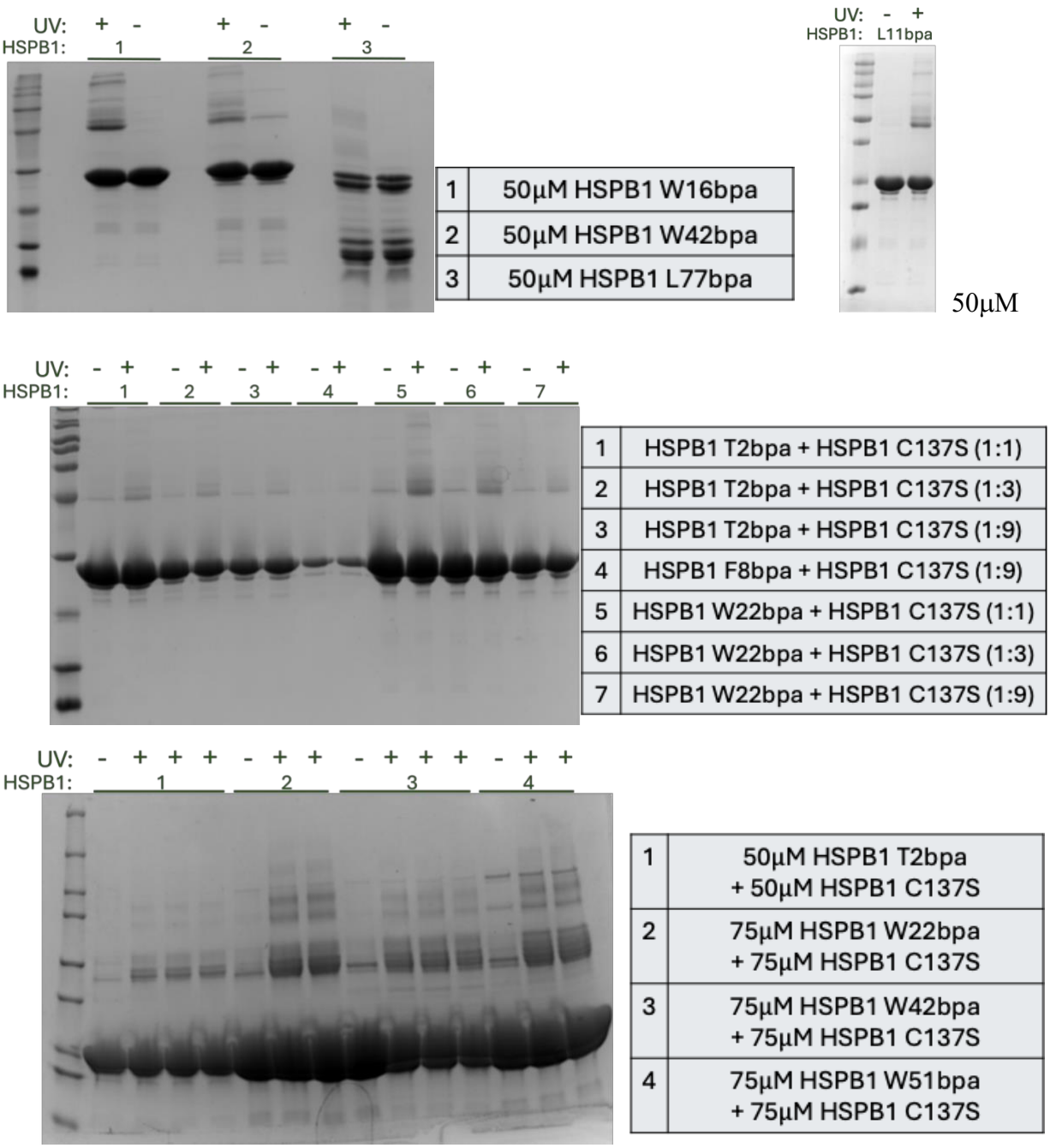

Supplemental Figure 6 (Chapter 4): HSPB1 and HSPB6 BPA crosslink reactions by SDS-PAGE after UV-Crosslink reactions.